

Equilibration and deformation of glass-forming polymers : molecular simulation via connectivity-altering Monte Carlo and scale-jumping methods

Citation for published version (APA):

Mulder, T. (2008). *Equilibration and deformation of glass-forming polymers : molecular simulation via connectivity-altering Monte Carlo and scale-jumping methods*. [Phd Thesis 1 (Research TU/e / Graduation TU/e), Applied Physics and Science Education]. Technische Universiteit Eindhoven.
<https://doi.org/10.6100/IR633474>

DOI:

[10.6100/IR633474](https://doi.org/10.6100/IR633474)

Document status and date:

Published: 01/01/2008

Document Version:

Publisher's PDF, also known as Version of Record (includes final page, issue and volume numbers)

Please check the document version of this publication:

- A submitted manuscript is the version of the article upon submission and before peer-review. There can be important differences between the submitted version and the official published version of record. People interested in the research are advised to contact the author for the final version of the publication, or visit the DOI to the publisher's website.
- The final author version and the galley proof are versions of the publication after peer review.
- The final published version features the final layout of the paper including the volume, issue and page numbers.

[Link to publication](#)

General rights

Copyright and moral rights for the publications made accessible in the public portal are retained by the authors and/or other copyright owners and it is a condition of accessing publications that users recognise and abide by the legal requirements associated with these rights.

- Users may download and print one copy of any publication from the public portal for the purpose of private study or research.
- You may not further distribute the material or use it for any profit-making activity or commercial gain
- You may freely distribute the URL identifying the publication in the public portal.

If the publication is distributed under the terms of Article 25fa of the Dutch Copyright Act, indicated by the "Taverne" license above, please follow below link for the End User Agreement:

www.tue.nl/taverne

Take down policy

If you believe that this document breaches copyright please contact us at:

openaccess@tue.nl

providing details and we will investigate your claim.

Equilibration and deformation of glass-forming polymers: molecular simulation via connectivity-altering Monte Carlo and scale-jumping methods

PROEFSCHRIFT

ter verkrijging van de graad van doctor aan de
Technische Universiteit Eindhoven, op gezag van de
Rector Magnificus, prof.dr.ir. C.J. van Duijn, voor een
commissie aangewezen door het College voor
Promoties in het openbaar te verdedigen
op donderdag 20 maart 2008 om 14.00 uur

door

Tim Mulder

geboren te Eindhoven

Dit proefschrift is goedgekeurd door de promotor:

prof.dr. M.A.J. Michels

Copromotor:
dr. A.V. Lyulin

Druk: Universiteitsdrukkerij Technische Universiteit Eindhoven

CIP-DATA LIBRARY TECHNISCHE UNIVERSITEIT EINDHOVEN

Mulder, T.

Equilibration and deformation of glass-forming polymers: molecular simulation via connectivity-altering Monte Carlo and scale-jumping methods / door T. Mulder. - Eindhoven : Technische Universiteit Eindhoven, 2008. - Proefschrift.

ISBN 978-90-386-1226-3

NUR 971

Trefwoorden: amorfe polymeren / glas / mechanische eigenschappen / deformatie / Monte Carlo methoden / multischaal modellering / polyetheen / polystyreen

Subject headings: amorphous polymers / glass / mechanical properties / deformation / equilibration / Monte Carlo methods / connectivity altering / coarse graining / multi-scale modeling / scale jumping / polyethylene / polystyrene

This work forms part of the research programme of the Dutch Polymer Institute (project 487).

Voor het gebruik van supercomputerfaciliteiten bij dit onderzoek is subsidie verleend door de Stichting Nationale Computer Faciliteiten (NCF), met financiële steun van de Nederlandse Organisatie voor Wetenschappelijk Onderzoek (NWO).

Contents

1	Introduction	1
1.1	Polymers and their mechanical behavior	2
1.2	Experimental knowledge	3
1.3	Existing theoretical and simulation approaches	6
1.4	Multi-scale modeling	9
1.5	Our project	11
2	Molecular simulation methods for polymers	13
2.1	Molecular simulations of polymers: basic methods and state of art with respect to length and timescales	14
2.2	Molecular simulation of polymer mechanical deformation	19
2.3	Equilibration of condensed polymer systems - an overview	23
2.3.1	Approaches to equilibration of condensed polymers	23
2.3.2	End-bridging Monte Carlo	26
2.4	Methodologies employed in this thesis	33
3	Monte Carlo simulation of uniaxial tension of an amorphous polymer glass	35
3.1	Introduction	36
3.2	PE model and simulation algorithm	39
3.3	Preparation of the initial polymer melt	42
3.3.1	Equilibration at 450 K	42
3.3.2	Cooling process	43
3.4	Uniaxial deformation	44
3.4.1	Stress-strain behavior	44
3.4.2	Evolution of internal-energy contributions and stress partitioning	47
3.5	Conclusions	53
4	Constraints in Monte Carlo simulations of deformation	55
4.1	Introduction	55
4.2	Model, MC algorithms and stress calculation	57
4.3	Results and discussion	59
4.3.1	Equilibration at 450 K	59

4.3.2	Cooling to 200 K	61
4.3.3	Uniaxial deformation	61
4.3.4	Stress-strain behavior	62
4.3.5	Stress partitioning and energy partitioning	63
4.3.6	Structural properties	67
4.4	Conclusions	69
5	Generalization of the EBMC algorithm to polymers of type (AB)_n	73
5.1	Introduction	74
5.2	Coarse-grained polymer models and generalization of EBMC	76
5.2.1	The 2:1 coarse-grained model of PS	76
5.2.2	Generalization of EBMC to simulate coarse-grained systems	82
5.3	Testing the algorithm on small molecules	83
5.4	Equilibration of long-chain polymer melts	84
5.5	Conclusions	90
6	Structural properties of atactic polystyrene	93
6.1	Introduction	95
6.2	Reinsertion of atomistic detail	97
6.3	Structural properties of aPS resulting from the multi-scale preparation method	99
6.4	Comparison of structural properties obtained from the different cooling rates	105
6.5	Conclusions	107
7	Molecular-dynamics simulation of PS under deformation	111
7.1	Introduction	112
7.2	Details of the simulations	113
7.3	Differences between CGEB and ECC samples	114
7.3.1	Structural properties prior to deformation	114
7.3.2	Stress-strain behavior	116
7.3.3	Stress partitioning and energy partitioning	117
7.3.4	Evolution of structures	120
7.4	Conclusions	125
8	Conclusions and outlook	127
8.1	Main results	128
8.2	Outlook	130
	Summary	141
	List of publications	143
	Dankwoord	145
	Curriculum Vitae	147

Chapter 1

Introduction

ABSTRACT

This Chapter starts with a general introduction into polymers and their mechanical properties. Subsequently an overview is given of the experimental knowledge with regard to mechanical behavior of pure, synthetic-polymer materials that have been investigated in this thesis work. Modeling approaches are given in a next Section. Finally the goal of the work and the outline of this thesis are presented.

1.1 Polymers and their mechanical behavior

Polymers form a relatively new group of materials. Although polymers have been present all over the place since time immemorial, they were not recognized as an apart group of materials before the 20th century. For a long time, polymers were viewed as colloids. This view lasted till the 1920s, when Staudinger came up with his macromolecular hypothesis, i.e., the hypothesis that polymers are molecules made of covalently bonded elementary units, called monomers. This hypothesis gave a plausible explanation for the fact that polymers exhibit colloidal behavior in all solvents in which they dissolve, whereas normal colloids fall apart in small molecules in good solvents. This important insight can be considered as the start of the field of polymer science. It results in the development of basic synthetic routes for producing polymers and developing the first theoretical concepts. Till World War II synthetic polymers were regarded as substitutes for existing natural polymers, such as rubber and silk. From the 1940s polymers were developed with properties fairly different from known natural ones. Ever since, polymers have been increasingly important, as supplement and also as replacement for traditional materials. Via synthesis and further processing it appeared possible to produce polymer materials with widely different chemical, electrical and physical properties, resulting in many opportunities for applying those polymers. Nowadays polymers can be found in many and widely different applications and products, such as food conservation, all kinds of packaging, housing of electrical apparatus, paint and coatings, clothes, fibers and semiconductor devices.

One of the main advantages of polymers is that these materials are easy to process. Many processing routes are available, such as injection molding, compression molding, extrusion, melt spinning, cold drawing, solution spinning, and so on. Injection molding, where molten plastic is injected at high pressure in a mold, is used on a large scale for a wide range of products, from small Lego parts to large car parts. During compression molding the molding material is first placed in an open mold; the mold is then closed and pressure is applied to force the material into contact with all mold areas, and until the molding material has cured, heat and pressure are maintained. In extrusion the polymer material is pushed or drawn through a die, to obtain long objects with a fixed cross-sectional area and shape. Melt spinning, cold drawing and solution spinning are techniques in which polymer chain alignment can be promoted. Using one or more of these techniques a wide range of products can be made. One of the advantages of polymers is the ease at which these materials can be shaped. A consequence is that the number of parts in products can be reduced, as compared to a situation where only traditional materials are applied, by combining parts into one piece. Another crucial point is that polymer materials can be processed at a much lower temperature (about 1000 K lower) than for example most common metals, which means an enormous cost reduction because of considerably lower energy costs and also because the processing is less demanding for processing equipment.

In many applications of polymers, the favorable mechanical properties in combination with the low specific weight are important. These mechanical properties can be influenced by a

multitude of methods. Both chemistry issues and processing issues can be decisive for final mechanical properties. It is essential which polymer or copolymer has been chosen, whether it has been blended with another polymer and in what proportions, whether additives and what additives are used, whether one has a composite or not, and so on. But processing issues are equally important, e.g. temperature and pressure conditions, melt or solution processing, absence or presence of a flow field. And finally the conditions under which the final polymer product is used and kept are important, for example temperature and UV-radiation promote degradation of various polymers.

Although there exists a vast amount of possibilities to influence the mechanical behavior of polymer materials, a thorough understanding of all principles and mechanisms underlying this behavior is often lacking. Much of the knowledge is full of empirical rules. Even for a pure polymer material it is not evident what exactly determines its mechanical properties, and what makes its properties different from another polymer? What makes a polymer stiff, what makes it brittle or tough or what determines the impact resistance of a polymer material? And also, what is the structural evolution, referred to as aging, that translates in an evolution of the mechanical properties of a polymer material during its service life? All these issues are central to this thesis; the remainder of this Chapter will provide the reader with the necessary background information on these and closely related problems.

1.2 Experimental knowledge

Many polymers used for different practical applications are in a glassy state. The glassy state of matter originates from the liquid state upon cooling below the so-called glass-transition temperature T_g . In approach of T_g , the relaxation times of the liquid increase very rapidly, whereas one can hardly see any accompanying change in the static structure of the material at hand [1, 2]. Usually, the glass-transition temperature T_g is arbitrarily defined as the temperature at which the viscosity reaches 10^{12} Pa s. The glassy state of matter and the glass transition itself are still great, ill-understood problems in condensed matter physics, certainly for polymers, because of their complex microstructure and the multitude of length and time scales. No wonder that the mechanical properties of glassy polymers [3–7], which are central to this thesis, are not too well understood either.

Many important mechanical properties can be obtained from straightforward tensile and compression tests. In the left panel of Figure 1.1, typical room-temperature stress-strain curves are given for atactic polystyrene (aPS) and bisphenol-A-polycarbonate (PC) in a uniaxial compression test. These curves can be divided in a number of different regimes, labeled 1 through 4 in this Figure. Deformation starts with a linear-elastic response (regime 1). The slope of the curve in this regime is the E-modulus, which is a measure of the stiffness. The onset of plastic deformation, termed the yield point, is indicated by 2. The subsequent decrease in the stress (regime 3) is called strain softening. This strain softening is very pronounced for PS. The eventual increase of the stress with strain (region 4) is

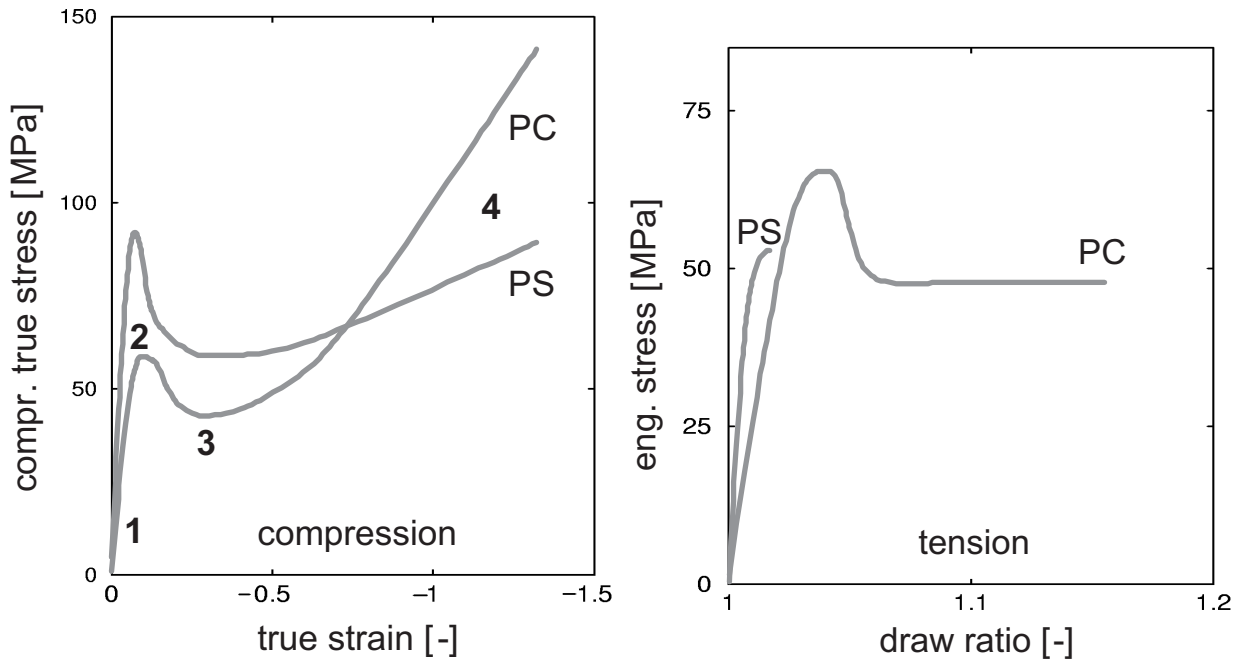


Figure 1.1: a) Typical room temperature stress-strain curves for PS and PC during uniaxial compression testing. Four characteristic regimes can be distinguished: the region of initial quasi-elastic response (region 1), the yield point (region 2), strain softening (region 3) and strain hardening (region 4). b) Room temperature stress-strain curves for PS and PC during a uniaxial tensile test. PS fails brittle at a few % deformation, PC fails ductile at much larger deformations. Reprinted from Van Melick et al.[8].

referred to as strain hardening. From the slope of this final part of the stress-strain curve the strain hardening modulus is usually obtained. It is found that the yield stress increases with increasing strain rate, decreasing temperature and increasing pressure [9]. The post-yield strain-hardening behavior is found to strongly depend on the state of deformation [10], for example uniaxial or plane strain, and involves also the density of cross-links or entanglements of the polymer material [8].

Differences in the mechanical properties among chemically different polymers also clearly manifest themselves in the stress-strain curves. In Figure 1.1a one can observe a larger yield stress and strain softening for PS than for PC. PC, on the contrary, shows a stronger strain hardening. Another clear signature of the differences between these two polymers is given in Figure 1.1b, where typical stress-strain curves for PC and PS under tension have been plotted; polycarbonate behaves ductile (can be deformed well beyond the yield point) and polystyrene behaves brittle (there is only very little plastic deformation before failure occurs due to the formation of a localized crack). However, in the 1980s Kramer and Berger [11] proved that it was possible to measure the intrinsic large-deformation stress-strain behavior at a microscopic scale, with the surprising result that e.g. PS is at that level far more ductile than PC. In fact, there turns out to exist an excellent correlation between

the microscopically measured maximum extension ratio and the theoretical maximum extension ratio of a single strand in the polymer entanglement network. Furthermore, the picture is more complex than this, since the macroscopic deformability of polycarbonate disappears if a specimen is notched and tested under impact conditions.

On top of the intrinsic differences between chemically different polymers, there exist huge processing-related variations in the mechanical behavior of chemically identical polymer materials. It is found that by mechanical treatment PS and PC can both macroscopically become very ductile and can be made to deform by shear yielding. However, this effect is only of temporal nature; the relaxation back to the original state is orders of magnitude faster for PS than for PC [12, 13].

Important in relation to these processing-related observations is the phenomenon of *physical aging*. It was introduced by Struik [14] and refers to the slow structural relaxation processes, not involving chemical reactions, in polymer materials below their glass transition. The age of a material increases with time and aging is fastest just below T_g . Physical age is essential to mechanical properties of amorphous polymers [14, 15].

The height of the yield peak and the degree of strain softening increase with the age of a polymer [16]. The opposite of aging, termed *rejuvenation*, can be accomplished either by heating above T_g followed by quenching into the glassy state, or by subjecting the polymer to a mechanical pre-treatment [17]. By rejuvenation, the yield peak can be lowered and the strain softening can be partially or fully removed. The ultimate consequence of rejuvenation is a brittle polymer such as PS becoming tough, albeit temporarily [17]. The term rejuvenation can further be rationalized by the fact that after the yield point the stress drops to a value which is independent of aging time, and it has been concluded that mechanical extension erases the polymer thermal history [15]. Recently, however, experiments on calorimetry [18] and positron-annihilation lifetime spectroscopy [19] have shown that yielding does not rejuvenate the polymer material, but brings it to a different "equilibrium state".

In summary one may conclude that the mechanical behavior of glassy polymer materials is very rich and there are many ways to manipulate it. To understand all the generic and chemistry-specific mechanisms of polymer structural relaxation, determining both the communalities and wide differences in the mechanical behavior of different amorphous polymers, is of utmost technological importance and forms a big challenge in condensed-matter science. And in addition there is the intriguing role of the influence of processing. A overview of the theoretical understanding up-to-date is given in the next Section.

1.3 Existing theoretical and simulation approaches

Many theoretical, both analytical and simulational, studies have been carried out on many aspects of elastic response, yielding, strain softening, and strain hardening of glassy polymers. Already in 1968 Haward and Thackray [20] proposed a model considering the large-strain deformation of glassy polymers with the help of two separate processes. The first process is the deformation-rate-dependent plastic flow of polymer-chain segments, which can be described by an Eyring viscosity. The second process is related to the chain alignment resulting from the plastic-flow process and is modeled using a finite extendable Langevin spring. The Haward and Thackray model was further extended to a spatial 3-D description by Boyce, Parks and Argon [21]. In order to describe the plastic flow the BPA model takes into account the pressure dependence and a phenomenological description of intrinsic strain softening. The strain hardening was modeled by using the three-chain approach of Wang and Guth [22]. Later the modeling of strain hardening was improved by Arruda and Boyce [10] by using the more realistic eight-chain model. Another modification of the BPA model was considered by Wu and Van der Giessen [23], where the 3-chain model is replaced by a network.

Later contributions concern for example the approach as presented by Tervoort et al. [24]. They described the non-linear viscoelastic polymer behavior with the help of a compressible version of the Leonov fluid model [25], as originally proposed by Baaijens [26]. The Leonov model is a three-dimensional constitutive equation comprising an Eyring dashpot for non-linear visco-elastic behavior and a neo-Hookean spring for strain-hardening behavior. Govaert et al. [27] later added pressure dependence and (phenomenological) strain softening to this model.

Smit [28] was able to do the first multi-level micro-macro finite-element modeling, with large-strain micro-macro homogenization; a finite-element model of the microstructure (morphology) serves as a constitutive model for the calculations at the macroscopic scale. They were thus able to predict the global mechanical behavior of filled amorphous polymers under different loading conditions from their microstructure and microscopic properties.

These phenomenological models successfully describe the localization phenomena in polymers such as shear banding, necking, and crazing. It became clear that the strain localization is caused by the strain softening. An important new insight is that what matters is not so much the absolute value of the yield stress, but more the balance between the post-yield stress dip and the strain hardening [28]. Ultimately this balance between polymer strain softening and further hardening determines whether a material deforms macroscopically ductile or brittle.

All constitutive-modeling efforts resulted in constitutive models that do perform well; experimentally observed stress-strain behavior can, at least for simple geometries be reproduced for various polymers. The downside of these models, however, is that they are phenomenological. It is not revealed what are the molecular mechanisms at work during the

various stages of deformation, i.e., linear-elastic response, yield, strain softening and strain hardening. For example aging and rejuvenation are not very well understood. Rejuvenation is considered the opposite of aging because it has the opposite effect on strain softening, whereas experiments have shown that yielding does not rejuvenate the polymer material, but brings it to a different "equilibrium state". This last point of view is supported by modeling studies of Stillinger et al. [29] and Isner et al.[30]. What exactly happens in terms of structural evolution, during aging or rejuvenation, is still a big open problem. As regards strain hardening, one of the established viewpoints that the entropic response of a rubbery entanglement network is responsible here is problematic. The values of the strain-hardening moduli of polymer glasses are typically two orders of magnitude larger than the corresponding E-moduli in the rubber state; in addition the strain-hardening modulus is observed to decrease linearly with temperature, whereas entropic elasticity would predict a linear increase with temperature [31]. Which mechanisms are really responsible for the experimentally known values of strain-hardening moduli has not been unambiguously revealed. And as a consequence of these observations, what molecular processes underly the differences between chemically different polymers remains a puzzle.

For a proper understanding of the mechanisms at work at the molecular level during deformation of a glassy polymer, it is essential to understand the segmental dynamics, from the level of an atom to the level of multiple statistical segments (Kuhn segments, see [5, 32]) of polymers in the glassy state. Computer simulations and theoretical results [33, 34] provide direct evidence that the collective character of molecular motion is responsible for the slowing down of mobility in polymer glasses but conclusions are still made mainly on toy chain models. Although the cooperative dynamic behavior in the vicinity of the polymer glass transition appears to be a generic phenomenon, also polymer-specific chemistry plays an important role. The influence of details of the chemical structure of polymers on the collective segmental dynamics is not known.

The difficulty in establishing the nature of the molecular mobility lies in the complex polymer microstructure, giving rise to various types of interatomic interactions, and the many length and time scales characterizing polymer structure and dynamics. The possibility to carry out atomistic simulations of glassy polymers for realistic length and time scales has only become possible recently. Han, Gee and Boyd [35] demonstrated that molecular-dynamics (MD) simulation results for $V - T$ curves could be used to locate the volumetric glass-transition temperature T_g reliably for a rather large set of polymers. Their reproduced T_g values span a range of 200 K, from 170 to 370 K. Detailed atomistic simulation of the structural properties and segmental mobility in the vicinity of the glass transition in atactic polypropylene [36], amorphous polyethyleneterephthalate [37], atactic polystyrene [38] and many other results show reasonable agreement with experimental calorimetric data, X-ray scattering data, dielectric- and NMR-spectroscopy results.

Brown and Clarke [39] performed one of the first detailed MD computer simulations of an amorphous polyethylene-like polymer under uniaxial tension. They prepared initial samples of 1000 united atoms which after equilibration at melt temperature are cooled

down at a rate of 10^{12} K s⁻¹ and subsequently equilibrated for 1 ns. Thereafter uniaxial deformation was simulated with various tension rates (corresponding to deformation rates of the order of 10^9 s⁻¹). A loose-coupling constant-pressure molecular-dynamics simulation was carried out for times up to 1 ns. The simulated elastic deformation, yield and plastic flow at low temperatures show similarity with laboratory results obtained on time scales that are many orders of magnitude longer. This pioneering work was followed by many other contributions.

In the work of Brown and Clarke and to a lesser extent in later simulation work on glassy-polymer deformation, the time scales for cooling and deformation are many orders of magnitude larger than in experimental reality, which is a shortcoming of all molecular-simulation work on this topic. Still useful information can be extracted from these simulations. The reason is probably that, both in simulations and in experimental situations, the time scale of deformation lies in the same physical regime, namely the Rouse regime [5].

Various studies at the molecular level focussed on evolution of structure under deformation. MD simulation of the anisotropic mechanical properties of oriented amorphous polyethyleneterephthalate, PET, has been reported by Zhou et al. [40] up to a draw ratio $\lambda = 3.9$. Eight chains of PET consisting of only ten monomers each were first randomly packed into a rectangular box at $T = 300$ K. They were then uniformly deformed by constant NVT MD such that they end up as a cube. The observed rapid development of the benzene-rings orientation with deformation is in good agreement with the results of polarized infrared spectroscopy, but it should be noticed that the simulation cells develop orientation more rapidly than is seen in the experiment. The development of main-chain-bonds orientation in the direction of stretching was observed by Ogura and Yamamoto [41] in the MD simulation of a polymethylene melt.

In other deformation studies, using molecular simulation, segmental mobility issues have been addressed. An early example is the Brownian-dynamics work of Neelov, Darinskii and Clarke [42] for a toy-model single polymer chain in an external field of dipolar symmetry. This study reveals the significant change of the local segmental mobility under deformation. It was shown that the extension of the polymer chain proceeds in two stages. During the first stage the extension involves the redistribution of the coiled and extended rotational isomers along the chain, the overall conformational composition being retained. The extension during the second stage involves the transition of coiled isomers to extended isomers. It was shown that near the extended conformations (gauche-trans transitions), the local conformational mobility increases, whereas it decreases in the coiled conformation (gauche-gauche transitions). Later, Capaldi et al. [43] studied the behavior of a glassy PE-like polymer undergoing active compressive deformation by MD. They found that deformation increases the transition rate between different dihedral-angle states and promotes propagation of dihedral-angle flips along the chain.

Increased mobility under deformation has also been observed experimentally. Important in this context is the work of Loo, Cohen and Gleason [44], who observed, using solid-state

deuterium NMR, increased mobility of chains in the amorphous region of nylon 6 near its glass transition during active uniaxial elongation. The mobility increase was maximum at the yield point and decayed once the deformation was stopped. Comparable observations were done by Capaldi, Boyce and Rutledge [45] recently in MD simulations of a model glassy amorphous polyethylene in compression at a strain rate of 10^{10} s^{-1} . They found that deformation increases the transition rate between different dihedral-angle states and promotes propagation of dihedral-angle flips along the chain. This enhanced transition rate returns to the rate before deformation when active deformation ceases, in agreement with the NMR results of Loo et al.[44].

More recently, Lyulin et al. [46] showed that it was possible to simulate by MD both glassy atactic polystyrene and glassy bisphenol-A polycarbonate, using chemically realistic models, under uniaxial mechanical deformation, employing a deformation rate of 10^8 s^{-1} . The initial samples were cooled down from the melt at a speed of $5 \cdot 10^{10} \text{ K s}^{-1}$. It was shown that the simulated Young moduli, yield stresses and strain-hardening moduli were in fair agreement with existing experiments. An important observation is that the mobility of the PS segments in the deformation direction is increased drastically beyond the yield point. A weaker increase is observed for PC.

In summary, one observes that phenomenological constitutive models are quite successful in reproducing and predicting mechanical behavior of glassy polymers. However, proper explanations of phenomena like aging, rejuvenation and strain hardening are lacking. Molecular simulations are being used to obtain more insight in mechanisms at the molecular level. Most studies at the molecular level have focussed on evolution of structure and on changes in local mobility; in these studies molecular simulations are often used. The downside of molecular simulations however is that the accessible length and time scales are orders of magnitude smaller than typical experimental scales for glassy-polymer deformation. Despite all these efforts, many important questions regarding the characteristic features of typical stress-strain curves of glassy polymers and differences between chemically different polymers remain unanswered and a lot of work still has to be done.

1.4 Multi-scale modeling

One major obstacle in developing deep insights in mechanical behavior of polymer materials lies in their extremely broad range of length and time scales. Length scales cover a range from the typical size of chemical bonds, 1\AA , to the size of different phases in for example immiscible polymer blends, above $1\mu\text{m}$. The range of time scales is even many orders of magnitude wider and ranges from 10^{-14} s for bond vibrations to hours or more for structural relaxation in the glassy state.

To obtain a thorough understanding of polymer materials, their behavior at all length and time scales has to be investigated. This can not be achieved using just one experimental or

modeling technique. Such a technique does not exist. This is the reason that mechanical behavior of polymers is studied by employing a multitude of techniques, each suitable for different time and spatial windows.

At the macroscopic level of modeling, one has the top-down approach of continuum mechanics, where extensive use is made of advanced finite-element calculations based on phenomenological constitutive models, see the previous Section. At the other extreme is the molecular level, where a bottom-up approach should still be able to link with the synthetic chemistry that attempts to develop materials with better mechanical properties. The ultimate goal would be to relate these extreme levels. To make this possible, a scale-jumping approach between intermediate levels is essential. Multi-level finite element calculations, e.g. by Smit et al. [28], which enables the incorporation of morphology, form a first step beyond a pure continuum approach. One level more detailed, there exist various network models like the lattice-based model of entanglement networks at polymer interfaces of Terzis et al. [47–49], or the primitive-path analyses of various polymers in the melt by for example Everaers et al. [50] and Tzoumanekas et al. [51]. Below the level of entanglement networks, one gets to the level of molecular models, with various degrees of detail. The most coarse molecular models are bead-joint models, one joint representing typically a Kuhn segment; the most fine models are the atomistic models. In between there are the various coarse-graining levels, at which one coarse-grained particle is representing a small amount of atoms, typically less than ten.

Especially in molecular modeling knowledge exists how to establish links between different levels. This can be done by systematic coarse graining [52, 53], which results in model parameters that describe a physical system at a particular level and that are based on structural and dynamical properties of a model, of the same physical system, at a finer level.

Scale-jumping is especially advantageous in cases where one is interested in material behavior at both short length and time scales and at longer length and time scales. For example one can use simulation at a coarser level to evolve to a system at macroscopic length and time scales, and interrupt such a simulation to jump to a finer level, and obtain insight in how the system evolves at that level.

Finally, besides coarse-graining, other routes have been developed to have access to larger length and time scales, namely via advanced Monte Carlo (MC) algorithms; with such algorithms it turned out possible to explore larger parts of configuration space and calculate much more accurately equilibrium properties of polymer systems than in for example MD simulations, because MC algorithms use discrete jumps through configuration space, without having to follow the system's dynamics. Very important in this context is the work of Theodorou and coworkers [54, 55], who, in the second half of the nineties, introduced and developed an MC algorithm for the equilibration of PE in the melt. Their algorithm makes use of connectivity-altering MC moves; in this way the slowest dynamical processes, i.e., the Rouse motions associated with the lowest-order Rouse modes [5] and reptation motions

[5], could be circumvented. The first connectivity-altering MC technique that Theodorou et al. presented was the "end-bridging" (EB) technique; this method made the preparation of well-equilibrated long-chain (more than 100 monomer segments) PE in the melt possible for the first time.

1.5 Our project

The purpose of our project is to have access to a wider range of length and time scales, starting from the atomistic level, for polymers that are relevant in relation to the study of mechanical behavior, such as PS and PC. A wider range of length scales and time scales is important to simulate cooling from the melt and deformation in the glass. An additional very important aspect is to have well-equilibrated initial polymer melt structures, which are the input for cooling and deformation simulations. Preparation and equilibration of initial polymer samples in the melt, prior to cooling and deformation, is a non-trivial task, that does often not receive the attention it should get. Often a random-walk or self-avoiding-random-walk process is used to create an initial sample, sometimes followed by an energy-minimization step; finally MD simulation is used to equilibrate the sample. This procedure is insufficient to obtain polymer structures that are equilibrated on all scales, in particular on the scales relevant to entanglements and reptation motion.

The goal of our research was to develop connectivity-altering Monte Carlo methods for more complex polymers than PE, in particular for PS. This polymer has an A-B monomer structure, with A ($=\text{CH}_2$) and B ($=\text{CHC}_6\text{H}_5$) different chemical groups, also with large size differences. So for the development of connectivity-altering methods that should generate well-equilibrated structures, PS can be regarded as a good prototype.

Since the application of connectivity-altering techniques is not trivial the project started with a study on amorphous PE samples. An existing end-bridging Monte Carlo (EBMC) algorithm is used to obtain well-equilibrated PE samples in the melt. Subsequently we simulate PE under deformation, for this purpose MC with local moves is used; we estimate that one local move per particle in the system corresponds to a time interval of 10^{-13} s, enabling us to deform hundred times slower than in typical MD simulations of deformation. Insight is obtained from simultaneous study of structural properties and contributions of different interaction types to stress and energy, see Chapter 3. Furthermore a study, on the same and similar systems, has been devoted to a comparison of different ways to simulate deformation, and on how to deal with constraints such as fixed bond lengths, see Chapter 4.

As a next step, we generalize the existing EBMC algorithm for PE to an algorithm that is suitable for the equilibration of polymers which monomers can be modeled as two connected spherical particles of different size. The result is an algorithm for the equilibration of various polymers at a slightly coarse-grained level. The algorithm is demonstrated for PS, see Chapter 5. Subsequently atomistic detail can be reintroduced to obtain well-

equilibrated atomistically detailed structures; this is done for PS and the resulting structure is extensively compared to experimental data from literature in Chapter 6.

Finally, in Chapter 7, the well-equilibrated PS structures have been used in simulation of glassy polymer deformation and an elaborate comparison has been made with deformation of samples obtained from less sophisticated equilibration methods. Conclusions and suggestions for further research are given in Chapter 8.

Chapter 2

Molecular simulation methods for polymers

ABSTRACT

The basics of molecular-simulation methods are discussed, together with the state of the art in terms of accessible length and time scales. Subsequently an overview is given on existing molecular-simulation approaches to glassy-polymer deformation. In addition various methods for preparing well-equilibrated polymer samples are discussed. In the final Section our own approaches are explained in technical detail.

2.1 Molecular simulations of polymers: basic methods and state of art with respect to length and timescales

Computer simulation of physical processes in condensed-matter physics is regarded as the 'third way' of doing research, besides experiments and analytical theories. With more chemically-realistic models and ever increasing computer power, computer simulation of low-molecular-weight and polymer materials has become in the last half century a reliable and accurate tool to study physical processes at the molecular and atomic scales. The big advantages of computer simulations are their relatively low costs, compared to performing actual experiments, the possibility to investigate physical processes under conditions that cannot be easily realized in the laboratory (e.g. extremely high pressures or high temperatures), the possibility to "measure" properties that are difficult or impossible to measure in real experiments, and the option to artificially adapt the molecular reality to single out specific effects of interest.

The term "molecular simulation" refers to a group of simulation techniques in which physical systems consist of particles, representing (groups of) atoms, interacting via a force field [56, 57]. The particles are subjected to boundary conditions, defining the ensemble [58]; in this Chapter basic principles will be explained using the NVT ensemble, i.e. N particles in a simulation box of volume V at a temperature T . Furthermore there is a mechanism to generate microstates [58], defined by the positions and momenta of all particles in the system. From trajectories, i.e., sequences of microstates in time, observables can be calculated, as ensemble averages, using the statistical-mechanics formula:

$$\langle A \rangle = \frac{\int d\vec{p}^N d\vec{r}^N A(\vec{p}^N, \vec{r}^N) \exp[-\beta H(\vec{p}^N, \vec{r}^N)]}{\int d\vec{p}^N d\vec{r}^N \exp[-\beta H(\vec{p}^N, \vec{r}^N)]} \quad (2.1)$$

with A the observable, \vec{r}^N and \vec{p}^N the particle positions and momenta respectively, H the Hamiltonian of the system and $\beta = 1/k_B T$.

One common technique to generate microstates is Monte Carlo (MC), so called because of the role that random numbers play in the method. MC dates from 1953, when the first computer simulation of a liquid was carried out at the Los Alamos National Laboratories in the United States by Metropolis, Rosenbluth, Rosenbluth, Teller and Teller [59]. This very early work laid to the foundations of modern MC simulations. The precise technique employed in that study is still widely used, and is referred to as 'Metropolis Monte Carlo'. This technique is based on a clever way of calculating observables from microstates. In order to calculate observables one has to evaluate the integrals in Equation 2.1. In general this has to be done numerically. Simple numerical quadrature is not feasible for this purpose [57]. Also random sampling of the integrands is not a good idea, since most computing

time is spent in regions where Boltzmann's factor is negligible. The key idea of MC is to devise a scheme in which the chance $N(o)$ to sample a particular microstate o relative to the chance $N(n)$ to sample another microstate n equals the ratio $\exp[-\beta(U(o) - U(n))]$ of their Boltzmann weights. As a consequence, the unweighed average of the observable A measured in the various microstates gives an estimate for $\langle A \rangle$.

An MC simulation is a repetition of *moves*, of a simulated system, from one state to another. The probability $\pi(o \rightarrow n)$ of going from one (old) state o to another (new) state n , must satisfy the condition that equilibrium once reached is not disturbed. That is, the probability to leave state o should be equal to the probability to enter it from another state. A stronger, more simple criterion, known as the detailed-balance condition, states that the number of transitions ($o \rightarrow n$) equals the number of transitions ($n \rightarrow o$):

$$N(o)\pi(o \rightarrow n) = N(n)\pi(n \rightarrow o) \quad (2.2)$$

To be more precise, a MC move consists of two stages. In the first stage a trial move is performed from state o to state n with a probability $\alpha(o \rightarrow n)$, in the second this move is accepted with a probability $\text{acc}(o \rightarrow n)$. In case α is symmetric ($\alpha(o \rightarrow n) = \alpha(n \rightarrow o)$), Equation 2.2 can be reduced to:

$$N(o)\text{acc}(o \rightarrow n) = N(n)\text{acc}(n \rightarrow o) \quad (2.3)$$

so that:

$$\frac{\text{acc}(o \rightarrow n)}{\text{acc}(n \rightarrow o)} = \frac{N(n)}{N(o)} = \exp(-\beta[U(n) - U(o)]) \quad (2.4)$$

To satisfy this condition Metropolis used:

$$\text{acc}(o \rightarrow n) = \begin{cases} \frac{N(n)}{N(o)} = \exp(-\beta[U(n) - U(o)]) & N(n) < N(o) \\ 1 & N(n) \geq N(o) \end{cases} \quad (2.5)$$

In case of non-symmetric α one could obviously use:

$$\text{acc}(o \rightarrow n) = \begin{cases} \frac{N(n)\alpha(n \rightarrow o)}{N(o)\alpha(o \rightarrow n)} & N(n)\alpha(n \rightarrow o) < N(o)\alpha(o \rightarrow n) \\ 1 & N(n)\alpha(n \rightarrow o) \geq N(o)\alpha(o \rightarrow n) \end{cases} \quad (2.6)$$

MC is used mainly to obtain information about equilibrium properties. To obtain the dynamic properties of many-particle systems, it is usually the molecular-dynamics technique that is preferred. Molecular dynamics (MD) is based on obtaining the time evolution of a system by integrating the classical equations of motion (Newton's equations). A suitable integration scheme is the Verlet scheme:

$$\vec{r}(t + \Delta t) = 2\vec{r}(t) - \vec{r}(t - \Delta t) + \frac{\vec{f}(t)}{m}\Delta t^2 + O(\Delta t^4) \quad (2.7)$$

Velocities are obtained from:

$$\vec{v}(t) = \frac{\vec{r}(t + \Delta t) - \vec{r}(t - \Delta t)}{2\Delta t} + O(\Delta t^2) \quad (2.8)$$

The first MD simulation was accomplished by Alder and Wainwright [60, 61] for a model liquid made of hard spheres. For that system, the particles move at constant velocity between perfectly elastic collisions, and it is possible to solve the dynamic problem without making any approximations, within the limits imposed by machine accuracy. It took several years before a successful attempt was made to solve the equations of motion for a set of particles interacting via the Lennard-Jones potential [62]. For that system, an approximate, step-by-step procedure is needed, since the forces change continuously as the particles move.

Computer simulations are usually performed on a small (of the order of $N 10^4 - 10^5$) number of molecules or atoms. The size of the simulated system is limited mainly by the speed of execution of the program. For the case of pair potentials used to describe inter-particle interactions the time needed to evaluate the forces or the potential energy is proportional to N^2 . Special techniques, such as the use of Verlet lists [63] or cell lists [64], may reduce this dependence to $O(N)$, but the force/energy calculation almost inevitably dictates the overall speed, and, clearly, smaller systems will always be less expensive computationally.

A major obstacle for the simulation of bulk liquids or melts is the large fraction of molecules that lie on the surface of a small simulation sample; these molecules on the surface will experience quite different forces than molecules in the bulk. This problem of surface effects can be overcome by implementing periodic boundary conditions. The simulation box is replicated throughout space to form an infinite lattice, see Figure 2.1. In the course of the simulation, as a molecule moves in the original box, its periodic image in each of the neighboring boxes moves in exactly the same way. Thus, as a molecule leaves the central box, one of its images will enter through the opposite face. As will be shown in the following chapters these periodic boundary conditions should be properly taken into account when studying the stress-strain properties for melts of long polymer chains.

Computer simulation of long polymer molecules in the condensed state faces a few funda-

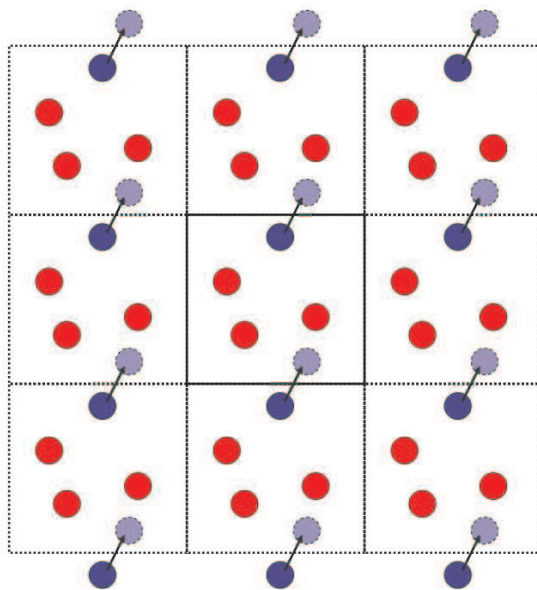


Figure 2.1: To remove surface effects in a simulation, periodic boundary conditions are being used. That is, the simulation box is continued periodically.

mental challenges that are related to the existence of polymer segmental-relaxation processes on different time scales, spanning 13-14 decades, from picoseconds to tens or hundreds of seconds, and length scales ranging from angstroms to tens of nanometers. One consequence is that the preparation of equilibrated polymer structures, which should provide a good starting point to any molecular simulation, is a non-trivial task. Furthermore it is difficult to sample large parts of phase space and calculate reliable values for observables, because the available CPU time is often not sufficient to affect the system on the largest length scales. Finally, for the same reason, it is not feasible to study the dynamics of the slowest processes in polymers. Given the intrinsic problems of molecular simulation, nowadays it is possible to simulate, using MD, a system of the order of $N = 10^3$ particles for 100 ns using one CPU (e.g. one Intel Itanium 2 processor (1,3 GHz, 3 Mbyte cache) on an SGI Altix 3700 system) for one week.

Despite the limitations of molecular-simulation techniques lots of successes have been obtained with them in polymer science. Molecular-simulation methods have been applied to virtually any physical system involving polymers; applications include polymers in the melt, in the rubbery state, in the glassy state and in a solution; to bulk material, thin films and interfaces; to homopolymers, copolymers and blends, and more. [65–67]. So the limitations of conventional molecular-simulation techniques, even using a single-processor machine, do not render them useless. However there is a lot to gain. To simulate larger systems for longer times two routes can be pursued, either the one of parallelization or the one of coarse graining. An example of parallelization is to run a number of similar systems

simultaneously, which is good to improve estimates for static properties or short-time dynamical properties of a simulated system. To enable the extension of the time frame of the simulation, in order to study long-term dynamical behavior, domain decomposition [68–70] is a suitable technique. This technique results in a scaling of CPU-time with almost $1/P$, P being the number of CPUs available to a particular molecular-simulation job. Coarse graining means a reduction in the number of degrees of freedom and thereby an increase in the typical length and time scales of description; this enables the simulation of larger systems. Typically the number of particles is reduced by one order of magnitude. In addition, coarse-grained potentials are much softer than atomistic potentials, so larger time steps can be used. Usually the time step is increased by a factor of 10–100. Finally, another option if one is purely interested in the static properties of a system, is to apply advanced MC moves such as in the connectivity-altering methods [54, 55, 71, 72]. In Section 2.3 more elaborate information is given on these MC techniques.

2.2 Molecular simulation of polymer mechanical deformation

To simulate glassy-polymer deformation, almost all existing molecular-simulation techniques have been applied, albeit some with more success than others. In most studies MD has been used, but MC, Brownian Dynamics (BD) and energy-minimization approaches have been employed as well. In this Section MD, energy minimization and MC techniques, respectively, are discussed.

In one of the earliest MD approaches to polymer deformation, by Brown and Clarke [39], an external-pressure tensor \mathbf{P}^0 is prescribed. A glassy polymer system is coupled to this pressure tensor by allowing the size and shape of the system, represented by a matrix \mathbf{h} made up of basis vectors \vec{a} , \vec{b} and \vec{c} , to respond to imbalances between internal-pressure tensor \mathbf{P} and \mathbf{P}^0 :

$$\dot{\mathbf{h}} = \frac{\mathbf{P} - \mathbf{P}^0}{M} \quad (2.9)$$

in which M is an empirically chosen coupling constant. Similarly to the "loose-coupling method" introduced by Berendsen et al.[73], all monomer positions are scaled affinely with \mathbf{h} . Using this method, the equations of motion become:

$$\dot{\vec{r}}_i = \mathbf{h}\dot{\vec{s}}_i + \dot{\mathbf{h}}\vec{s}_i = \frac{\vec{p}_i}{m_i} + \dot{\mathbf{h}}\mathbf{h}^{-1}\vec{r}_i \quad (2.10)$$

in which scaled coordinates $\vec{s}_i = \mathbf{h}^{-1}\vec{r}_i$, with \vec{r}_i the position of the i^{th} monomer, have been used. The two contributions to the motion are integrated separately. The first term is integrated using a standard Verlet scheme; integration of the second term gives:

$$\vec{r}_i(t + \Delta t) = \mathbf{h}(t + \Delta t)\mathbf{h}^{-1}(t)\vec{r}_i(t) \quad (2.11)$$

Note that the result of this method is not that the whole sample evolves in an affine way; this is prevented by the first term in the equation of motion.

Brown and Clarke use this method to simulate the uniaxial tension of an amorphous polyethylene-like polymer. They prepare initial samples of 1000 united atoms which after equilibration at melt temperature are cooled down at a rate of 10^{12} K s⁻¹ and subsequently equilibrated for 1 ns. Thereafter uniaxial deformation is simulated with various tension rates dP_{xx}^0/dt (corresponding to deformation rates of the order of 10^9 s⁻¹). The simulated elastic deformation, yield and plastic flow at low temperatures show similarity with laboratory results obtained on time scales that are many orders of magnitude longer. The

method of Brown et al. is later also used by for example Ogura et al. [41]. They deform adiabatically at a rate of 10^{10} s^{-1} . They obtain very pronounced orientation of local chain segments in the direction of active deformation, and extremely pronounced density fluctuations are observed; a Poisson ratio below 0.1 is observed, whereas typical experimental values are of the order 0.30-0.35. With this deformation rate, apparently the polymer can not relax its density.

In later MD approaches [43, 45, 46] often strain is prescribed instead of an external pressure field. In this case the positions of monomers are rescaled every time step Δt by a factor $\frac{x_i}{L}\dot{L}\Delta t$, with x_i the component of the position vector in the direction of deformation, L the box size and \dot{L} the deformation velocity. Using prescribed-strain MD, Capaldi et al. [45] simulated uniaxial compression, employing a strain rate of 10^{10} s^{-1} , of a polymer glass; during deformation, an enhanced transition rate between different dihedral-angle states and propagation of dihedral-angle flips along the polymer backbone were observed. Lyulin et al. [46] performed uniaxial-tension simulations of PS and PC at a strain rate of 10^8 s^{-1} and found a fair agreement of E-moduli, yield-stresses and strain-hardening moduli with experiments, albeit at cooling and deformation rates that are orders of magnitude larger than in experiments; furthermore an increased segmental mobility beyond the yield point has been observed for both polymers, and the effect is the most pronounced for PS.

There is no reason to state that prescribed strain is better than prescribed stress. Prescribing strain may be the most logical choice if one aims at simulating uniaxial deformation, which is experimentally done by controlling the strain; in prescribed-stress simulations one has only indirect control over the strain. In other situations, for example if a creep process is simulated, prescribing stress has the preference.

Also energy-minimization routes have been followed, e.g. by Mott et al. [74] and by Utz et al. [75]. These approaches consist of a repetitive application of strain increment followed by an energy-minimization procedure. Although the absence of temperature may not resemble experimental reality (room temperature), this approach enables one to study the separate influence of deformation on structural relaxation processes.

As mentioned, MC techniques have been applied to deformation of glassy polymers as well. Lattice-based and continuum polymer models can be distinguished. In the lattice-based MC simulations, deformation is often incorporated as an additional term in the system's Hamiltonian. This can be done by adding a term corresponding to a bulk force, which could be implemented as:

$$H_{deform} = - \sum_{i=1}^N |\vec{F} \cdot (\vec{r}_i - \vec{R}_0)| \quad (2.12)$$

where N is the number of monomers in the system, \vec{F} the force exerted on the sample, \vec{r}_i the position of monomer i and \vec{R}_0 the origin of the coordinate system, which is chosen

as the original center of mass of the sample, prior to deformation. This approach was followed for example by Ospina et al. [76, 77] in their 2D lattice simulation of glassy-polymer deformation. Although simple, the method gave reasonable results; one observes qualitatively correct temperature and strain-rate dependence for example and slight alignment of polymer chains with the direction of the force. Alternatively a surface force can be incorporated. Hölzl et al. [78] did so in their simulation of uniaxial deformation of an initially cubic sample. They used a 3D version of the bond-fluctuation model (BFM), invented by Carmesin et al. [79] and extended to 3D by Deutsch et al. [80], and adequate MC moves for this model were used. Tensile normal forces on two diametrically opposite boundaries of the sample were realized by coupling the monomers at those boundary surfaces to harmonic springs, see Figure 2.2. The deformation term in the Hamiltonian then became:

$$H_{deform} = c \sum_{i=1}^{2n} (r_{x,i} - R_{x,i}^s)^2 \quad (2.13)$$

in which c represents a spring constant, $r_{x,i}$ and $R_{x,i}^s$ are the x -components of the position of boundary monomer i and the position of the minimum of the potential of spring i , respectively, and n is the number of springs per boundary layer. Deformation is performed stepwise by discrete shifts to the left (right) of the minima of the spring potentials, for the springs at the left (right) side of the sample; after each step the system is relaxed for a number of Monte Carlo steps (MCS), where one MCS corresponds with the number of attempted Monte Carlo moves being equal to the number of monomers in the system. Using their method, which is very efficient, Hölzl et al. have access to larger time windows than typical for the MD methods discussed earlier. They are able to simulate for 10^7 MCS, corresponding to deformation rates of 10^{-5} s^{-1} to 10^{-6} s^{-1} ($1 \text{ MCS} \equiv (10^{-12}-10^{-13}) \text{ s}$ [81, 82]). There are problems however: the Poisson ratio does not exceed 0.15 (experimental values are 0.30-0.35) and pronounced voids are observed; large structural effects in terms of bond orientations and chain elongations are observed near the system boundaries where the forces are applied, whereas in the central region, in between the boundaries on which the forces work, no such structural effects are seen at all.

MC in combination with continuum models has also been used, by for example Chui et al. [9] and Li et al. [83]. Chui et al. use, in order to simulate a cross-linked polymer network, a repetition of affine strain increments ($\vec{r}_{i,new} = \vec{r}_{i,old} + \frac{x}{L} \Delta L \vec{e}_x$, where $\vec{r}_{i,new}$ and $\vec{r}_{i,old}$ are the positions of monomer i before and after a strain increment ΔL , L the size of the initially cubic box and x the component of $\vec{r}_{i,old}$ in the direction of deformation \vec{e}_x), followed by a number of MCS for relaxation. Deformation methods involving simple shifting of the boundaries of the simulation box require many relaxation steps ($\gg 100$ MCS) for artificially sparse or dense regions caused by the displacement of boundaries to diffuse through the system. Chui et al. use strain increments $\Delta L/L = 2.5 \cdot 10^{-3}$ and 100 MCS in between strain increments, giving a deformation rate $2.5 \cdot 10^{-5} \text{ MCS}^{-1}$, which

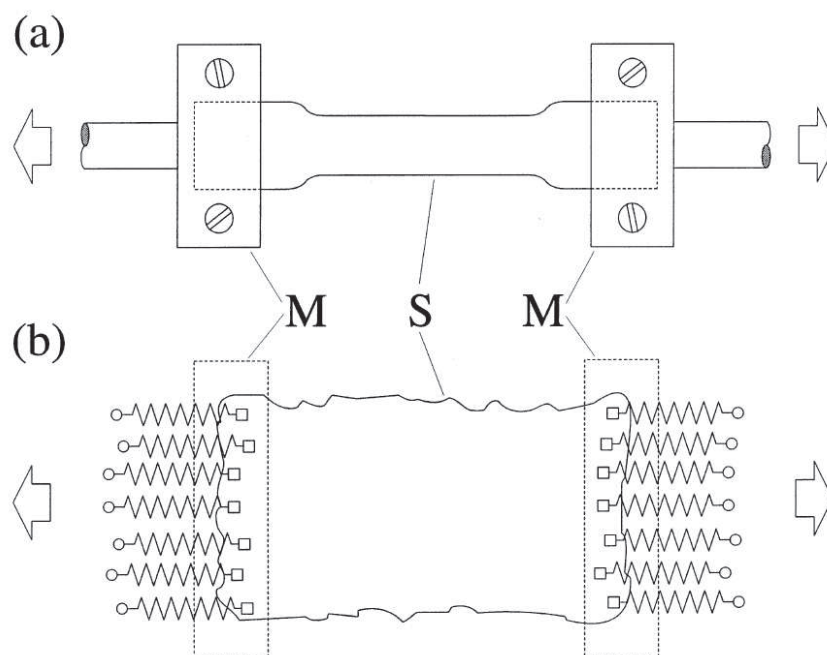


Figure 2.2: Polymer sample in a uniaxial tensile test (a) and its equivalent in a BFM simulation (b). The tensile forces acting on two surfaces opposite to each other are modeled using harmonic springs attached to the monomers close to those surfaces. Reprinted from Hölzl et al.[78]

they estimate to correspond to $10^8 - 10^9 \text{ s}^{-1}$. They obtain a realistic density evolution, qualitatively correct stress-strain relations and dependencies of stress-strain relations on temperature and strain rate, and finally they are one of the first to obtain insight by looking at the contributions of different interactions to stress and energy.

In summary one may conclude that most available molecular simulation methods can be helpful in unraveling the molecular mechanisms responsible for the typical features observed in deformation of glassy polymers. In general methods in which affine deformation is prescribed or in which bulk forces are applied are strongly preferred over techniques where only sample boundaries are displaced or in which surface forces are used to effect deformation. Finally, lattice-based models may be often too simple to incorporate all chemical details and polymer specific interactions and may therefore be inadequate comparing different polymers on their mechanical behavior.

2.3 Equilibration of condensed polymer systems - an overview

To create well-equilibrated initial polymer samples in the melt, for subsequent use in computer simulations, many methods have been proposed in literature. Only a few of them are discussed here, since other methods are often based on similar principles. Particular attention is given to the so-called end-bridging Monte Carlo, which is an example of a connectivity-altering MC method, since this technique is applied throughout this thesis work.

2.3.1 Approaches to equilibration of condensed polymers

McKechnie et al. [84] compare two methods of generating dense polymer melts. The first is chain growth including excluded volume (EV) and the second is phantom-chain growth (PCG) followed by the introduction of excluded volume. In both methods samples are grown chain-by-chain and atom-by-atom in a periodic box. In the EV method new atoms are added as follows: a new trial position for an atom to be added is based on the three previous atoms in the chain, the equilibrium bond length, the equilibrium bond angle and a randomly chosen dihedral. The total energy change $\Delta\Phi$ associated with adding the new atom is calculated. Subsequently, to decide on whether to accept or reject the trial position for the atom to be added, the corresponding Boltzmann factor is compared to a random number between 0 and 1. Important now is that in the calculation of $\Delta\Phi$, apart from the energy of the new dihedral angle, also all excluded-volume interactions are taken into account. The important downside of this method is that there is an increasing discrimination against trans states as the growth proceeds. The reason is the following: in the beginning of the chain-growth process there are no excluded-volume effects and the dihedral angle distribution is dictated by the relative energies of the trans and gauche states. As the growth proceeds, the growing chain hits more often upon already occupied space and needs to change its growth direction by adopting a gauche conformation for the dihedral associated with the last atom added.

In the PCG method it is assumed, after Flory [32], that successive torsion angles in a chain occur with a probability which is related to immediately adjacent torsion angles only. Long-range Van der Waals interactions are ignored, except between atoms separated by less than three other atoms, to take into account the "pentane" effect (Certain combinations of consecutive dihedrals in a polymer chain are highly improbable, since these would induce very strong excluded-volume interactions. By taking into account the relevant excluded-volume interactions in the generation process, these highly improbable combinations of dihedrals can be prevented.). This approach considerably reduces the occurrence of unlikely torsion pairs. The method inevitably leads to spatial overlaps between atoms, which have to be relaxed in subsequent MD simulations. Immediate introduction of the full Lennard-

Jones potential would result in a crash of the MD simulation due to diverging forces for very small interatomic distances. Moreover the chain conformations created in the previous step would be distorted. To relax the overlaps, initially the repulsive part of the Lennard-Jones potential is replaced by a weaker potential. This weaker potential is gradually turned into the full Lennard-Jones potential.

Methods based on first generating reasonable initial-chain conformations and then enabling local relaxing of the structures, such as the PCG method of Brown and Clarke and similar methods, can be unfeasible for polymers containing large monomer units [85]. A method to prepare well-relaxed glass structures of polymer consisting of bulky monomers was introduced by Khare, Paulaitis and Lustig [86] in 1993. Actually it concerned an extension of the technique of Rigby and Roe [87], who prepared systems of short-chain alkanes by "polymerizing" monomers placed randomly in a simulation box.

The approach consists of three stages: (1) placing monomers on random positions in the simulation box, (2) connecting monomers to create polymers and (3) minimizing the energy, locally, to obtain well-relaxed polymer glass. In stage (1) monomers are first placed on a regular array in the simulation box. Subsequently the system is relaxed at elevated temperature by MD, in order to achieve a uniform spatial distribution and a random orientational distribution of the monomers in the simulation box. In the second stage monomers are connected to obtain polymers of the desired degree of polymerization. Subsequently, the chains are subjected to a procedure in which the sequence of monomers in the chains is modified iteratively in order to form the shortest polymer chain. The result is polymers with bond lengths and bond angles that are far from equilibrium. This problem is tackled in the last stage, where the potential energy is minimized using a combination of energy minimization and molecular dynamics at elevated temperature.

Unfortunately the equilibration stages in the methods discussed up to now do not guarantee the correct chain statistics. Both deviations from a Gaussian coil conformation [32] and incorrect distributions of dihedral angles occur. Kotelyanskii et al. [88] came up with a way to generate atomistic amorphous polymer structures starting from configurations on a lattice. Their method guarantees Gaussian chain statistics and enables control over chain tacticity and monomer sequence. Severe overlaps in the initial stage of preparing the polymer structures are avoided.

In some more detail, the approach starts with self-avoiding walks on a cubic lattice, occupying all lattice sites in order to have a uniform spatial distribution. The trajectories of these walks become the chain backbones, which are then decorated by atoms according to the specific chemical structure of the polymer. First the lattice sites connected along the chain contour are populated with building blocks containing the atoms of the monomer unit. Subsequent proper placement and orientation of atoms within the building blocks simultaneously avoids overlaps and minimizes, to some extent, distortions in bond lengths and valence angles. Of course some equilibration is still required afterwards.

Müller, Nievergelt, Santos and Suter [89, 90] developed the PolyPack algorithm to generate

polymer structures with the experimental density, fulfilling pairwise torsional distributions in agreement with probabilities from RIS theories [32, 91] and avoiding atomic overlap. In their approach polymer packing is treated as a geometric optimization problem. Bond angles and bond lengths are considered constant. Torsion angles are considered the only degrees of freedom (besides the overall molecular position parameters). The PolyPack algorithm is able to find sets of torsional angles for which: (1) a prescribed density is obtained, (2) hard-sphere overlaps are prevented, and (3) (pairwise) distribution of torsion angles approaches the distribution given by RIS models [32, 91].

Starting point of the algorithm is a polymer structure with polymer chains obeying RIS statistics [32, 91], at a prescribed density. Torsional angles of this structure are optimized in a random order as follows. After an angle Φ has been chosen, the set of available RIS states D involving this angle is systematically checked. For each conformation D both a function $cost(D, ..)$, related to bead overlap, and the RIS probability $prob(D, \Phi)$ are evaluated. Subsequently, all values of Φ that yield values of function $cost(D, ..)$ exceeding a certain preset threshold c_{goal} are rejected. Finally one of the remaining Φ -values is picked according to its probability $prob(D, \Phi)$. If none of the states D yields $cost(D, ..) < c_{goal}$, then the state giving the lowest value of $cost(D, ..)$ is selected.

With this method it turned out to be possible to generate dense conformations of atomistic PS that correspond to large extent to experimental statistical data and that largely preserve these properties during subsequent MD simulations.

Auhl et al. [92] studied several methods that start off from an ensemble of chains with the correct end-to-end distance arranged randomly in the simulation cell. Subsequently excluded volume has to be introduced. In one procedure, often used to prepare melt configurations, the excluded-volume interactions are introduced rapidly (on a timescale in the order of the fastest Rouse modes [5]). This is termed fast push-off. A result of this procedure is that, at short length scales, polymer chains exhibit deformations (overstretching), which only vanish after chains have moved their own size.

To prevent these local deformations, alternative procedures are needed. In one alternative, the chains that have been randomly arranged in the simulation cell are first subjected to a prepacking procedure, in which density fluctuations are strongly reduced. Subsequently, excluded-volume interactions are introduced slower (at the time scale of Rouse modes involving N_d polymer segments, N_d being the maximum range on which polymers are deformed during fast push-off) than in the first method. In addition, full 1-5 excluded-volume interactions, i.e., excluded-volume interactions between segments separated by four other segments, are taken into account during the whole process. Finally there is another alternative, in which double-bridging moves [92] are used.

2.3.2 End-bridging Monte Carlo

A completely different strategy to generate a well-equilibrated condensed polymer system is the application of connectivity altering, i.e., addition and removal of chemical bonds. Theodorou et al. [54, 55, 93] came up with an MC algorithm in which a number of different types of MC moves is employed, one type being a connectivity-altering move called end-bridging (EB) move. With this technique, large displacements of the polymer system in configuration space [58] are very feasible in terms of CPU-time requirements. This has two very pleasant consequences. The first is that, almost regardless of the position in configuration space at which the MC run starts, the polymer system will quickly evolve to a very probable state, i.e., near equilibrium. The second result is the ability to calculate reasonable estimates of observables in the simulation. After all, the system is navigated through configuration space, thereby visiting the most probable states, which is inherent to any MC method. At the time this thesis is written, for a polymer-melt system of the order of 10^4 particles and an average chain length of the order of a few hundred particles, configuration space can be fully sampled in one or two week's time, using one Intel Itanium 2 processor (1,3 GHz, 3 Mbyte cache) on an SGI Altix 3700 system.

In the remainder of this Section, the EB method will be explained for a model system, resembling polyethylene (PE), consisting of spherical beads connected in linear chains, all beads being of the same type. For more complicated polymers, the philosophy of the method remains the same, however there are many practical issues to be dealt with. In Chapter 5, the implementation of the method for coarse-grained polymers, in which one monomer is represented by two beads, is explained.

Procedure

During an EB move, see Figure 2.3, two melt chains are selected so that the end of one of those chains is within a certain bridgeable distance from a backbone segment of the other. A trimer (i, j, k) , centered at this latter backbone segment, is excised from the second chain, thus defining two sub-chains. The end of one of these sub-chains is connected to the end of the first chain by constructing a bridging trimer (i', j', k') , forming a new chain with prescribed molecular geometry (bond lengths and bond angles). Clearly, the EB move alters the lengths of chains participating in it. To control the chain-length distribution, chemical potentials are defined for all chain lengths.

In more detail the procedure works as follows. A chain end p is selected at random, and in addition an atom in another chain is selected at random from a list of proximate atoms; to be precise those atoms which are within a range, from the chosen chain end, that can be bridged by the trimer. This so-called bridgeable distance equals $4l_0 \sin(\theta_0/2)$, with l_0 the equilibrium bond length and θ_0 the equilibrium bond angle. As an extra check, after

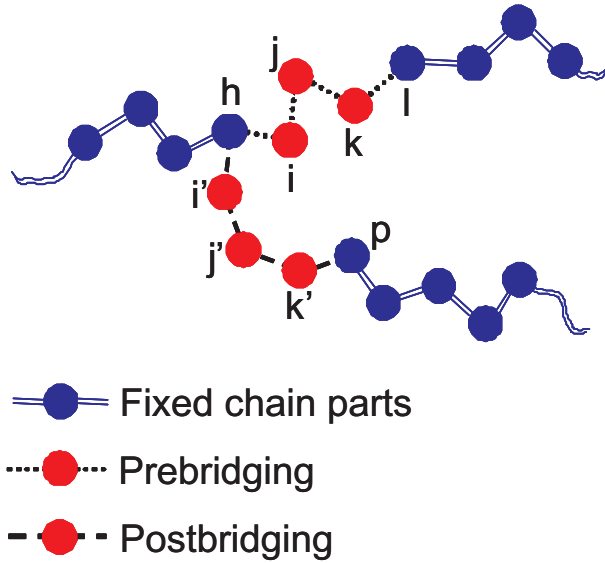


Figure 2.3: The end-bridging move displayed here is a connectivity-altering MC move, in which a trimer (i, j, k) is excised from one chain, and reused to connect one of the two parts of the chain resulting after the excision to the chain end p of another chain. The trimer in its new position is given the label (i', j', k') .

a chain end and a bridgeable neighbor have been picked, it is always verified whether the distance between them is bridgeable.

The next step is to find the solutions to the problem, termed the geometrical-bridging problem [54, 55], of finding the positions $(\vec{r}_{i'}, \vec{r}_{j'}, \vec{r}_{k'})$ of the trimer atoms fulfilling the requirement that all bond angles and all bond lengths involving the trimer, have predefined values; a practical choice is to put all those bond angles equal to θ_0 and all bond lengths equal to l_0 . Subsequently, all solutions are subjected to two tests for quick rejection. In the first test the torsional energy change ΔE_{tor} is calculated and compared to a preset maximum increase $\Delta E_{tor,max}$; all solutions for which $\Delta E_{tor} > \Delta E_{tor,max}$ are not considered anymore. The second test concerns the removal of all solutions which result in hard-sphere overlaps of non-bonded atoms, i.e., solutions resulting in a distance, between atoms in different chains or atoms in the same chain but separated by at least three chemical bonds, smaller than some predefined value $R_{overlap}$. From the remaining solutions one is chosen with a probability $\alpha_{tor}(m \rightarrow n)$:

$$\alpha_{tor}(m \rightarrow n) = \frac{\exp(-E_{tor}(n)/k_B T)}{\sum_{n'=1}^{N(n)} \exp(-E_{tor}(n')/k_B T)} \quad (2.14)$$

where m and n represent the states of the system before and after the EB move, and $N(n)$ represents the number of solutions after quick rejection.

After choosing a solution n , this solution has to be subjected to a final Metropolis acceptance procedure. To guarantee detailed balance, a number of factors regarding the forward move ($m \rightarrow n$) and the reverse move ($n \rightarrow m$) have to be incorporated in this acceptance test. The first ingredients are the Boltzmann factors $\exp(-E_m/k_B T)$ and $\exp(-E_n/k_B T)$ associated with states m and n . In addition, the chance $1/N_{bridge}(p)$ has to be taken into account that upon end-bridging from chain end p , see Figure 2.3, a particular bridgeable atom h is chosen and the chance $1/N_{bridge}(l)$ that in the reverse move upon end-bridging from chain end l again atom h is chosen. Furthermore, both the probability $\alpha_{tor}(m \rightarrow n)$ for selecting a trimer-bridging solution m for the forward move ($m \rightarrow n$) and the probability $\alpha_{tor}(n \rightarrow m)$ for selecting a trimer-bridging solution n for the reverse move ($n \rightarrow m$) must enter into the Metropolis acceptance criterion. The last issue to deal with is the fact that in the procedure to solve the trimer-bridging problem use is made of coordinate transformations from a Cartesian coordinate system to a coordinate system using constrained coordinates, see refs [55, 94]. In this constrained coordinate system the problem is actually solved. The solution is finally transformed to Cartesian coordinates again. This procedure effects that some regions are more intensely scanned for solution of the trimer-bridging problem than other regions. To correct for this, Jacobian determinants associated with these coordinate transformations, $J(n)$ for the forward move and $J(m)$ for the reverse move, have to be incorporated in the acceptance as well. Taking all these factors into account, the probability $P(m \rightarrow n)$ for going from state m to state n equals:

$$P(m \rightarrow n) = \min \left[1, \frac{\frac{1}{N_{bridge}(l)} \alpha_{tor}(n \rightarrow m) \exp(-\frac{E_n}{k_B T}) J(n)}{\frac{1}{N_{bridge}(p)} \alpha_{tor}(m \rightarrow n) \exp(-\frac{E_m}{k_B T}) J(m)} \right] \quad (2.15)$$

in which $N_{bridge}(l)$ is the number of bridgeable neighbors from chain end l .

Practical aspects

To make the EB algorithm efficient, many lists are used. First of all there are lists containing connectivity information, such as a list with the number of atoms per chain, a list containing the number of the chain and the position within that chain for every atom in the system, and a list containing, for any position in any chain, the number of the atom at that position. These lists have to be updated after every accepted EB move.

Another list, the "overlap list", is created by dividing the sample in cubic cells of size $\sigma_{LJ}(1 + \delta)$, where σ_{LJ} is the length parameter of the Lennard-Jones potential and $0 < \delta \ll 1$, and allocating all atoms in the system to one of those cells. This list is used to quickly reject attempt moves that result in excluded-volume overlaps. As a complement to this list, there is a list giving for any atom the number of the cell in which it is contained.

A third list is the "linked-cell list". This list is created by dividing the system into cells of size $R_{cutoff}(1 + \Delta)$, where R_{cutoff} is the Lennard-Jones cutoff radius and Δ defines a skin

layer [57]. All atoms are allocated to one of those cells again; there is also a list containing for any atom in the system the linked cell in which it resides.

A final important list, which was already briefly mentioned, is the "end-bridging list", which contains, for each chain end, all candidate atoms in other chains to which the chain end can be attached using a trimer bridge. The criterion is that candidate atoms must be internal atoms of another chain within the all-trans bridging distance $4l \sin(\theta/2)$ of a particular chain end, with l the bond length and θ the bond angle. For each chain c the number of bridgeable neighbors $N_{bridge}(c)$ is administrated, since it is a necessary ingredient to the acceptance criterion, see above.

Control over molecular weight distribution

Obviously an EB move could easily result in two chains with different molecular weights than the original two chains, before the move. However, there is a means to exert control over the molecular weights via the chemical potentials for different particles, i.e., polymer chains with different molecular weights, present in the system.

The physical system dealt with in an EB Monte Carlo simulation is an $NnpT\mu^*$ ensemble, where N is the number of chains, n the number of monomers, p the pressure, T the temperature and μ^* a spectrum of reduced chemical potentials, associated with the different chain lengths k , which can be related to the normal chemical potentials μ_k . In case of the more simple μVT ensemble, one has to treat the normal chemical potentials as natural variables. However, in the EB simulations considered here, the constraints that the number of chains N and the number of monomers n in the system are conserved have to be taken into account. Therefore two additional chemical potentials $\mu^{(N)}$ and $\mu^{(n)}$ associated with N and n have to be introduced, and, simultaneously, two arbitrarily chosen components i and j have to be eliminated then. The reduced chemical potentials are related to the normal ones as:

$$\mu_k^* = \mu_k - \left(\frac{k-i}{j-i}\right)\mu_j - \left(\frac{k-j}{i-j}\right)\mu_i \quad (2.16)$$

and the chemical potentials $\mu^{(N)}$ and $\mu^{(n)}$ are given by:

$$\mu^{(n)} = \frac{\mu_i - \mu_j}{i - j} \quad (2.17)$$

$$\mu^{(N)} = \frac{i\mu_j - j\mu_i}{i - j} \quad (2.18)$$

The partition function \tilde{Y} for this ensemble can be derived by using the relations between

the $NnPT\mu^*$ ensemble and the canonical ensemble NVT , with $\mathbf{N} = \{N_k\}$, N_k being the number of particles of type k (here the number of chains of length k monomers), and V the volume. The thermodynamic potential A of the NVT ensemble, i.e., the Helmholtz free energy, and the thermodynamic potential Y for the $NnPT\mu^*$ ensemble, can be related via Legendre transforms [58]:

$$Y = A - \sum_{k=1, k \neq i, j}^m \mu_k^* N_k + pV \quad (2.19)$$

The corresponding total differential is:

$$dY = -SdT + Vdp - \sum_{k=1, k \neq i, j}^m N_k d\mu_k^* + \mu^{(n)} dn + \mu^{(N)} dN \quad (2.20)$$

where V is the volume and S is the entropy. The partition function \tilde{Y} for the $NnPT\mu$ is therefore also related to the partition function Q for the NVT ensemble:

$$\tilde{Y}[N, n, p, T, \mu^*] = \sum_{\{N_1, \dots, N_m\}} \exp[\beta \sum_{k=1, k \neq i, j}^m \mu_k^* N_k] \frac{1}{V_0} \int dV \exp(-\beta pV) Q(\dots) \quad (2.21)$$

in which

$$Q(V, T, N_1, \dots, N_m) = \frac{1}{N_1! \dots N_m!} \frac{1}{\Lambda^{3n}} Z(V, T, N_1, \dots, N_m) \quad (2.22)$$

with

$$Z(V, T, N_1, \dots, N_m) = \int d\vec{r}_1 \dots d\vec{r}_n \exp[-\beta E(\vec{r}_1 \dots \vec{r}_n)] \quad (2.23)$$

Λ is the thermal wavelength of a monomer, \vec{r}_i is the position of monomer i and E the internal energy. The summation in Equation 2.21 is restricted to combinations $\{N_1, \dots, N_m\}$ for which two constraints are fulfilled:

$$f_{c1} \equiv \sum_{k=1}^m N_k - N = 0 \quad (2.24)$$

$$f_{c2} \equiv \sum_{k=1}^m kN_k - n = 0 \quad (2.25)$$

So the probability of a particular microstate in the $NnPT\mu^*$ ensemble is:

$$P^{NnpT\mu^*}(V, \vec{r}_1, \dots, \vec{r}_N; \text{connectivity}) \propto \exp[\beta \sum_{k=1, k \neq i, j}^m \mu_k^* N_k - \beta pV - \beta E(\vec{r}_1 \dots \vec{r}_n; \text{connectivity})] \quad (2.26)$$

where *connectivity* represents a particular connectedness of monomers by chemical bonds. To relate N_k to the reduced chemical potential μ_k^* , two assumptions are essential. The first is that the configurational integral Z depends solely on the monomer density and the number-averaged molecular weight:

$$Z = Z(V, T, N, n) \quad (2.27)$$

This is justified [54] for systems without very short chains, so that the monomer density and the density of chain ends are the only relevant parameters of the molecular-weight distribution. A second assumption, valid for large N and n , is that a maximum-term approximation can be used for \tilde{Y} :

$$\tilde{Y} = \frac{\exp[\beta\mu_k^* N_k]}{N_k!} \times R(..) \simeq \frac{\exp((\beta\mu_k^* + 1)N_k)}{N_k^{N_k+1/2}} \times R(..) \quad (2.28)$$

where $R(..)$ does not depend on N_k . Subsequently, using the thermodynamic relation $Y = -k_B T \ln(\tilde{Y})$ and the requirement that in equilibrium $\partial Y / \partial N_k - \xi \partial f_{c1} / \partial N_k - \psi \partial f_{c2} / \partial N_k = 0$, where ξ and ψ are Lagrangian multipliers, one finds:

$$\ln N_k = \beta\mu_k^* + \xi + \psi k \quad (2.29)$$

giving

$$N_k = cy^k \exp(\beta\mu_k^*) \quad (2.30)$$

Now the molecular-weight distribution can be controlled by choosing μ^* . Constants c and y are then found by substituting this expression in the constraint Equations 2.3.2. An example is the uniform distribution, which can be obtained by taking:

$$\mu_k^* = \begin{cases} -\infty & k < \bar{X} - l \cup k > \bar{X} + l \\ 0 & \bar{X} - l < k < \bar{X} + l \end{cases} \quad (2.31)$$

with $\bar{X} = n/N$. This has as a solution $y = 1$ and $c = \frac{N}{2l+1}$.

Concluding remarks

Various methods for preparing well-equilibrated polymer samples have been discussed. The excluded-volume (EV) method produces wrong dihedral-angle distributions and is therefore not advisable. Phantom-chain growth (PCG) is better, but does not work for polymers with bulky monomers, such as PS. A method consisting of polymerizing a monomer liquid does not guarantee correct chain statistics.

There are more successful methods however. One such method is the method of Kotelyanskii et al. [88], starting from chain configurations on a lattice. Another is the PolyPack method [89, 90], where polymer packing is treated as a geometric optimization problem. A third successful approach, presented by Auhl et al.[92], consists of placing chains with correct end-to-end distances in a simulation box, reducing density fluctuations and finally introducing an excluded-volume potential very slowly.

Here we decide to use none of these methods, but again another method, namely connectivity-altering MC. This method generates well-equilibrated polymer conformations on all length scales, and is relatively insensitive to details of the starting conformations of the chains in the system. Furthermore, the method can be used not only for sample preparation, but also for calculating equilibrium properties, whereas in other methods MD is often used to calculate physical properties after preparation. The advantage is then that with connectivity-altering MC larger parts of configuration space can be sampled.

Connectivity-altering algorithms exist for the equilibration of PE in the melt. For this thesis an end-bridging code for PE has been used to obtain well-equilibrated PE samples, to be used for subsequent deformation simulations. To be able to equilibrate other polymers as well, an end-bridging code has been developed to simulate polymers of type $(AB)_n$; this code is subsequently used to equilibrate PS at coarse-grained level of description (a PS monomer is represented by two beads, A and B).

By first equilibrating at the coarse-grained level and subsequently reintroducing atomistic detail, well-equilibrated PS structures at the atomistic level can be obtained. For the reinsertion the "back-mapping" method of Harmandaris et al. [95] is used.

2.4 Methodologies employed in this thesis

All simulation work presented in this thesis concerns bulk polymer material, either in the melt or in the glassy state. We perform simulations of polymers both under isotropic conditions and under the influence of mechanical deformation. The polymers studied are PE and PS. PE has been chosen for its simple chemical formula and the fact that many algorithms are available or relatively easy to develop. PS has been investigated, because there exist a lot of data, from experiments and from finite-element modeling, on its mechanical properties.

In all simulations one or more of the following tasks have to be dealt with:

1. Creating well-equilibrated polymer samples in the melt and calculating physical properties from subsequent melt simulations;
2. Obtaining polymers in the glassy state and determining physical quantities in that state;
3. Subjecting a glassy polymer to deformation.

In all these tasks both MD and MC techniques have been employed. Typically, the simulated polymer systems consist of 5000 monomers in the bulk phase. The common way to simulate the bulk phase is by using periodic boundary conditions, see Section 2.1. In all simulation work presented in this thesis, orthorhombic periodic boundaries have been used.

Exclusively off-lattice models have been used for the work presented in this thesis. One of the reasons is the availability of force fields. In lattice approaches, often polymer models are used that have general polymer-like features, but do not originate from one specific polymer. So by using off-lattice models we could in principle compare different polymers. In addition to this argument, there is the question to what extent the reduction of the infinite number of possible configurations in continuum space to a finite number of possible configurations on a lattice is valid.

The elementary particles used to represent PE or PS polymer chains in the simulations are united atoms, i.e., carbon atoms plus the hydrogen atoms covalently bound to it. PE, both during isotropic simulations and under deformation, is modeled exclusively at the united-atom level. For PS different levels of description have been used. During sample preparation both descriptions at the united-atom level and at the (2:1) level of coarse-graining, see Chapter 5, have been used; during deformation only a united-atom model is applied.

The various force fields used will be explained in the different result Chapters. These force fields have some commonalities though, that can be mentioned here already. Bond lengths are always treated as constraints or as harmonic springs, and bond angles as harmonic springs. Dihedral angles are modeled in various ways, sometimes including or excluding 1-

4 non-bonded interactions [56]. For the united-atom simulations of PS, improper torsional potentials [96] have been used, in order to incorporate tacticity [96] in united-atom polymer models of polymers with side groups. Non-bonded interactions are Lennard-Jones like; details of the cutoff radius are different for the various force fields used.

Equilibration

In equilibration, always the end-bridging technique has been applied, both to obtain well-equilibrated PE and PS. The chemical potential is always such that a uniform mass distribution results. For PE, EB can be applied, at the united-atom level of description. For PS the situation is more complicated. Equilibration has been performed in two stages. During the first stage the focus is on equilibration of length scales beyond that of a few chemical bonds. For that purpose end-bridging Monte Carlo has been used. At this stage the PS polymer is described at the (2:1)-level of coarse graining, that is PS monomers are represented by two coarse-grained particles. This level of description is desirable for end-bridging, to make implementation feasible, to make applicability of the developed algorithm more general, and to obtain a non-negligible acceptance of the end-bridging move. Further details are provided in Chapter 5. In a second stage atomistic detail is reintroduced and the smallest length scales are equilibrated as well, using the molecular-dynamics technique, see Chapter 6.

Deformation

To simulate deformation of PE, MC has been used, whereas MD has been employed for simulation of PS under deformation. In either case strain was prescribed, and not stress. And in both cases affine deformation was prescribed, because of the problems with approaches where only boundary displacements or boundary forces were incorporated, see Section 2.2. All deformations are uniaxial.

For PS a united-atom level of description has been used for deformation, and not a coarse-grained description. Coarse-grained descriptions are often developed for reproducing structural properties; in their development structural data from atomistic simulations or experiments are being used; dynamic properties are often not rigorously taken into account during the development of coarse-grained models. As a result, the dynamic properties of coarse-grained polymers are in general distinct from those of actual polymers or their atomistic models.

Chapter 3

Monte Carlo simulation of uniaxial tension of an amorphous polyethylene-like polymer glass

ABSTRACT

Atomistic Monte Carlo (MC) simulations of uniaxial tension of an amorphous linear polyethylene(PE)-like polymer glass have been carried out. A united-atom model has been used where PE chains are represented by beads connected by flexible springs. Highly efficient end-bridging MC moves have been used to first equilibrate the polymer in the melt and then cool to a temperature below its glass transition temperature. A mix of efficient MC moves has also been used to simulate the deformation dynamics. Upon uniaxial deformation the stress response to the strain is initially linearly elastic, subsequently as the strain increases further yielding is observed, and finally strain hardening is developed. The simulated Young modulus and Poisson ratio take realistic values. Furthermore the temperature and strain-rate dependencies of stress-strain curves have been investigated and the results are in qualitative agreement with the experimental observations. Chain conformation and energy- and stress partitioning with increasing strain are followed in detail. During the deformation the chains adopt more extended conformations and the fraction of dyads in the trans state increases. In the elastic region mechanical work done on the sample, is primarily stored as non-bonded internal energy, whereas from the yield region onwards the intra-chain contributions start to play a role.

3.1 Introduction

A long-standing problem in polymer science concerns the mechanical behavior of glassy amorphous polymers under deformation. Numerous experimental and theoretical efforts have been put on investigating elastic response, yielding (the stress stops increasing with strain at the onset of yielding), strain softening (a drop in the yield stress with strain), and strain hardening (the steep increase of the stress with strain at large strain values). It is found that the yield stress increases with increasing strain rate, decreasing temperature and increasing pressure [9], the post-yield strain-hardening behavior is found to strongly depend on the state of deformation [10] and involves also the cross-linked or entangled polymer network which is loaded at large strains [8]. Nevertheless, the direct connection between the network density and strain-hardening modulus and the physical origin of strain softening are not well understood [8].

Molecular simulations provide a route to investigate polymers at the molecular level, thus to obtain more detailed information on the static and dynamic properties than can be extracted from experimental measurement. Molecular dynamics (MD) and Monte Carlo (MC) have proved to be successful tools for exploring the structure and properties of bulk amorphous polymers at the molecular level. One of the first detailed MD computer simulations of an amorphous polyethylene-like polymer under uniaxial tension was performed by Brown and Clarke [39] in 1991. They prepared initial samples of 1000 united atoms which after equilibration at melt temperature are cooled down at a rate of 10^{12} K s^{-1} and subsequently equilibrated for 1 ns. Thereafter uniaxial deformation was simulated with various tension rates (corresponding to deformation rates of the order of 10^9 s^{-1}). A loose-coupling constant-pressure molecular-dynamics simulation was carried out for times up to 1 ns. The simulated elastic deformation, yield and plastic flow at low temperatures show similarity with laboratory results obtained on time scales that are many orders of magnitude longer. In spite of the problems such as a small system size and huge cooling and deformation rates, MD has proved to be a useful tool in studying deformation behavior of amorphous polymers. Capaldi et al. [43] for instance studied, in 2004, the behavior of a glassy PE-like polymer undergoing active compressive deformation by MD. They found that deformation increases the transition rate between different dihedral-angle states and promotes propagation of dihedral-angle flips along the chain. Recently Lyulin et al. [46] showed that it was possible to simulate by MD both glassy atactic polystyrene and glassy bisphenol-A polycarbonate, using chemically realistic models, under uniaxial mechanical deformation, employing a deformation rate of 10^8 s^{-1} . The initial samples were cooled down from the melt at a speed of 10^{12} K s^{-1} . It was shown that the simulated Young moduli, yield stresses and strain-hardening moduli were in fair agreement with existing experiments. An important observation is that the mobility of the PS segments in the deformation direction is increased drastically beyond the yield point. A weaker increase is observed for PC.

Apart from limitations mentioned above, a serious drawback of MD simulations is the prob-

lem of preparing well-equilibrated initial samples at melt temperature. Typically chains are first generated by some (self-avoiding) random-walk process, and subsequently equilibrated by MD [39, 41, 97]. However the equilibration achieved in such a simulation is far from complete. The longest relaxation time rapidly increases with chain length; even for relatively short chains (a few tens of monomers) the longest relaxation time will exceed the accessible computer time. As a consequence the large-scale configurational characteristics of the polymer system will hardly evolve and the system will remain close to its initial position in phase space. The result is an inefficient sampling of phase space and unreliable estimations of both statistical and dynamical properties. In some cases use has been made of MC simulations for sample equilibration. Capaldi et al. [43] for example used MC with single-atom-displacement moves for equilibration. The local nature of this kind of moves does not solve the equilibration problem either. In the course of time lots of efforts have been made in improving upon the situation at hand by developing advanced MC moves. Vacatello et al. [98] introduced the “reptation” (REP) move, where a monomer is cut off from a randomly selected chain end and subsequently attached to the other end of the same chain. In a so-called “configurational bias” (CB) move [99], a randomly selected chain is cut in two pieces, one of which is removed and then regrown segment by segment, avoiding overlap with surrounding segments. Dodd et al. [94] came up with the “concerted rotation” (CONROT) move, where one trimer is excised from a chain, the two adjacent atoms are displaced by changing their dihedral angles, and finally the trimer is placed in between the adjacent atoms (at their new positions). In the nineties it appeared possible with these moves to fully equilibrate polymer chains up to 30 monomers. For longer chains descriptors such as the end-to-end distance vector did not completely forget the values they had in the beginning of the simulation [55, 100]. A real breakthrough came when Pant and Theodorou [54] introduced their so-called “end-bridging” MC move. This move, which alters the connectivity of chains, made very large steps in phase space possible. The long relaxation times that scale with the degree of polymerization could be circumvented. Besides equilibration, the energy-based MC method appeared to be a useful tool in the study of non-equilibrium dynamical processes, such as polymer deformation, as well. Typically in such simulations one type of move is used, and an estimate is made of the corresponding timescale. Wittkop et al. [101] used lattice Monte Carlo (MC) simulations to study the deformation behavior of a bond-fluctuation polymer-chain model under an external force in 2D and 3D, and found a good agreement in the chain end-to-end distance over a large force range between simulation results and theoretical estimations. Hölzl [78] used MC simulations employing the same lattice model to investigate deformation of polymer melts and observed that the sample significantly shrinks laterally near the glass-transition temperature. Below T_g voids are produced and chains are extremely stretched. Recently Ospina et al. [76, 77] simulated by MC the initial stage of deformation of linear polyethylene (PE) using a 2D lattice model and observed a stress-strain behavior comparable to what is observed in experiments [102], but neither strain softening nor strain hardening was reported. 3D off-lattice MC simulations of PE-like crosslinked networks have been performed recently by Chui and Boyce [9] to study the mechanical-deformation process under various loading conditions. Their model has been found to qualitatively capture the rate-

and temperature dependence of deformation observed experimentally for real amorphous polymeric materials. Chui and Boyce perform a careful study of the separate contributions of the non-bonded as well as the various bonded interactions to both the internal energy and the stresses. Their main conclusions are that the strain softening is a result of the evolution of intermolecular contributions to the response whereas the strain-hardening phenomenon is a result of evolution in the intramolecular contributions. Chui and Boyce used one type of (local) MC move, in which one particle is selected at random and its position is perturbed by a small random displacement. They estimate that, by using these very local moves, the deformation rate in their simulations equals $10^8 - 10^9 \text{ s}^{-1}$.

Here an MC study is reported to investigate the uniaxial tension (up to 80 % strain) of an amorphous non-crosslinked PE-like glass. Special attention is given to producing well-equilibrated initial samples, by employing advanced MC moves that enable equilibration at the timescale of the longest relaxation times. Subsequently deformation of the polymer samples is simulated with MC at an estimated deformation rate of 10^8 s^{-1} or slower.

Extensive simulations, using advanced MC moves such as REP, CONROT and EB moves, have been performed to prepare well-equilibrated initial samples of 5000 monomers in the melt. Especially EB had proved to be of great help in efficiently sampling the configuration space of systems of long-chain polymers. After subsequent cooling, we used MC to simulate the uniaxial tensile deformation of PE by employing efficient local moves, primarily CONROT. By doing so it should be possible to obtain effective deformation rates that are lower than so far achieved in simulations; in the present implementation we estimate our rates to be about 10^8 s^{-1} . To validate our simulations, properties such as stress-strain behavior and its dependence on temperature and strain rate have been studied to check if experimental dependencies are at least qualitatively reproduced. As an extra check we have studied the calorimetric behavior and compared the results to experimental data from Hasan and Boyce [15]. Subsequently, following Chui and Boyce, to obtain insight in the role of the different bonded and non-bonded interactions during deformation, the evolution of contributions from the different interactions to internal energy and internal stress, at various stages of the deformation process, has been investigated. In addition the evolution of chain conformations have been examined and compared to previous simulations [9, 43, 45].

In Section 3.2 the PE model, the details of the MC algorithms, the different types of moves used in the present study, as well as details of the stress calculations are explained. The equilibration and cooling is elaborated on in Section 3.3. In Section 3.4 the stress-strain relations are discussed. Subsequently the evolution of the internal-energy contributions upon deformation are treated, together with the evolution of chain conformations. Finally, in Section 3.5, conclusions are drawn.

3.2 PE model and simulation algorithm

We studied a united-atom model of linear PE, where each CH₂ group is considered as a bead and each chemical bond on the backbone is represented by a spring via a harmonic bond-stretching potential U_l . The valence angle is governed by a harmonic angle-bending potential U_θ . The Ryckaert-Bellemans torsional potential U_ϕ [103] is used, and interactions between beads on different chains and beads separated by more than three bonds on the same chain are described by the Lennard-Jones potential. The exact functional forms and values of the parameters associated with these potentials are given in Table 3.1. The Lennard-Jones potential is truncated at 2.3σ and a quintic spline was used from 1.45σ to 2.3σ [93]; long-range interactions are left out since no attempt is made to compare the results accurately with experimental values.

The equilibrium internal-stress tensor of a periodic monatomic system can be calculated using the expression [56, 104]:

$$\tau^{\alpha\beta} = \left\langle -\frac{1}{V} \sum_i \frac{p_i^\alpha p_i^\beta}{m_i} - \frac{1}{2V} \sum_i \sum_j (r_i^\alpha - r_{j_{\min}(i)}^\alpha) F_{ij}^{\min,\beta} \right\rangle + \tau_{\text{tail}}^{\alpha\beta} \quad (3.1)$$

where $\tau^{\alpha\beta}$ is the $\alpha\beta$ component of the stress, V is the system volume, p_i^α is the α component of the momentum of site i with mass m_i . \vec{r}_i is the position vector of site i , $j_{\min}(i)$ denotes the minimum image of site j with respect to site i , and \vec{F}_{ij}^{\min} is the force on i due to the interaction with $j_{\min}(i)$. τ_{tail} in Equation 3.1 is a tail contribution from the interactions U_{tail} beyond the potential-cutoff distance, which are neglected in the present study.

In a system of polyatomic molecules, \vec{F}_{ij} includes non-bonded forces from the excluded-volume interactions and bonded forces from the bonds, the valence angles and the dihedral angles. It was pointed out in [104] and [105] that the contribution of valence angles and dihedral angles to the trace of the instantaneous value of the stress tensor is zero. In other words, the pressure is governed only by the non-bonded forces and the bond-stretching forces. However, valence-angle and torsional forces do affect the instantaneous values of the individual normal as well as shear stresses in the system. The momentum term on the right-hand side of Equation 3.1 can not be calculated directly in an MC simulation. However for equilibrium situations it is often assumed that on-diagonal elements of the kinetic part of the stress tensor are simply related to temperature and that off-diagonal elements are zero, that is the kinetic term can be written in terms of the system temperature as $\langle -\frac{N}{V} \rangle k_B T \delta_{\alpha\beta}$, where N is the total number of monomers in the periodic box and $\delta_{\alpha\beta}$ the Kronecker delta [104]. In this study we go one step further in that Equation 3.1 is used during deformation (non-equilibrium simulations) as well. The internal pressure in the present MC simulations is calculated as the negative trace of the stress tensor in Equation 3.1.

PE chains are contained in an orthorhombic box, which starts (before deformation) as a

cubic box of size 50 Å, with periodic boundary conditions. (Although simple to implement, orthorhombic periodic boundary conditions do not allow one to control or respond to off-diagonal components of the stress. However in our study we observed that the off-diagonal elements are very small, and equal to each other within the statistical errors.) The chain-length distribution is uniform in the interval from $\bar{X}(1 - \Delta)$ to $\bar{X}(1 + \Delta)$, where \bar{X} is the number-average degree of polymerization and Δ the half-width of the chain-length distribution reduced by the number-average chain length. A geometrical builder is used to create initial PE samples of 5000 monomers with $\bar{X} = 50$ and $\Delta = 0.5$. (Preliminary results on longer chain systems, for example $\bar{X} = 500$ and $\Delta = 0.5$, resulted in the same qualitative picture of deformation.) The initial temperature is 450 K. During this sample-building process hard-sphere overlap is prevented.

Table 3.1: The force field. Parameter values are taken from [55], except the value of the bond stretching potential k_l , which is taken from [9].

Interaction type	Functional form	Parameters
Bond stretching	$U_l = \frac{1}{2}k_l(l - l_0)^2$	$k_l = 1674 \text{ kJ}\text{\AA}^{-2}\text{mol}^{-1}$, $l_0 = 1.54 \text{ \AA}$
Angle bending	$U_\theta = \frac{1}{2}k_\theta(\theta - \theta_0)^2$	$k_\theta = 481.8 \text{ kJ rad}^{-2}\text{mol}^{-1}$, $\theta_0 = 1.955 \text{ rad}$
Torsion	$U_\phi = \sum_{k=0}^5 c_k \cos^k(\phi)$	$c_0 = 9.279 \text{ kJ mol}^{-1}$, $c_1 = 12.16 \text{ kJ mol}^{-1}$, $c_2 = -13.12 \text{ kJ mol}^{-1}$, $c_3 = 3.060 \text{ kJ mol}^{-1}$, $c_4 = 26.24 \text{ kJ mol}^{-1}$, $c_5 = 31.49 \text{ kJ mol}^{-1}$
Non-bonded	$U_{\text{LJ}} = 4\epsilon \left[\left(\frac{\sigma}{r}\right)^{12} - \left(\frac{\sigma}{r}\right)^6 \right]$	$\epsilon = 0.410 \text{ kJ mol}^{-1}$, $\sigma = 3.94 \text{ \AA}$

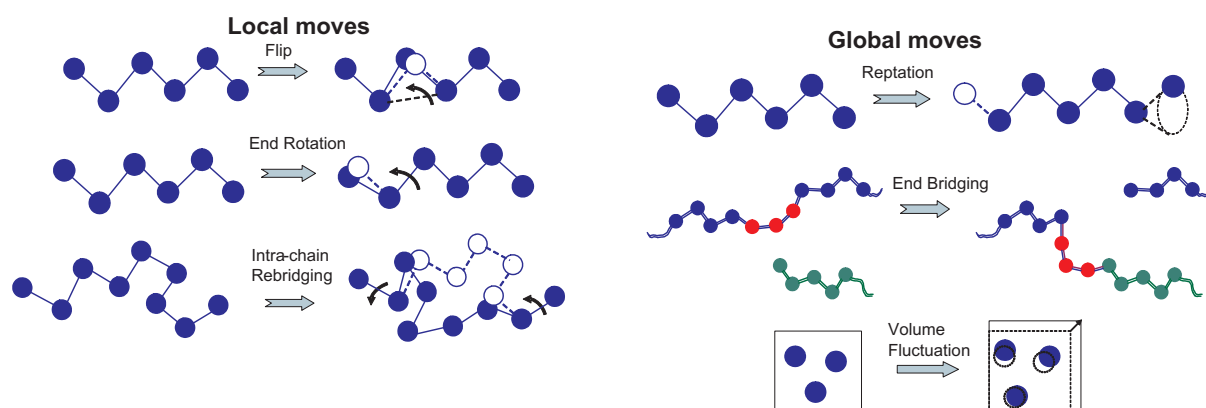


Figure 3.1: Local MC moves (left) and global MC moves (right) implemented in the present study.

In the present study six types of moves have been used: three local and three global types of MC moves, see Figure 3.1. During a “flip” move, a trimer in the middle of a

chain is selected at random, and subsequently the apex atom is rotated by a small angle along the line connecting the two neighboring atoms, which are kept fixed in the move. During an “end rotation” move a chain end (start) is selected at random, and the last segment is rotated around the neighboring bond by changing the torsional angle defined by the last (first) four beads of the chains. The “intra-chain rebridging” or “concerted rotation” (CONROT) move as well as the REP move have been explained before. In order to efficiently apply the MC technique to a long-chains polymer melt, Theodorou et al. [55, 93] developed the connectivity-altering EB MC move. During an EB move, two melt chains are selected so that the end of one is within a certain bridgeable distance from a backbone segment of the other. A trimer centered at this latter backbone segment is excised from the second chain, thus defining two sub-chains. The end of one of these sub-chains is connected to the end of the first chain by constructing a bridging trimer, forming a new chain with prescribed molecular geometry (bond lengths and bond angles). Clearly, the EB move alters the lengths of chains participating in it. To control the chain-length distribution, any trial move which makes the length of any chain fall outside the prescribed range of chain lengths is immediately rejected. Finally, a “volume fluctuation” move modifies simultaneously the box sizes in all directions i ($i \in x, y, z$) affinely with the coordinates of all atoms: the box size L is increased by ΔL and the i -coordinate $i(j)$ of the position of a site j is shifted by $\Delta i(j) = \Delta L \frac{i(j)-i_0}{L}$, with i_0 the position of the face of the box that keeps its position (the opposite face is displaced ΔL in the i -direction).

The initial PE samples are first equilibrated in the NPT ensemble at melt temperature $T=450$ K and isotropic external pressure $P=0.1$ MPa. The question of the equilibration of a (non-deformed) PE melt was given special attention in the present study. A mix of MC moves with different attempt probabilities is used, similar to the mix of moves used by Mavrantzas et al. [55]: 6% reptation, 6% end rotation, 6% flip, 32% intra-chain rebridging, 49% end-bridging and 1% volume fluctuation. This choice was made in order to make especially the end-bridging move efficient. To obtain such efficiency the “shuttling effect”, i.e., the occurrence of successive accepted EB moves that annihilate each other by performing transitions twice, in forward and backward direction, has to be reduced as much as possible. This can be done by considerably updating, between two end-bridging moves, the lists of chain ends and backbone segments in other chains to which they can bridge [72]. It is observed that at 450 K the energy and the density achieve equilibrium values after $4 \cdot 10^4$ MCS, where 1 MCS (Monte Carlo Step) is the number of moves divided by the total number of monomers in the system. After this initial equilibration the sample is further cooled down to 100 K, 200 K and 300 K, at a rate of 1 K every 20 MCS, until it reaches the desired temperatures. It is difficult to give an estimate for the timescale of the cooling process. Above the glass transition one could claim that one cools on the timescale of the slowest processes by using the EB move, i.e., on the scale of the disengagement time (quasi-statically). As soon as the system becomes glassy, only local moves have a non-negligible chance of acceptance. In the latter case we estimate the cooling rate to be 10^{11} K s⁻¹. Then the equilibration has been continued with the temperature fixed at its target value until the energy and the density reach stable values.

The equilibrated samples at different temperatures and at atmospheric pressure ($P = 0.1$ MPa) are uniaxially deformed at constant effective velocity in the z-direction: the box size L_z is increased by $\Delta L_z = 0.1 \text{ \AA}$ every 100-200 MCS. All positions of sites in the box are scaled affinely with the box size, i.e., $\Delta z = \Delta L_z \frac{(z-z_0)}{L_z}$, where z is the position of a site, z_0 the position of the face of the box that keeps its position (the opposite face is displaced ΔL_z in the z-direction). Besides a “lateral size fluctuation” move (comparable to the volume fluctuation move) that modifies simultaneously the box sizes in directions x and y, during deformation only local moves (primarily the CONROT move) are used, to avoid a direct intervening in the slowest processes (that take place on time scales that also exceed experimental timescales of the order of seconds or larger). The exact mix of moves is: 55.88% CONROT, 34% flip, 10% end rotation and 0.12% lateral size fluctuation. We use as estimate for the time corresponding to one MCS (one Monte Carlo Step per monomer), the time in which the MSD (Mean Square Translational Displacement) of a monomer in a united-atom MD simulation of PE equals the average bead displacement due to a typical CONROT move (average of a few tens of CONROT moves). This time is approximately 10^{-13} s. This would imply a deformation rate of the order of 10^8 s^{-1} . However since the time estimate is very crude it is dangerous to draw final conclusions regarding cooling rates or deformation rates.

3.3 Preparation of the initial polymer melt

3.3.1 Equilibration at 450 K

During the initial equilibration the energy and the density of a PE sample are calculated every move, while the stress is calculated at every 20 MCS. The density evolution in Figure 3.2 (a) shows the fast equilibration of the sample by the MC algorithms. Within $2 \cdot 10^3$ MCS the system evolves to an equilibrium density of 0.81 g cm^{-3} . As the purpose of the present study is not to reproduce the experimental density, the parameters of the implemented force fields are not carefully calibrated versus the available experimental results. Similar to the density, the energy also reaches equilibrium quickly after $2 \cdot 10^3$ MCS. The equilibrium total energy is $2.21 \cdot 10^4 \text{ kJ mol}^{-1}$ (Figure 3.2 (b)). The instantaneous pressure calculated in the present study is given in Figure 3.3 and the contributions to the pressure from different types of interactions are listed in Table 3.2. It is found that for the equilibrated PE sample in the melt state (450 K) negative contributions come from bond lengths and intermolecular non-bonded interactions, whereas a positive contribution comes from intramolecular non-bonded interactions. The fluctuations in the pressure, which are of the order of 30 MPa, are mainly caused by changes of the chemical-bond lengths during volume-fluctuation moves.

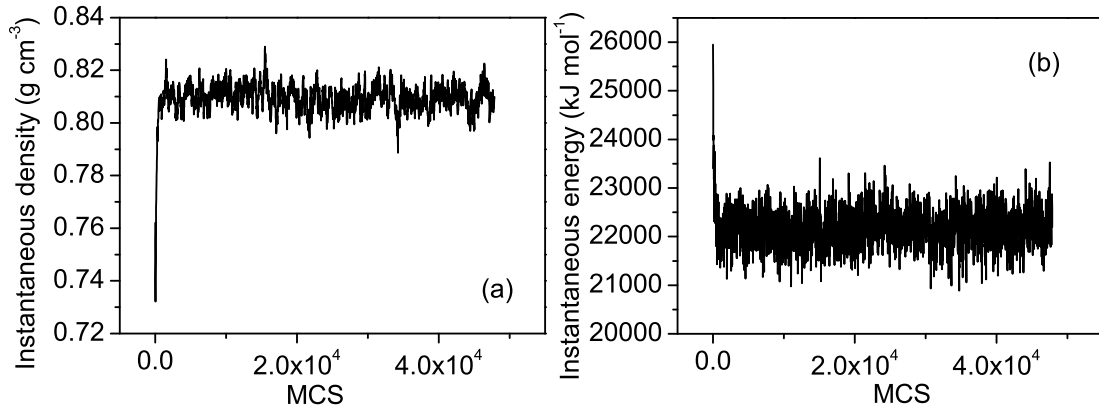


Figure 3.2: The density (a) and total energy (b) evolution during the equilibration of the initial samples at 450 K and 0.1 MPa. Results are plotted every 20 MCS. The average equilibrium density and energy of the initial samples are 0.81 g cm^{-3} and $2.21 \cdot 10^4 \text{ kJ mol}^{-1}$.

3.3.2 Cooling process

After the equilibration at $T=450 \text{ K}$ the cooling process is conducted by gradually cooling the PE sample down at a rate of $5 \cdot 10^{-2} \text{ K MCS}^{-1}$ to the final target temperature, followed by the equilibration at that temperature. The evolution of the instantaneous density and total energy in the cooling process from the melt temperature (450 K) to the three target temperatures, 100 K, 200 K and 300 K, is plotted in Figure 3.4. In the cooling to 300 K the density quickly reaches the equilibrium value of 0.85 g cm^{-3} ($4 \cdot 10^3 \text{ MCS}$ after the cooling stops), while the densities keep increasing as the cooling stops at 200 K and 100 K. The evolution of the density during and after the cooling to these two low temperatures are very similar, suggesting a very slow relaxation at these temperatures. Probably the PE samples investigated in this study have a T_g in the range $200 \text{ K} < T_g < 300 \text{ K}$ (the experimental value equals 252 K [106]), and both samples (cooled down to 200 K and 100 K) are frozen in some amorphous states. The continuous decrease of the total energies after cooling to 200 K and 100 K also indicates the slow structural-relaxation process in these samples below T_g . We found that the changes of the internal structure during cooling are responsible for the large decrease of the total energy. These structural changes can be seen in Figure 3.5 (left) where the monomer-monomer pair correlation function before and after cooling to 200 K is plotted. Figure 3.5 (right) shows the average internal pressure (average of all values from the first move till the last move performed) calculated from the atomic stress theorem, Equation 3.1. The cooling process does not influence the consistency of the internal and the imposed pressures. However, the internal balance of different contributions does change; upon cooling the intermolecular interactions instead of

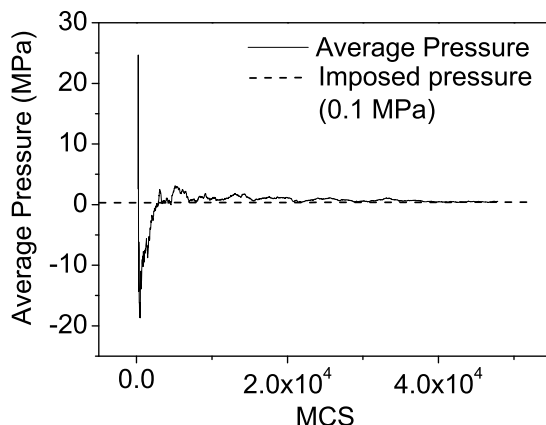


Figure 3.3: The average pressure (average of all values from the move at which the monitoring was started, after 200 MCS, till the last move performed) obtained from the equilibration of the initial PE sample at 450 K and 0.1 MPa. Results are plotted every 20 MCS.

the intramolecular bond-stretching start to play a dominant role in balancing the kinetic motion to keep the system stable, as shown in Table 3.2.

3.4 Uniaxial deformation

3.4.1 Stress-strain behavior

The PE samples are uniaxially deformed at various temperatures and strain rates. The calculated (true) stress-strain relations are shown in Figure 3.6. Here the strain ϵ is defined as $(L_z - L_{z,0})/L_{z,0}$, with $L_{z,0}$ the box length prior to deformation. The calculated stresses (Figure 3.6) are higher than the typical stresses of high-density PE (HDPE), 10 - 50 MPa, observed in tensile experiments at room temperature [107]. That is probably because of the high deformation speed in the present simulations as compared to the experiments. Typically the strain rate used in experiments is about 0.1 s^{-1} [107], whereas the strain rate in the simulations is in the range of $(1 \cdot 10^{-5} - 2 \cdot 10^{-5}) \text{ MCS}^{-1}$ (As mentioned earlier this corresponds to a strain rate of approximately 10^8 s^{-1}). For clarity, the deformations take place at constant velocity; the deformation rates mentioned are the deformation rates at the start of the deformation. Apart from a difference in deformation velocity, a comparison with experimental observations is difficult because in reality PE is semi-crystalline, whereas the sample used in our calculations is amorphous. Therefore experimental values are only

Table 3.2: Comparison of the pressure contributions from different types of interactions, before and after the cooling process to 200 K. The data before cooling are the average values over the equilibration interval at 450 K, while those after cooling are average values over the interval from $4 \cdot 10^4$ MCS (counted from the moment the cooling was started) till the end of the "equilibration-after-cooling" process. The indicated error is the standard deviation of the distribution of all measured values. The total pressure hardly changes during the cooling, but the different contributions do change; whereas in the melt kinetic motion is balanced by bond-stretching forces, in the glassy state non-bonded interactions (mainly intermolecular) keep the system stable.

Pressure contribution	Before cooling (MPa)	After cooling (MPa)
Kinetic	216 ± 1	111.5 ± 0.3
Bond	$-(2.4 \pm 0.3) \cdot 10^2$	$-(3 \pm 2) \cdot 10^1$
Valence angle	$\equiv 0$	$\equiv 0$
Torsional angle	$\equiv 0$	$\equiv 0$
Intermolecular	-10 ± 8	-73 ± 7
Intramolecular	30 ± 4	-10 ± 2
Total	0 ± 30	-0 ± 20

mentioned at a few instances in this paper, to give an idea to what extent the simulated material is or behaves different than real PE.

Because of the complications mentioned above, no attempt will be made to reproduce all experimental values, but on this point the aim is to show that the qualitative dependence of the stress-strain relation on temperature and strain rate can be obtained, and to see how the results compare to those of previous simulation studies, e.g. by Capaldi et al. [43], who report E-moduli of order 2.5 GPa, or by Brown and Clarke [39], who observe an E-modulus of 2.5 GPa at 100 K and half an order lower at room temperature. In the left panel of Figure 3.6 the stress-strain behavior for the temperatures at 100 K, 200 K and 300 K at a strain rate of $2 \cdot 10^{-5}$ MCS⁻¹ can be seen. All curves show an initial elastic region (for strain values below 0.1), followed by yielding (the steep increase of stress with strain levels off at this point). The sample deformed at 100 K shows a clear transition to strain hardening at a strain of 0.5. The elastic deformation at small strains shows larger moduli for lower-temperature samples. The elastic moduli, which are obtained from a linear fit to the stress-strain data for strains smaller than 0.02, are given in Table 3.3. These values are similar to the values found in other computational studies, e.g. by Brown and Clarke [39], and for temperatures below T_g they are of the same order of magnitude as measured in the laboratory (of the GPa order [7]). At higher temperatures the moduli decrease by half an order of magnitude, which is far less than observed in experiments. These results can be understood by realizing that the material behaves elastic at low temperature, and therefore the deformation timescale is not relevant. For higher temperature the behavior is more viscous and the time scale of deformation is deciding for the moduli. The yield point was determined as an intersection of the stress-strain curve with its tangent at zero strain (with

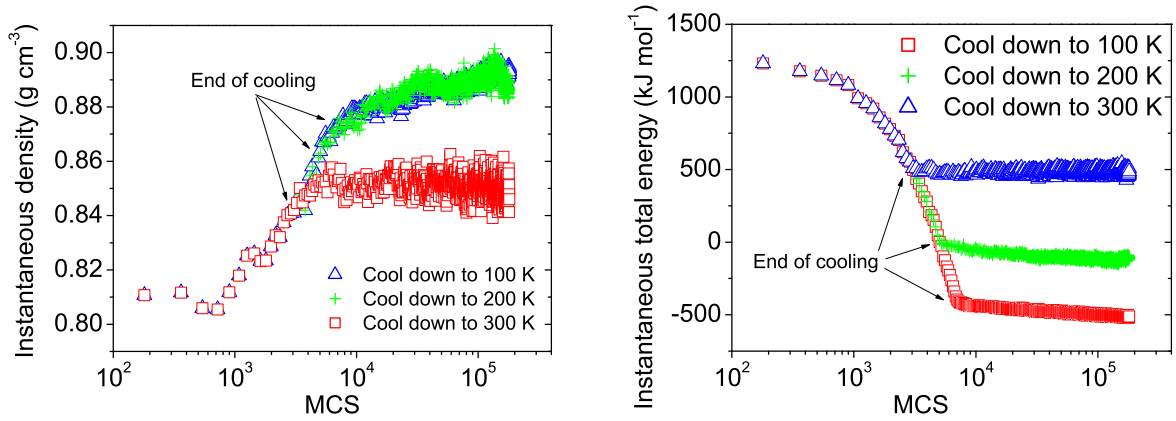


Figure 3.4: The evolution of the instantaneous density (left) and total energy (right) during the cooling process from 450 K to three lower temperatures. Results are plotted every 180 MCS. The sample which stays at the higher temperature shows the lower equilibrium density and higher equilibrium total energy. The slow relaxation processes at low temperatures require more than $2 \cdot 10^5$ MCS for the samples to be equilibrated.

Table 3.3: Young moduli, yield stresses, yield strains and strain hardening moduli of PE glass deformed at various temperatures and strain rates.

T (K)	$\dot{\epsilon}$ (MCS $^{-1}$)	E (MPa)	σ_y (MPa)	ϵ_y (-)	G_R^ϵ (MPa)
100	$2 \cdot 10^{-5}$	$(4.0 \pm 0.3)10^3$	170 ± 2	0.06 ± 0.005	$(1.27 \pm 0.03)10^3$
200	$1 \cdot 10^{-5}$	$(1.3 \pm 0.2)10^3$	90 ± 5	0.09 ± 0.005	$(2.5 \pm 0.3)10^2$
200	$1.3 \cdot 10^{-5}$	$(1.9 \pm 0.2)10^3$	90 ± 5	0.07 ± 0.005	$(2.6 \pm 0.3)10^2$
200	$2 \cdot 10^{-5}$	$(2.5 \pm 0.2)10^3$	115 ± 2	0.07 ± 0.005	$(4.2 \pm 0.3)10^2$
300	$2 \cdot 10^{-5}$	$(1.2 \pm 0.4)10^3$	36 ± 2	0.05 ± 0.005	$(9 \pm 3)10^1$

slope equal to the E-modulus) but shifted over 0.02 along the strain axis [7]; the values of the yield stress and yield strain are given in Table 3.3. These values are slightly higher than experimental values (for room temperature the yield stress is in the range 18-32 MPa [107]), but lower than values obtained in other simulations (for example Capaldi et al. [45] find 200-300 MPa for deformation rates of $5 \cdot 10^9 - 5 \cdot 10^{10} \text{ s}^{-1}$ at 200 K), which is probably due to the better equilibration of the present PE melts and to a lower deformation rate. Eventual strain hardening is caused by increased bond lengths and valence angles (as compared to their equilibrium values), see Section 3.4.2. The strain-hardening moduli G_R^ϵ , obtained from a linear fit of the final parts of the stress-strain curves (final 10% of the deformation), are given in Table 3.3 as well. These values are extremely high in comparison to typical experimental results (at room temperature the strain-hardening moduli are typically in the range of 1-5 MPa [107]), which probably means that the extent to which the bond lengths and valence angles are increased is unrealistic. The values are comparable to the values

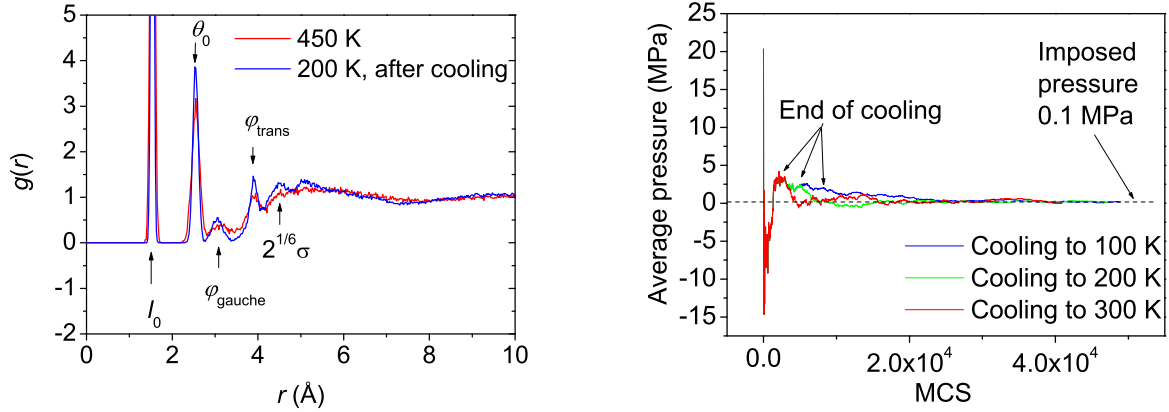


Figure 3.5: (Left) Pair correlation function for the equilibrium PE sample at 450 K and the PE glass at 200 K. The peaks corresponding to the equilibrium bond length l_0 , the equilibrium bond angle θ_0 , the gauche conformation ϕ_{gauche} , the trans conformation ϕ_{trans} and the equilibrium non-bonded distance $2^{1/6}\sigma$ are indicated by arrows. (Right) Evolution of the average internal pressure during the cooling process and further aging. The results are plotted every 20 MCS. After the cooling has stopped, the internal pressure evolves in approximately 10^4 MCS to the value of the external pressure.

that can be extracted from previous simulation results reported by Capaldi et al. [43], although they employed higher deformation rates.

In the right panel of Figure 3.6 the stress-strain relation is plotted for different strain rates: ($1.0 \cdot 10^{-5} \text{ MCS}^{-1}$, $1.3 \cdot 10^{-5} \text{ MCS}^{-1}$ and $2.0 \cdot 10^{-5} \text{ MCS}^{-1}$) at the same temperature (200 K). The initial elastic moduli, the yield points and the strain-hardening moduli can be found again in Table 3.3. The Young modulus increases with the deformation velocity, which is probably an artefact of the measurement, in which the modulus is chosen as the slope of the stress-strain curve for deformation up to 2%; at 2% deformation the departure from non-linear behavior is presumably too dramatic already at the higher strain rates. The yield stress and the strain-hardening modulus also depend on the deformation velocity, but the dependencies are much weaker. Qualitatively this picture is in agreement with the experimental [107] and computational [9, 39, 45] results mentioned before.

3.4.2 Evolution of internal-energy contributions and stress partitioning

To obtain insight in the molecular mechanisms at work during deformation of glassy amorphous PE, the evolution has been investigated of the various contributions to the internal energy from the bonded and non-bonded interactions at various stages of the deformation

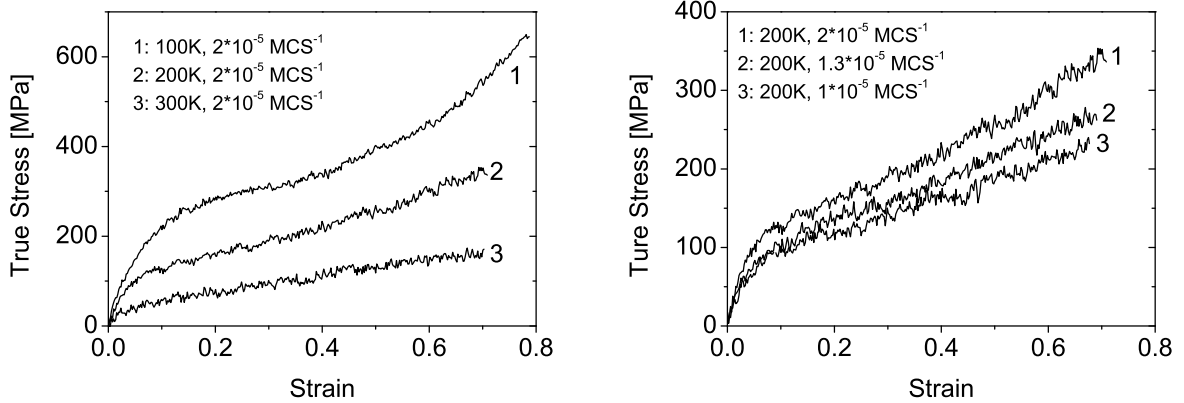


Figure 3.6: Stress-strain behavior during uniaxial deformation for various temperatures (left) and strain rates (right). A higher stress is observed for lower temperatures. Decreasing the strain rate results in a lower stress at fixed strain value. The initial elastic modulus is larger for lower temperature but the moduli from different strain rates under the same temperature are close to each other.

process, i.e., during initial linear-elastic response, yield, large deformation with low stress increase and strain hardening, respectively. In addition the contributions to the total stress have been studied. Finally the influence of deformation on distributions of bond lengths, bond angles, dihedral angles, as well as on the intra- and intermolecular pair distribution functions has been investigated.

In Figure 3.7 (left panel) the work, calculated as the area under the stress-strain curve, done on the PE glass during deformation is given for three different temperatures. The applied work during deformation at room temperature is of the same order of magnitude as what is experimentally found [15]. The evolution of the internal energy during deformation at 100 K is shown in Figure 3.7 (right). It can be seen that for strain values below 0.4 a substantial part ($\sim 30\%$) of the mechanical energy is converted into internal energy of the sample, mainly as an increase of the non-bonded energy. At intermediate strain values (0.4 - 0.6) almost all energy is dissipated. At larger strain values (above 0.6) the mechanical energy is partly turned into internal energy related to conformational changes in the chains. At the final strain (0.8) about one sixth of the applied work has been converted into internal energy. This is comparable to what is seen in experiments [15]. The energy from the Lennard-Jones interactions increases very fast up to the strain of 0.4 and then reaches a plateau, while the contributions from bonds and valence angles stay close to their initial values in the beginning, and start to increase only after the strain of 0.5. The contribution from dihedral angles decreases during deformation, indicating a re-distribution of dihedral angles, where the fraction of trans conformations increases.

The evolution of the different contributions to the stress τ^{zz} is shown in Figure 3.8. Initially

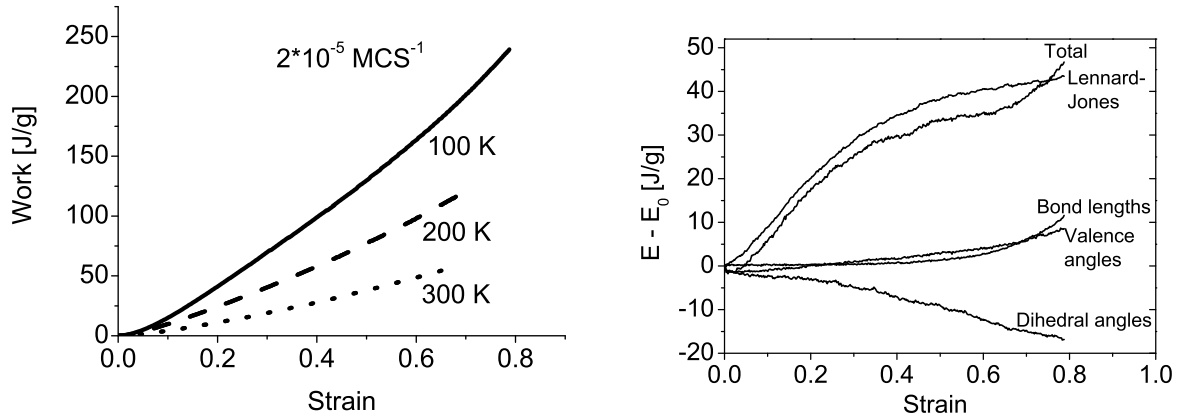


Figure 3.7: The work done at different temperatures and same strain rate ($2 \cdot 10^{-5} \text{ MCS}^{-1}$) (left), and the evolution of the internal-energy contributions associated with bond lengths, bond angles, dihedral angles and non-bonded interactions at 100 K and at a strain rate of $2 \cdot 10^{-5} \text{ MCS}^{-1}$ (right). E_0 , which denotes the initial energy of a certain contribution before the deformation, is subtracted for clarity.

the non-bonded interactions are tensile (give a positive contribution to the stress of the system), whereas the bonded interactions are compressive (give a negative contribution to the stress of the system); more specifically bond lengths give a compressive contribution, while bond angles and dihedral angles do not contribute. From a strain of 0.2 all contributions are tensile. (The only exception is the kinetic part of the stress, which is always compressive.) Upon deformation one observes initially a stiff response from both non-bonded and bonded interactions. As yielding sets in, the non-bonded contribution stops increasing, while the contribution from bonded interactions increases further at lower slope. Eventually, at strain values of 0.5-0.6, the contributions from bonded interactions, i.e., bond lengths and bond angles, start to increase more rapidly.

The facts above indicate that the deformation process can be divided in a few consecutive stages as follows: Initially, in the elastic regime and slightly beyond (up to the strain of 0.1), the non-bonded interactions are dominant, and bring the immediate response to the elongation. Subsequently, as the deformation progresses, the amount of mechanical energy from the external load converted into non-bonded energy decreases to zero. Simultaneously the bonded interactions become increasingly important in the response to the external loads. Dramatic changes of chain conformations occur. The probability densities of structural parameters before and at the end of the deformation at 100 K and at a strain rate of $2 \cdot 10^{-5} \text{ MCS}^{-1}$ are plotted in Figure 3.9. The unfolding of the chains results in the transformation of torsional angles from the gauche conformation to the trans conformation. The fraction of dyads in the trans conformation increases from 57% before deformation to 69% after deformation, as shown in Figure 3.9 (c), resulting in a decrease of the torsional

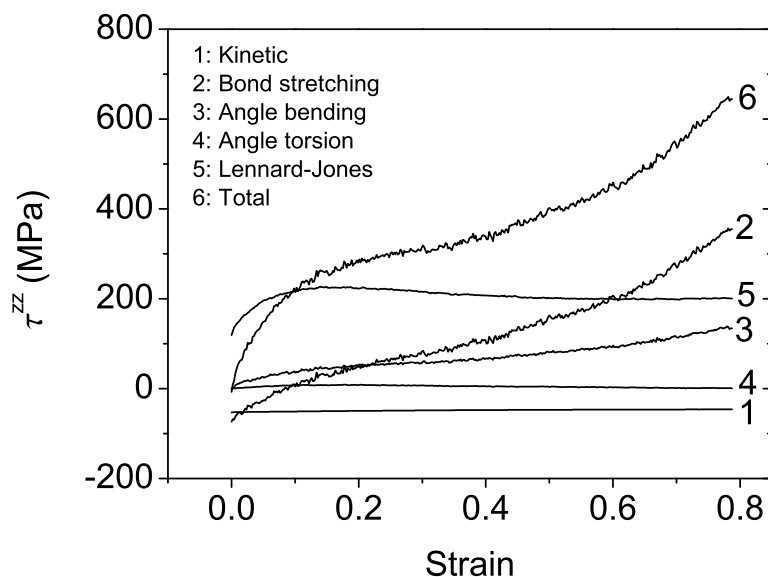


Figure 3.8: Stress partitioning in the sample during deformation: evolution of contributions from the different bonded and non-bonded interactions.

energy. The decrease, after deformation, in the intensity of the peak at intramolecular distances $2^{1/6}\sigma$ and the increase of the peaks at higher values, Figure 3.9 (d), indicates the transition of the chains to more extended conformations. The intermolecular distances shift to lower values. Apparently the space previously occupied by intramolecular neighbors is now occupied by intermolecular neighbors. Finally, at strain values larger than 0.5, the bond lengths and the bond angles start to absorb a considerable amount of energy and are responsible for a major contribution to the stress. This is the onset of strain hardening. It is clear from Figure 3.9 (a) and Figure 3.9 (b) that the distributions of the bond lengths and the bond angles shift towards higher values during deformation, corresponding to higher energies.

Although for PE-like crosslinked networks a similar approach was followed already by Chui and Boyce [9], to our knowledge this is the first study of the role of the different (separate) interactions during uniaxial deformation of an amorphous non-crosslinked PE-like glass. A comparison of the present Chapter with the results of Chui and Boyce is, though interesting, not without risk; apart from the topological differences (a crosslinked network vs a polymer melt) and the fact that Chui and Boyce study compression whereas the current paper concerns uniaxial extension, there are important differences in the PE force fields used in the two studies. Both Chui and Boyce and we use a Lennard-Jones potential for non-bonded interactions, but with different radii σ . Moreover Chui and Boyce directly

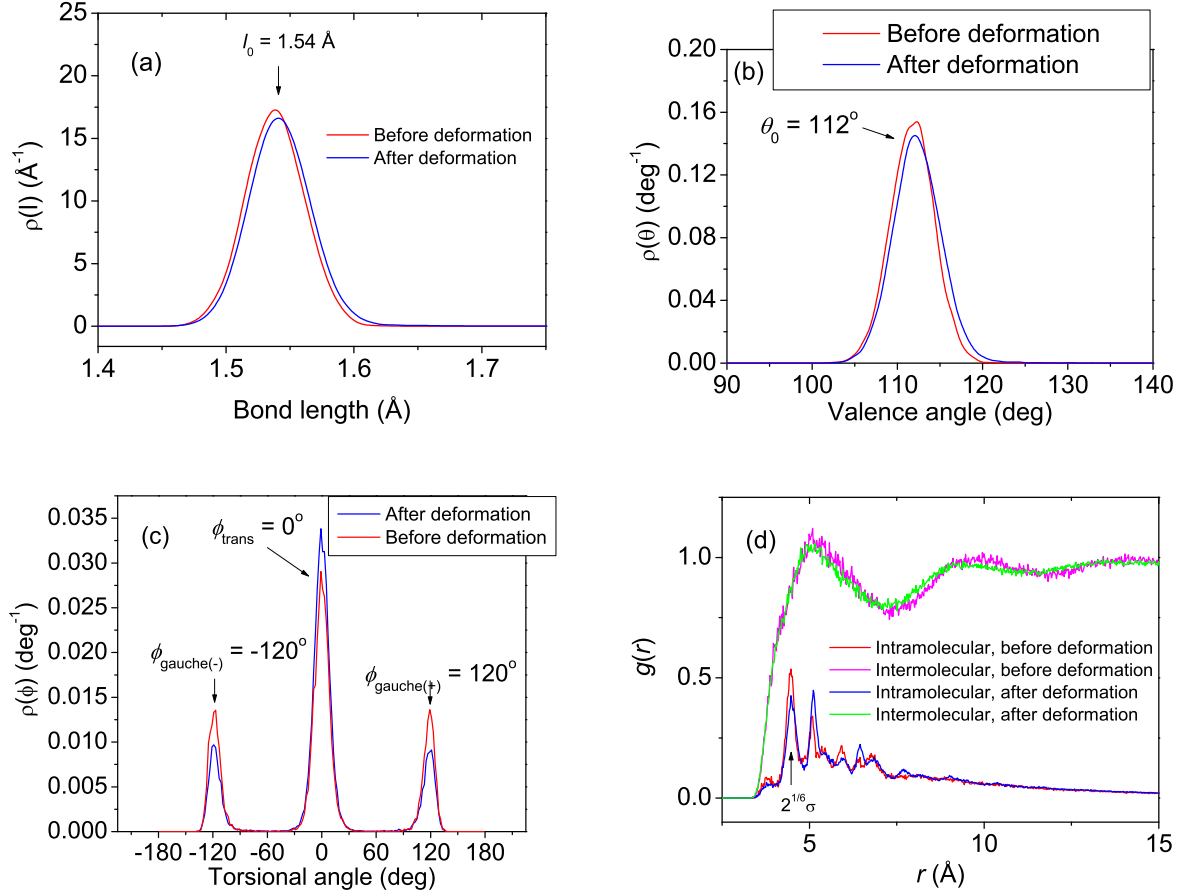


Figure 3.9: Comparison of the probability densities of (a) bond length, (b) valence angle, (c) torsional angle, and (d) non-bonded distance for the initial sample (before deformation) and the sample at the end of the deformation (after deformation) at 100 K and under a strain rate of $2 \cdot 10^{-5} \text{ MCS}^{-1}$.

calculate 1-4 non-bonded interactions, whereas we account for 1-4 non-bonded interactions by including them in the dihedral potential. This difference makes comparison of both contributions from non-bonded interactions and dihedral interactions to energy and stress complicated. Presumably it also explains why our results show tensile non-bonded interactions, whereas Chui and Boyce report compressive non-bonded interactions. In spite of the differences, there are some similarities in the results; the initially stiff response to deformation of our PE-like polymer melt, followed by leveling off of the contribution of non-bonded interactions to the stress and a less steep increase of the bonded interactions, is also observed by Chui and Boyce.

The evolution of the density of the system during deformation is also examined for different

temperatures at the same strain rate ($2 \cdot 10^{-5} \text{ MCS}^{-1}$) and for different strain rates at the same temperature (200 K). The sample deformed at 300 K, which is above T_g , shows initial dilation, after which the density fluctuates around a constant value during the rest of the deformation, see the left panel of Figure 3.10. At lower temperature the density keeps decreasing during the deformation, where the slope of the density curve increases with decreasing temperature. The influence of the strain rate is shown in the right panel of Figure 3.10: as the deformation rate decreases, the decrease of the density levels off and finally the density becomes constant. To facilitate a comparison with experimental results, use is made of the following ratio:

$$\mu = -\frac{\Delta L_{\perp}/L_{\perp}}{\Delta L_{\parallel}/L_{\parallel}} \quad (3.2)$$

which is calculated after every 0.002 strain increase. L_{\parallel} and L_{\perp} are the instantaneous lengths of the sample along the elongation direction and the perpendicular direction respectively, and ΔL_{\parallel} and ΔL_{\perp} denote the changes of the lengths L_{\parallel} and L_{\perp} since the last time the ratio was calculated. In the limit of zero strain, the ratio equals Poisson's ratio. At the lowest simulated temperature, 100 K (Figure 3.11), the value of Poisson's ratio is 0.34 ± 0.01 , which is in the experimental range 0.3 - 0.4 [108] for a typical amorphous polymer. As yielding sets in, the ratio μ starts to increase to 0.44 ± 0.03 at large strains,

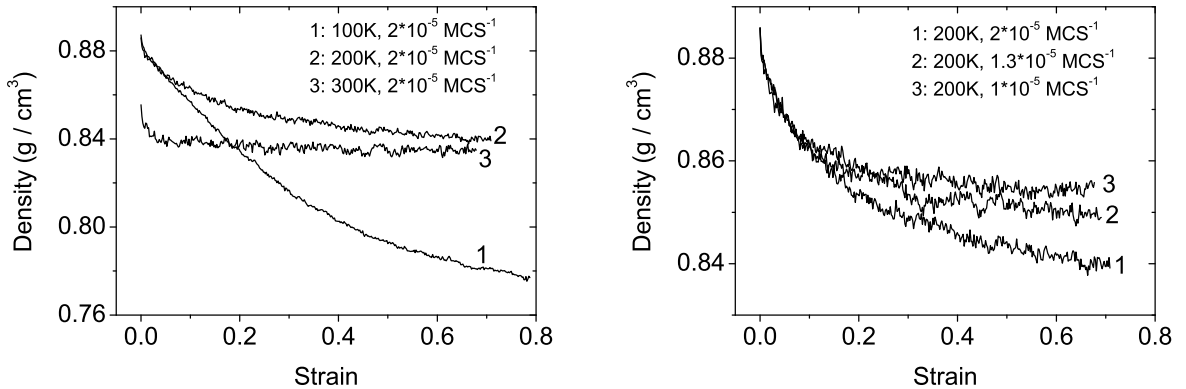


Figure 3.10: Density evolution during uniaxial deformation under different temperatures (left) and strain rates (right). All densities decrease, however at lower temperature or at higher deformation velocity the decrease is more pronounced and continues up to larger strain. The initial samples equilibrated under different temperatures show different initial densities.

indicating that the rate at which the density decreases goes down. At the highest temperature, 300 K, the density is constant in a large range of strains, which is consistent with μ fluctuating around an average value of 0.48 ± 0.04 during the deformation, and with a picture of local incompressible flow.

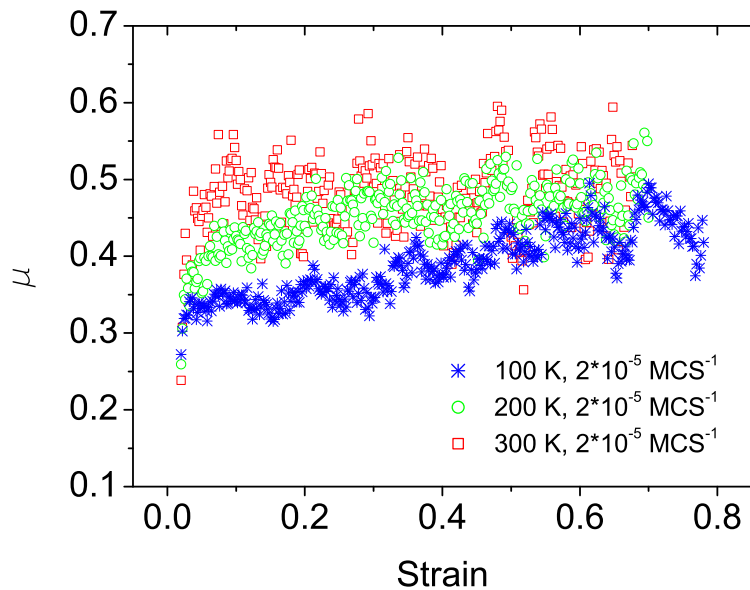


Figure 3.11: The evolution of the ratio $\mu = -\frac{\Delta L_{\perp}/L_{\perp}}{\Delta L_{\parallel}/L_{\parallel}}$ for the deformation at different temperatures (100 K, 200 K and 300 K) and the same strain rate of $2 \cdot 10^{-5} \text{ MCS}^{-1}$.

3.5 Conclusions

MC simulations have been performed of the uniaxial deformation of an amorphous PE-like polymer glass. A united-atom representation is used for the structure of PE. The MC algorithms used in the equilibration at the melt temperature are extensively described by Theodorou et al. [54, 55] and include local moves (flips, end- and concerted rotations) as well as reptation and connectivity-altering end-bridging moves. Especially the last two moves are important in order to produce well-equilibrated polymer samples before deformation is applied. By changing the connectivity of polymer chains, the mechanisms associated with the longest relaxation times are circumvented. After cooling to a temperature near or below T_g , uniaxial deformation of the equilibrated PE glass was performed by constant-velocity elongation at different temperatures, using partly the same MC moves. The results of the present study show that the extension of the MC algorithms of Theodorou et al. to uniaxial deformation provides a new approach for studying the mechanical behavior of model polymer systems. The stress-strain behavior we obtained shows the typical transitions from the elastic deformation in the beginning, to yield, then to large deformation with low stress increase and finally to strain hardening (even for the unentangled systems considered here), as observed in experiments. We also qualitatively reproduced the dependencies of the PE stress-strain behavior on temperature and strain velocity, where stress at the same strain was larger for lower temperatures and higher strain velocities. Moreover, in

spite of the large deformations in our simulations, realistic values are found for E-moduli, yield stresses and Poisson ratios. The evolution of the internal energy and chain conformations during the mechanical deformation indicate that the deformation process can be divided in a few consecutive stages as follows: In the elastic regime and slightly beyond (up to a strain of 0.1) the non-bonded interactions are dominant and density decreases. As the deformation progresses, the amount of mechanical work converted into the non-bonded energy decreases to zero, whereas the bonded interactions become increasingly important in the response to the external load. Chain conformations change considerably under deformation, while the density decrease diminishes. The unfolding of the chains results in the transformation of torsional angles from the gauche conformation to the trans conformation and a decrease of the torsional energy. The fraction of the trans conformations increases from 57% prior the deformation to 69% after deformation resulting in a decrease of the total torsional energy. Changes in both the intra- and inter-chain pair correlation functions imply a transition after yield to local flow of densely packed chains in more extended conformations. Strain hardening is observed at strain values larger than 0.5, where the chemical bonds and the valence angles start to absorb a considerable amount of energy and are responsible for a major contribution to the total stress.

Chapter 4

Use of constraints in Monte Carlo simulations of deformation of glassy polymers

ABSTRACT

The deformation of a glassy amorphous polymer has been simulated by Monte Carlo. A molecular model with constrained chemical bonds (rigid-bond model) and one with chemical bonds represented by Gaussian springs (flexible-bond model) have been compared. Furthermore two different deformation protocols have been tested. Comparisons on the basis of stress-strain behavior, contributions of various interactions to stress and energy, evolution of density and distribution of dihedral angles, and of pair correlation functions show that both the introduction of constrained bonds and the deformation protocol influence the results dramatically. The results obtained using the flexible-bond model, employing a deformation protocol in which all monomers are displaced affinely with the box size, show the best agreement with experimental facts.

4.1 Introduction

The mechanical behavior of glassy amorphous polymers during deformation is a long-standing problem in polymer science. Many experimental and theoretical studies have been performed to investigate phenomena such as strain softening and strain hardening [109–

119]. In a later stage computer simulations started to be employed as well to investigate deformation of glassy polymers at a molecular level [39, 46]. One of the first publications on molecular simulations of glassy polymers under mechanical deformation concerns the work of Brown and Clarke [39], who performed detailed molecular dynamics (MD) computer simulations of an amorphous polyethylene-like melt under uniaxial tension. With a tension rate of the order of 10^9 s^{-1} and time scales up to 1 ns, they found similar elastic deformation, yield and plastic-flow behavior at low temperatures as observed in the laboratory on time scales that are many orders of magnitude longer. In spite of problems such as small system sizes and huge cooling and deformation rates, MD has proved to be a useful tool in studying deformation behavior of amorphous polymers [39, 43, 46]. Although Monte Carlo (MC) simulation does not contain any dynamics, this tool is also starting to be used for the study of polymer deformation [9, 77]. Various lattice-model MC simulations have been used to study the deformation behavior of polymeric models [77, 101]. 3D off-lattice MC simulations of polyethylene(PE)-like cross-linked networks have been performed by Chui and Boyce [9]. Li et al. recently simulated the uniaxial extension of multi-chain PE-like systems employing a mix of very local atomic and more collective MC moves [83].

In many simulations of deformation the strain is prescribed by changing monomer positions affinely with the box size [9, 43, 45, 83]. Such a simulation protocol is not very efficient for polymers since it affects the hard degrees of freedom of the polymer molecules, i.e., bond length and valence angles. Changes in these hard degrees of freedom occur on very short time scales and simulating them requires a lot of computational resources [57]. By using constraints such as rigid (infinitely stiff) chemical bonds and bond angles the simulation of the deformation process can be speeded up. For simulation of deformation this means that one has to use a deformation protocol that keeps bond lengths and bond angles constant. The easiest way to do this is by changing the relative positions of the polymer chains, without changing the relative positions of monomers within the same chain. The consequences of introducing constraints and of changing the deformation protocol, which are not very well documented in literature yet, form the subject of the present study.

To gain some insight in the consequences of the introduction of constraints or of the deformation protocol, we have performed MC simulations of PE-like systems of 25 polymer chains with an average degree of polymerization of 200, in the NpT ensemble. MC simulations, using connectivity-altering moves [54], have been performed to produce well-equilibrated initial samples: both samples with flexible bonds (bonds represented by Gaussian springs) and samples with rigid bonds (bond represented by a rod with a fixed length). The behavior of samples with rigid bonds (the rigid-bond model) and that of samples with flexible bonds (the flexible-bond model) have been compared during deformation, employing a deformation protocol in which the relative positions of chains are altered. Furthermore deformation of a flexible-bonds system by changing monomer positions affinely with the box size has been compared to deformation of the same system by changing the relative positions of chains. For the different models and deformation protocols the comparisons have been made on the basis of stress-strain curves and density-strain curves, as well as on

stress partitioning and energy partitioning, i.e., the contributions of different interactions to the stress and to the internal energy of the system.

This Chapter is organized as follows: in Section 4.2 the model, the MC algorithms, the stress calculation and other relevant details of the simulation method are explained. All results, concerning the preparation and equilibration of initial samples as well as the uniaxial deformation via various constraint conditions and deformation protocols are extensively discussed in Section 4.3. Finally conclusions are drawn in Section 4.4.

4.2 Model, MC algorithms and stress calculation

In the present study a united-atom model of PE is used, in which each CH_2 -group is considered as a bead with its mass centered at the carbon atom of the backbone. Totally 5000 beads (monomers) are contained in an orthorhombic box of about 50 \AA with periodic boundary conditions [56, 57], constituting 25 chains with a number-averaged degree of polymerization $\bar{X} = 200$. The chain-length distribution is uniform in the interval from $0.5\bar{X}$ to $1.5\bar{X}$. In case of the flexible-bond model the monomers interact via a force field that employs a harmonic bond-stretching potential, a harmonic angle-bending potential for the valence angles, the Ryckaert-Bellemans potential for dihedral angles, and a Lennard-Jones-type potential for non-bonded interactions. The monomers in the rigid-bond model interact via the same force field without the harmonic bond-stretching potential. The details of both force fields have been explained in the previous Chapter.

The evolution of the system is realized by a mix of six types of MC moves including flip, end rotation, concerted rotation (CONROT), reptation (REP), end bridging (EB), and volume fluctuation, which have all been explained in ref. [83]. Flip, end rotation and CONROT are local-scale moves where only 4 - 9 monomers are involved, while REP, EB and volume fluctuation are large-scale moves which concern displacement of whole chains or displacement of all monomers in the system. All moves are in principle the same for both the flexible-bond model and the rigid-bond model, except the volume-fluctuation move. During a volume-fluctuation move the size of the box is changed isotropically. In case the flexible-bond model is used, either the coordinates of all monomers in the box are changed affinely with the box size or the center-of-mass(COM)-coordinates of the chains are changed; in the latter case the bond lengths and bond angles are not changed during a volume-fluctuation move. In case the rigid-bond model is used, only COM-coordinates of chains are changed affinely with the box size, so that the bond lengths and bond angles are always maintained constant during a volume fluctuation.

The initial sample is prepared by constructing polymer chains, one after the other, inside the box with periodic boundary conditions. The individual chains are created by placing the first monomer at a random position inside the box and then successively attaching the other monomers to the chain. A new monomer is added in such a way that the length of

the newly formed bond equals the equilibrium bond length, whereas the newly introduced bond angle and dihedral angle are selected from the Boltzmann distributions determined by their respective potentials. During the process of sample preparation hard-sphere overlap, i.e., the situation that the distance between monomers is so small that their potential energy is much larger than $k_B T$ is prevented.

It is proved by Theodorou et al. [55] that fast equilibration of PE in the melt can be well achieved with the combination of the moves mentioned above. In the present study we use a mix of moves similar to the one Theodorou used [55], both for the equilibration of our PE samples at melt temperature and for subsequent cooling to temperatures below the glass transition. After cooling the samples are deformed by stepwise deformation of the box size in one direction and changing either the monomer positions affinely with this box size or the positions of the COMs of chains affinely with this box size. The REP and EB move are switched off during deformation, to avoid direct intervening in the slowest processes (that take place on time scales that also exceed experimental timescales of the order of seconds or larger), other moves are performed in the same proportions as during equilibration. Further details on the equilibration, cooling and deformation are given below in the Results Section.

The stresses in the flexible-bond model are calculated from the standard atomic stress expression [56, 104]:

$$\tau^{\alpha\beta} = \langle \sigma_a^{\alpha\beta} \rangle = \left\langle -\frac{N_a k_B T \delta_{\alpha\beta}}{V} - \frac{1}{2V} \sum_i \sum_j (r_i^\alpha - r_{j_{\min}(i)}^\alpha) F_{ij}^{\min,\beta} \right\rangle \quad (4.1)$$

where $\tau^{\alpha\beta}$ is the $\alpha\beta$ component of stress, σ denotes the instantaneous mechanical quantity whose average gives the thermodynamic stress τ , and the subscript a indicates that the stress is calculated on the basis of interactions between *atoms*. N_a is number of atoms (or monomers), k_B the Boltzmann constant, T the system temperature, $\delta_{\alpha\beta}$ the Kronecker delta, V the system volume. \vec{r}_i is the position vector of atom i , $j_{\min}(i)$ denotes the minimum image [57] of atom j with respect to atom i , and \vec{F}_{ij}^{\min} is the force on i due to the interaction with $j_{\min}(i)$. Bonded and non-bonded forces \vec{F}_{ij} can readily be calculated from the system's potential energy U at any moment during the MC simulations by using $\vec{F}_{ij} = -\nabla_{r_i - r_j} U$. Thus the atomic stress can be explicitly calculated in the flexible-bond model.

Such a calculation of the atomic stress is not possible anymore when the rigid-bond constraint is introduced. To calculate the constraint forces one needs the atomic accelerations, which are not available in MC. Thus, the atomic stress expression, Equation 4.1, is unsuitable for the rigid-bond model. A molecular analogue of the double-summation form, Equation 4.1, has been invoked in equilibrium and non-equilibrium MD calculations [120, 121], with indices i and j labeling molecular centers of mass. This approach is correct as long as no periodic boundary conditions are used or for simulations of systems of

monatomic molecules. In simulations of polymer systems with periodic boundary conditions the approach of [120, 121] is inadequate, since in general the periodic box contains (parts of) more than one image of the same chain; all interactions between images of either different or the same molecules inside the periodic box have to be taken into account explicitly [104]. To calculate the thermodynamic stress τ in model systems with periodic boundary conditions Theodorou et al. [104] suggested a molecular stress expression (it does not require knowledge of bonded forces) in which all these interactions are taken into account:

$$\tau^{\alpha\beta} = \langle \sigma_m^{\alpha\beta} \rangle = \left\langle -\frac{N_m k_B T \delta_{\alpha\beta}}{V} - \frac{1}{2V} \sum_i \sum_j (r_{cm,c(i)}^\alpha - r_{cm,c(j_{\min}(i))}^\alpha) F_{ij}^{NB,\min,\beta} \right\rangle \quad (4.2)$$

where N_m is the number of polymer chains of the system. i refers to atom i and $j_{\min}(i)$ to the minimum image of atom j with respect to atom i . $c(i)$ indicates the chain image to which atom image i belongs and $r_{cm,c(i)}$ denotes the COM position of chain image $c(i)$. The subscript m means that the stress calculation is based on interactions between *molecules*, and the superscript NB denotes non-bonded interactions. Further details can be found in [104]. In the remaining Sections of the paper the calculation of stress is based on Equation 4.1 and Equation 4.2.

4.3 Results and discussion

4.3.1 Equilibration at 450 K

The initial PE sample is first equilibrated in the NpT ensemble at an external pressure of 0.1 MPa and at a temperature of 450 K, which is above the experimental melting temperature for this polymer. A mix of MC moves with different attempt probabilities is used, similar to that used by Mavrantzas et al. [55]: 6% reptation, 6% end rotation, 6% flip, 32% intra-chain rebridging, 49% end-bridging and 1% volume fluctuation.

It is shown in Figure 4.1 that density and total energy are equilibrated after 2×10^3 MCS, where 1 MCS (Monte Carlo Step) is the number of attempt moves divided by the total number of monomers in the system. The pressure reaches its equilibrium value after 10^2 MCS. The final values of the density and the total energy are different for the two models. It can be seen from Figure 1(c) that the pressures in both models show the same fluctuation of about 50 MPa. In the flexible-bond model these pressure fluctuations are caused by fluctuations of bond lengths during volume fluctuations (monomer positions are changed affinely with the box size), whereas in the rigid-bond model they are caused by fluctuations in the strength of intermolecular non-bonded interactions (relative positions of

chains are changed). The occurrence of these differences in the physical quantities according

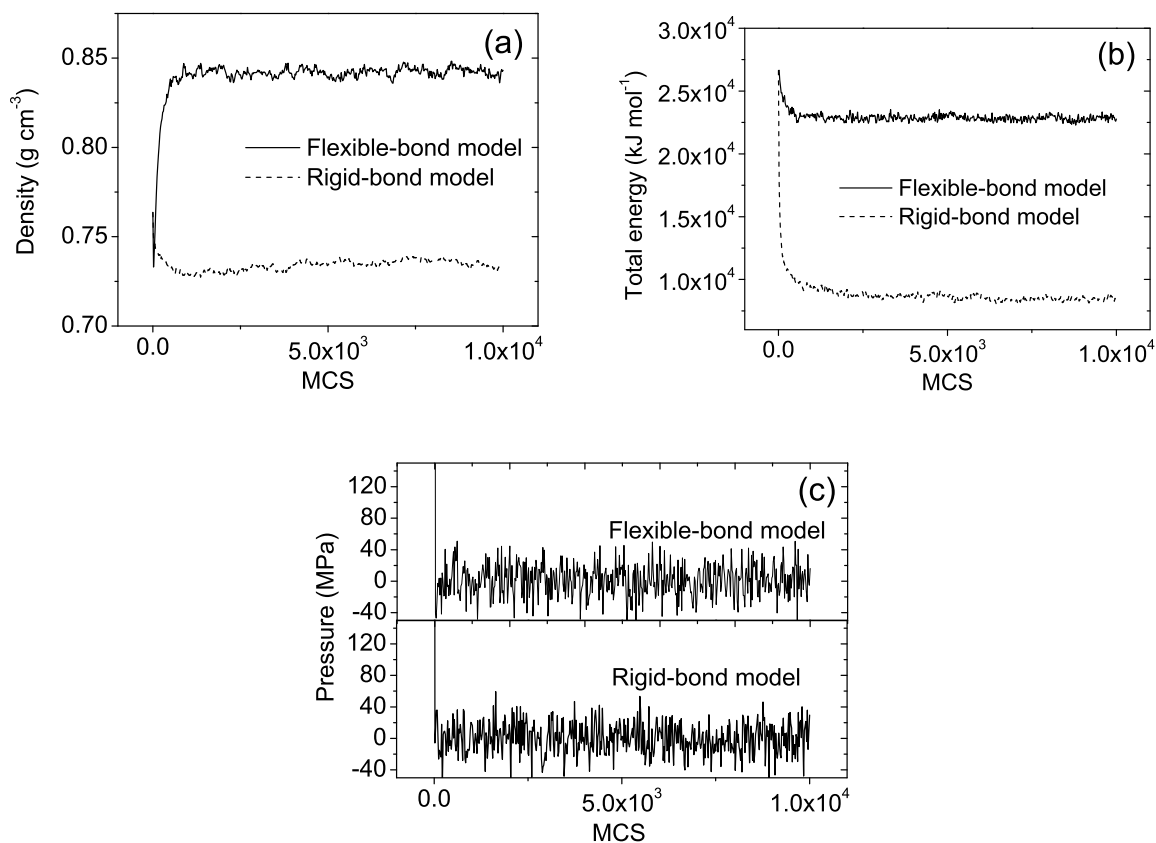


Figure 4.1: Equilibrations of (a) density, (b) total energy and (c) internal pressure at 450 K and at an external pressure of 0.1 MPa for the initial PE sample in the flexible-bond and in the rigid-bond model.

to the different models, shown in Figure 4.1, is almost inevitable. Since the purpose of this study is to determine the influence of the introduction of constrained bonds into the model, only the part of the force field that controls the bond lengths had to be changed. However, physical quantities are determined by all interactions in the system. If one type of interaction, e.g. the one controlling the lengths of chemical bonds, is changed, without any compensatory changes of other interaction type(s), the result will almost certainly be a change of the physical properties of the system.

4.3.2 Cooling to 200 K

After the equilibration at 450 K the cooling process is conducted by gradually cooling the PE sample down at a rate of 0.05 K MCS^{-1} (10^{11} K s^{-1} , see [83]) to the target temperature of 200 K, followed by the equilibration at that temperature.

As the temperature decreases, the density increases whereas the total energy decreases, as shown in Figure 4.2. The fast responses last until the cooling stops after $5 \times 10^3 \text{ MCS}$, after which the sample keeps on equilibrating at 200 K. It can be observed from Figure 4.2(a) that the density (total energy) keeps increasing (decreasing) after the cooling stops, and that the density (total energy) in the rigid-bond model shows a faster increase (decrease). Based on previous studies [83] we assume that the final structure after cooling to 200 K is glassy.

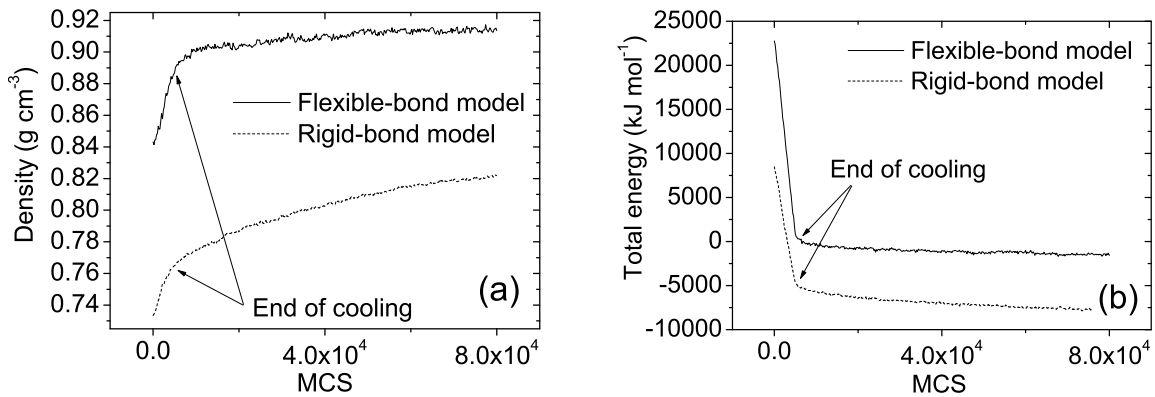


Figure 4.2: Evolution of (a) density and (b) total energy during the cooling process from 450 K to 200 K at a rate of 0.05 K MCS^{-1} .

4.3.3 Uniaxial deformation

The equilibrated samples are uniaxially deformed at constant velocity in the x-direction at 200 K and 0.1 MPa. Deformation is performed by stepwise increasing the box size L_x in the x-direction, once every 20 MCS, by an amount $\Delta L_x = 1 \times 10^{-4} L_{x0}$, where L_{x0} denotes the box length prior to deformation. This corresponds to a deformation rate of $5 \times 10^{-6} \text{ MCS}^{-1}$ ($5 \times 10^7 \text{ s}^{-1}$, see [83]). In between strain steps the following mix of moves is used: 13.3% end rotation, 13.3% flip, 71.1% intra-chain rebridging and, finally, 2.3% lateral-size fluctuation. The REP and EB moves are switched off during deformation, to avoid direct intervening in the slowest processes (that take place on time scales that also exceed experimental timescales of the order of seconds or larger), other moves are

performed in the same proportions as during equilibration. The "lateral-size-fluctuation" move (similar to a "volume-fluctuation" move) modifies simultaneously the box sizes in y- and in z-direction.

Three cases are studied. In the first place a simulation in which the flexible-bond model (F) is employed and coordinates of all atoms (AA) are changed affinely with the box size both in the direction of deformation and in the lateral directions by the "lateral-size-fluctuation" move (FAA). Secondly a simulation employing the flexible-bond model, in which COM-coordinates of all chains are changed affinely with the box size (FCOM). And finally a simulation, employing the rigid-bond model (R), in which, affinely with the box size, COM-coordinates are changed (RCOM).

4.3.4 Stress-strain behavior

The stress-strain curves are plotted for all three cases (FAA, FCOM and RCOM) in Figure 4.3. RCOM results in a very high stress value for all strain values. For FCOM this is also true at lower strain values, but to a lesser extent. Finally FAA gives reasonable results; the curve has the shape that is typical for glassy amorphous polymers and also the values for E-modulus and yield stress, see Table 1, have the right order of magnitude, i.e., of the order as experimentally found by for example Arruda et al. [10]. To facilitate quantitative comparison the values of E-moduli, yield stresses and -strains and strain-hardening moduli have been determined for all three cases, see Table 4.1. The E-moduli result from a linear fit to the stress-strain data for strains smaller than 0.02, for the yield point the intersection of the stress-strain curve with its tangent at zero strain, but shifted over 0.02 along the strain axis [7], is taken, and the strain-hardening moduli G_R^ϵ are determined as a linear fit to the final parts of the stress-strain curves (the final 0.1 strain increment). Although the definition of the strain-hardening modulus is somewhat arbitrary, it provides at least some lower bound to the value of the strain-hardening moduli in our systems. FAA results in E-

Table 4.1: Young moduli, yield stresses, yield strains and strain-hardening moduli of PE in both the flexible-bond model and the rigid-bond model deformed at temperature 200 K and strain rate 5×10^{-6} MCS⁻¹.

Model	Deformation Protocol	E (MPa)	σ_y (MPa)	ϵ_y (-)	G_R^ϵ (MPa)
F	AA	$(1.2 \pm 0.2) \cdot 10^3$	$(7 \pm 1) \cdot 10$	0.08	$(5.7 \pm 0.2) \cdot 10^2$
F	COM	$(4.1 \pm 0.1) \cdot 10^3$	$(1.2 \pm 0.2) \cdot 10^2$	0.05	$(-3 \pm 2) \cdot 10$
R	COM	$(1.6 \pm 0.0) \cdot 10^4$	$(4.5 \pm 0.3) \cdot 10^2$	0.05	$(3.5 \pm 0.0) \cdot 10^3$

moduli similar to those from other computational studies (e.g. by Brown and Clarke [39]) and of same order of magnitude as experimentally measured (of the order GPa [7, 10]) at temperatures below T_g . The values found for FCOM and those for RCOM are respectively about half an order and one order of magnitude too high.

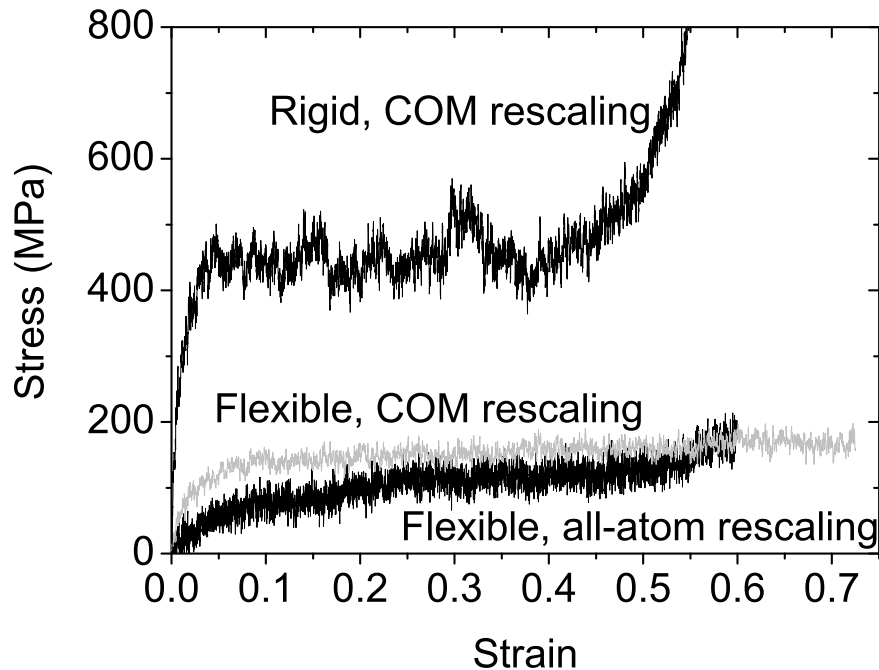


Figure 4.3: Stress-strain behavior of the PE samples in a constant-velocity deformation with strain rate $5 \times 10^{-6} \text{ MCS}^{-1}$ at 200 K and at imposed pressure 0.1 MPa.

The yield stress for FAA is comparable to experimental values as well [10]. The value is lower than found in some other computational results: for example Capaldi et al. [43, 45] find 200-300 MPa for deformation rates of 5×10^9 - $5 \times 10^{10} \text{ s}^{-1}$ at 200 K. This also supports our estimate [83] that our deformation rate is lower than in [43, 45]. So the FAA model and protocol results in feasible values for σ_y . The same is true for FCOM. RCOM gives values that are high both with respect to experiment and to existing computational results.

Values of strain-hardening moduli of glassy amorphous polymers are typically of the order of a few tens of MPa [119]. In the current study strain-hardening moduli are found by FAA and RCOM that are respectively one and two orders of magnitude too large. For the case of FCOM no strain hardening is found at all; from a strain of approximately 0.4 the stress-strain curve remains fluctuating around the same value.

4.3.5 Stress partitioning and energy partitioning

To obtain insight in the details of deformation, the contributions from various interactions to the total stress and to the total energy have been followed in their evolution with strain.

In the case of FAA, see Figure 4.4a, the stress contribution of the non-bonded interactions rises first, then at approximately strain 0.1 this contribution levels off. This picture of initial increase, followed by leveling off of (the contribution of non-bonded interactions to) the total stress is often seen; both for polymer glasses [9] and for monatomic glasses [122]. The contribution of the bonds shows an initial increase as well, although at a slower rate than the non-bonded contribution. At strain 0.2 the contribution of the bonds levels off, and eventually, at strain 0.45, rises again. The contributions of valence angles and dihedral angles are negligible. The large fluctuation in stress can be attributed mainly to a large fluctuation in the bond-lengths contribution. The contribution of the various

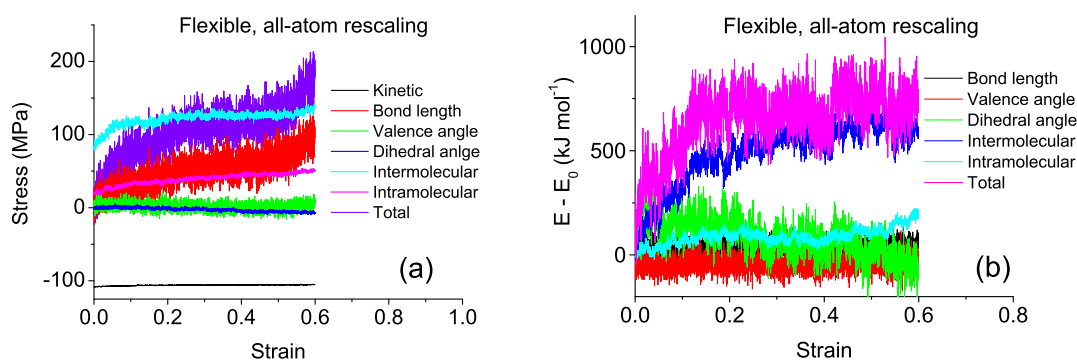


Figure 4.4: (a) Stress partitioning and (b) energy partitioning of PE samples during uniaxial deformation in the flexible-bond model, with coordinates of all atoms scaled affinely with the box size. The zero-strain values of all energy contributions have been shifted to zero.

interactions to the total energy has for the FAA case been shown in Figure 4.4b. Initially the work performed on the sample is converted (apart from heat) into non-bonded (both intermolecular and intramolecular) energy and to a lesser extent into torsional energy. As the deformation proceeds, the non-bonded energy of the system rises further at a slower rate and the torsional energy decreases. The amount of energy stored into bonds and bond angles is relatively small (whereas certainly the bonds contribute substantially to the total stress).

A possible explanation of these results is the following. Initial deformation is accommodated by a decrease in the density (an increase in the average distance between monomers) and by an increase of the bond lengths and the bond angles. At intermediate strain values a further increase of bond lengths and angles is prevented by conformational changes via dihedral angles; apparently the penalty for climbing the energy barriers of the torsion potential is smaller than the penalty for further increase of the bond lengths. In the final stage the amount of cheap conformational changes via the dihedrals is very limited; probably further conformational changes via dihedrals are accompanied by high non-bonded-energy

penalties. As a consequence the bond lengths increase further, resulting in an increase of the contributions from bond lengths to stress and energy.

For the FCOM case (Figures 4.5a and 4.5b) the picture is qualitatively similar to the FAA case for strains smaller than 0.4, although there are also essential differences for larger strain values. Whereas at strain values higher than 0.4-0.5 strain hardening, caused by a rise in the contribution of bond lengths and to a lesser extent of non-bonded interactions to the total stress, is observed for the FAA case; no strain hardening is observed for the case of FCOM. Furthermore an increase in the intramolecular non-bonded energy is observed in the FAA case. In the FCOM case this increase is absent. Quantitatively there are large differences. The amount of work turned into energy is more than twice higher than in the FAA case, which has to be attributed to the stronger increase of non-bonded energy in the FCOM-case. Furthermore the fluctuations of the total stress, primarily caused by the fluctuations of the bond lengths, are less than those in the FAA case. The differences

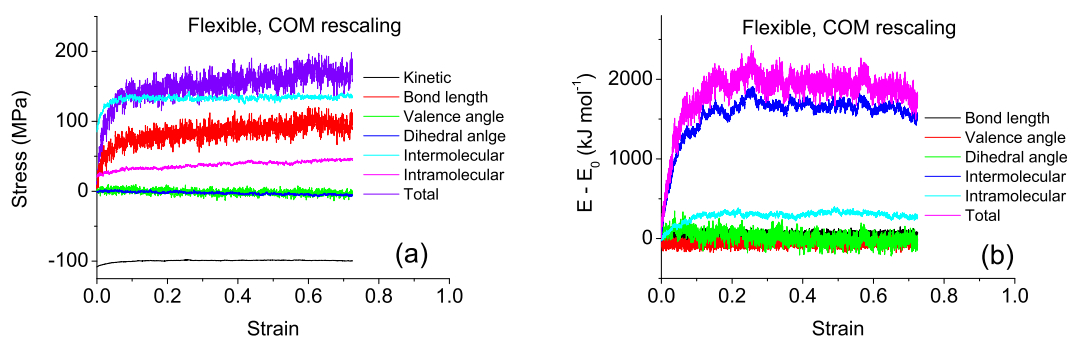


Figure 4.5: (a) Stress partitioning and (b) energy partitioning of PE samples during uniaxial deformation in the flexible-bond model, with COM-coordinates of all chains scaled affinely with the box size. The zero-strain values of all energy contributions have been shifted to zero.

between FAA and FCOM are not entirely clear. The fact that in both cases, in spite of the clear differences in the two deformation protocols, the contributions to stress from the non-bonded interactions and from the bond lengths first increase and then level off can be understood. In the FAA protocol the bond lengths are actively changed during deformation steps, and therewith the contribution of the bond lengths to the stress. In between deformation steps the bonds are relaxed to some extent, thereby transferring part of the stress to the non-bonded interactions. As a result both contributions from bond lengths and non-bonded interactions rise simultaneously. For FCOM the bond lengths and angles do not change during the deformation steps, however the deformation protocol can result in close approach of monomers in different chains. This results in very large contributions of intermolecular non-bonded interactions to the total stress. In between deformation steps part of the stress is transferred to the bonds. Therefore also for FCOM both contributions increase at the same time. Figure 4.6 shows two short parts of different

chains. Immediately after a deformation step (FCOM) monomers i and j are very close. Shortly after, adjacent bonds deform to increase the distance between monomers i and j . For intermediate strain values the contributions of non-bonded interactions and bond lengths level off, for both FAA and FCOM; further increase is prevented by conformational changes via dihedral angles. The reason for the different strain-hardening behavior is not clear. For FAA it can be explained that there is strain hardening, see above. However, the absence of strain hardening for FCOM is not obvious. It might have to do with the fact that in case of FCOM the initial density drop is larger, so that at larger strain values the chance of close approach of the two monomers is smaller. The larger fluctuations in the FAA case (as compared to FCOM) of the total stress, caused by the fluctuation of bond lengths, is caused by the fact that in both the volume-fluctuation move and the lateral-size-fluctuation moves all bond lengths are changed in the FAA case (for FCOM this does not hold). For the case of RCOM the information on the evolution of the various contributions

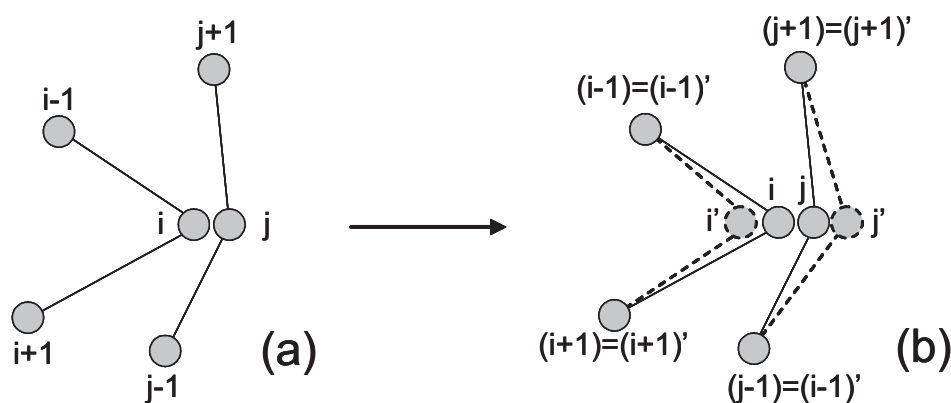


Figure 4.6: The COM deformation protocol can result in close approach of monomers, which is energetically very unfavorable; in (a) such a close approach between monomers i and j is shown immediately after a deformation step. Shortly after, adjacent bonds deform, see (b), to increase the distance between monomers i and j .

to the stress, see Figure 4.7a, is limited, because the stress was calculated according to Equation 4.2, based on interactions between chains. Since the kinetic contribution to the total stress is negligible, there is only one relevant contribution to the total stress, namely the intermolecular interactions, i.e., the non-bonded interactions between entire chain images, see Section 4.2. The evolution of the various contributions to the total energy is for RCOM given in Figure 4.7b. An even larger increase of non-bonded energy is observed than in case of FCOM. The torsional energy initially increases and then decreases again. At strain 0.5 all contributions go up sharply. The very high values of both stress and energy in case of RCOM with respect to FAA and FCOM can be understood from the fact that high non-bonded stress and energies caused by close approaches of monomers cannot be transferred to bond lengths, because the bonds are rigid. Only at intermediate strain values, between yield and strain hardening, this is less important, since in this strain

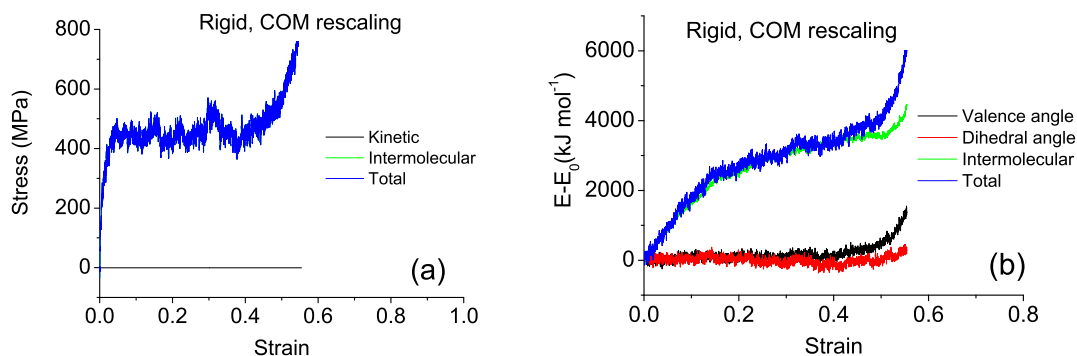


Figure 4.7: (a) Stress partitioning and (b) energy partitioning of PE samples during uniaxial deformation in the rigid-bond model, with COM-coordinates of all chains scaled affinely with the box size. The zero-strain values of all energy contributions have been shifted to zero.

region stress and energy increase are slowed down by conformational rearrangements via dihedrals.

In summary one may conclude that only the FAA case reproduces the typical stress-strain behavior of glassy amorphous polymers and produces reasonable values for quantities like E-modulus and yield stress. Furthermore it was shown that the non-bonded-interaction contributions to the total stress and to the total energy increase sharply in the initial stage of deformation in all three cases. Subsequently, at intermediate strain values, a decrease in torsional energy takes place in all three cases, indicating conformational changes involving the dihedrals. Finally stress and energy increase further, also via contributions involving the hard degrees of freedom (for FAA and RCOM only).

4.3.6 Structural properties

To verify our picture we also monitored the structural evolution of our sample during deformation. As shown in Figure 4.8 the densities evolve differently for all three cases. The density for FAA initially decreases in the elastic regime until the yielding sets in. After yielding, constant-volume deformation of the sample is observed. In case COM rescaling is used, and the same qualitative picture is obtained, however with an exaggerated initial decrease in volume. The density in the rigid-bond model keeps decreasing as deformation progresses, which is very unrealistic. To show more detail the probability densities of structural parameters before and at the end of deformation have been plotted, see Figure 4.9. The results for FAA (Figure 4.9a and 4.9b) are quite similar with what was observed in our previous study of the deformation of an amorphous PE-like polymer glass [83]. In Figure 4.9a it is shown that the fraction of dihedrals in the trans state grows under

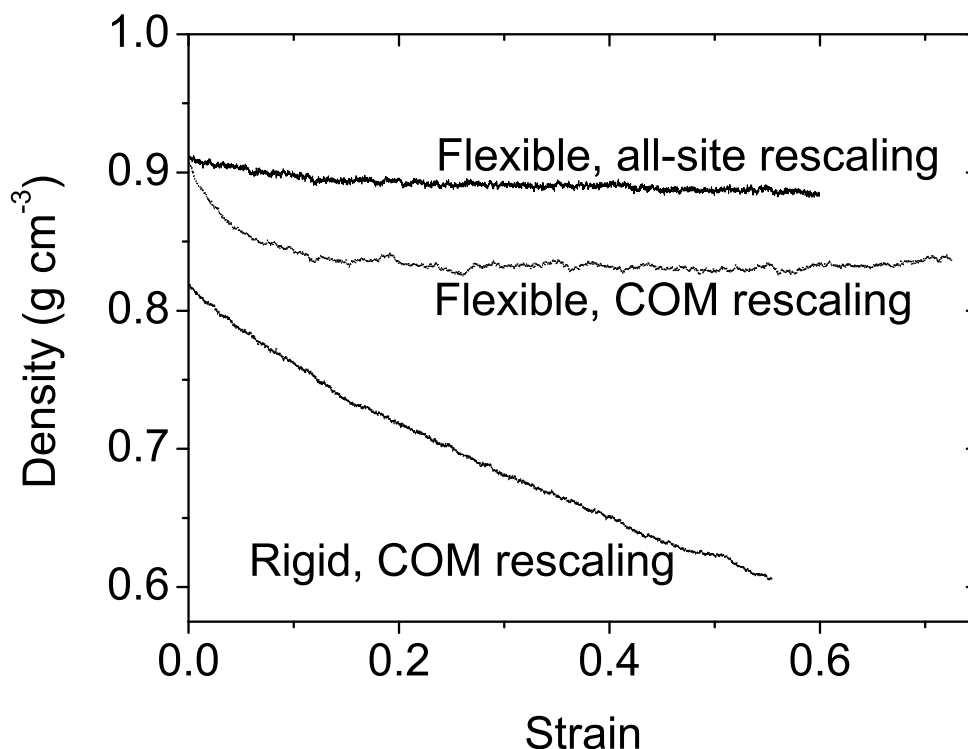


Figure 4.8: Evolution of densities during uniaxial deformation for both models.

deformation. Furthermore the intramolecular pair-correlation function, see Figure 4.9b, reveals that during deformation the heights of the peaks beyond the first peak (at $r = 2^{1/6}\sigma = 4.4 \text{ \AA}$) increase, indicating the unfolding of chains. For FCOM the same picture is obtained, although the intramolecular pair-correlation function shows a less pronounced increase of the peaks beyond the first peak.

For RCOM we observe once more an increase in the number of trans dihedrals and an increased height for peaks beyond the first peak of the intramolecular pair-correlation function. In addition all peaks of both the intramolecular and the intermolecular pair-correlation function rise during deformation, indicating larger spatial density fluctuations in the material after deformation than before. These strong spatial density fluctuations are also seen in Figure 4.10, where lateral snapshots are shown at the end of deformation both for FAA and for RAA. Clearly the density fluctuations are stronger for the RAA case. One point of concern when comparing FCOM and RCOM is the fact that in the two cases the starting materials are different (see Figure 4.9), e.g. the fraction of dihedrals in the trans state is quite different for the two models. It is not clear how this difference in materials, prior to deformation, contributes to the observed differences during deformation.

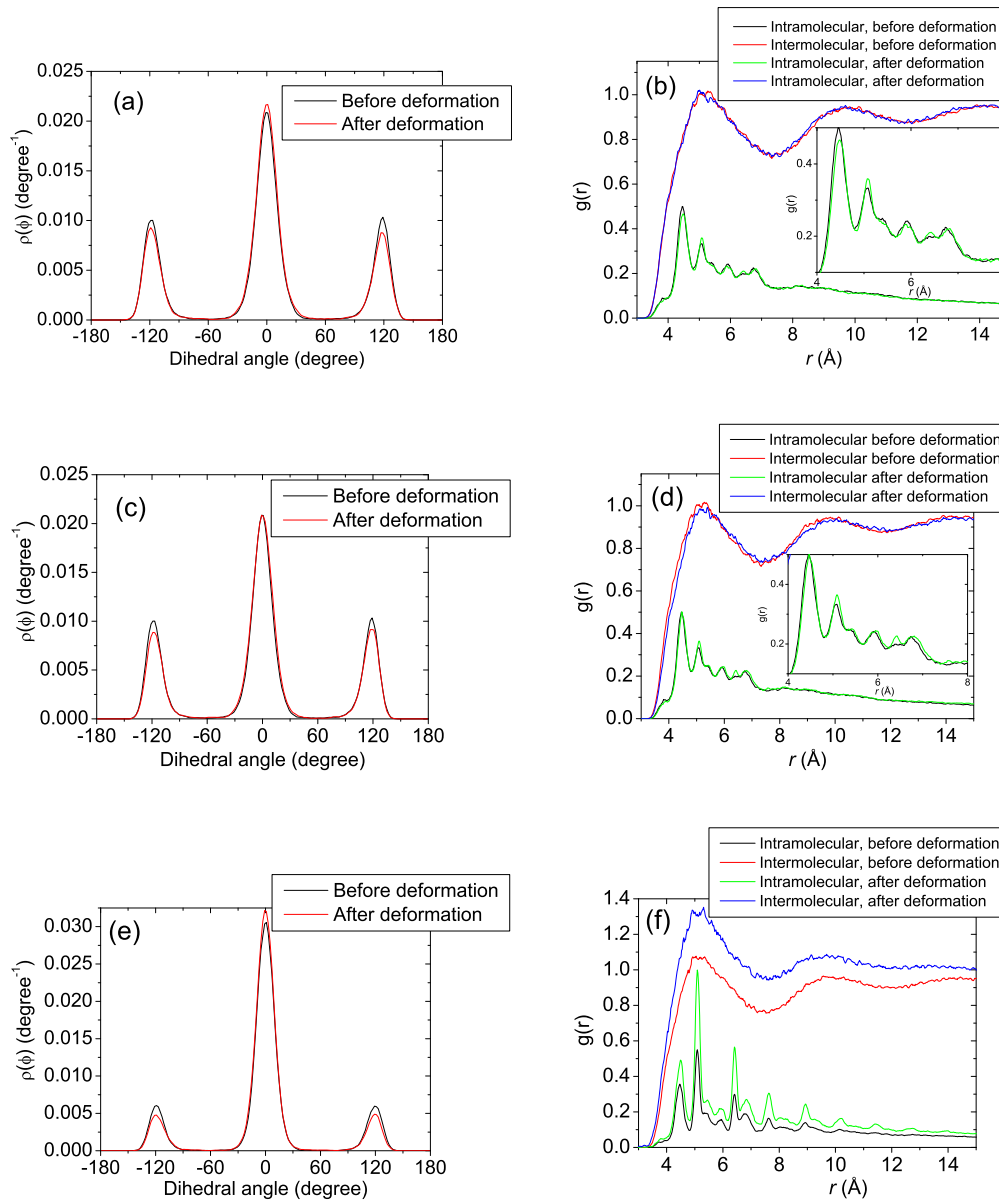
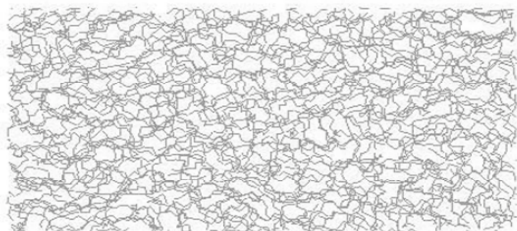


Figure 4.9: Probability densities of dihedral angle and non-bonded distance before and after deformation: in the flexible-bond model using AA ((a) and (b)), in the flexible-bond model using COM rescaling ((c) and (d)), and in the rigid-bond model using COM rescaling ((e) and (f)). The temperature is 200 K and the deformation velocity is 5×10^{-6} MCS $^{-1}$.

4.4 Conclusions

The deformation of glassy amorphous polymers has been studied by MC. The influence of both the internal molecular constraints and the deformation protocol on the details of the deformation process has been investigated.

(a) the flexible-bond model



(b) the rigid-bond model

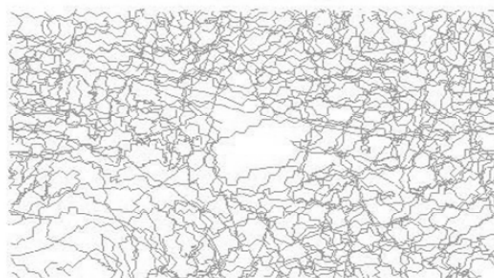


Figure 4.10: The lateral snapshots of the PE structures at the end of uniaxial deformation in (a) the flexible-bond model using AA and (b) the rigid-bond model using COM. The temperature is 200 K and the deformation velocity is 5×10^{-6} MCS $^{-1}$.

First well-equilibrated initial samples have been prepared in the melt. Subsequently these samples have been cooled into the glassy state. Finally the resulting samples have been deformed. Three cases have been investigated: 1) deformation of the model polymer without constrained bond lengths, employing a deformation protocol where the positions of all atoms (monomers) are scaled affinely with the box size (FAA), 2) idem, employing a deformation protocol where the COM-coordinates of all chains are changed affinely with the box size (FCOM), and 3) deformation of the model polymer with constrained bond lengths, employing a deformation protocol where the COM-coordinates of all chains are changed affinely with the box size (RCOM).

The different models and deformation protocols have been compared on the basis of stress-strain curves, density-strain curves, and contributions of different interactions to the stress and to the internal energy of the system. A comparison of the three cases on the basis of the stress-strain curve shows that only the FAA case gives the typical behavior of glassy, amorphous polymers, with realistic values for E-modulus and yield stress. For FCOM and RCOM the values of these quantities are respectively half an order and one order of magnitude too high. In none of the cases the strain-hardening moduli are reproduced, not even the order of magnitude is correct. From the comparison of the evolution of the contributions of various interactions to the total stress and total energy the following picture has been obtained. The non-bonded-interaction contributions to the total stress and to the total energy increase sharply in the initial stage of deformation in all three cases; in case of FAA and FCOM this is accompanied by an increase in the contribution of bond lengths. Subsequently, at intermediate strain values, stress and energy increase slow down; a decrease in torsional energy indicates that conformational changes involving the dihedrals take place in all three cases. Finally stress and energy increase further, also via contributions involving the hard degrees of freedom (for FAA and RCOM only).

Also only for the FAA case a realistic density evolution was observed. Both for FAA and

for FCOM an initial decrease in the visco-elastic regime is obtained, followed by constant-volume deformation after yield. However in FCOM the initial decrease is exaggerated. For the RCOM case the density keeps decreasing during the whole deformation. Closer inspection of evolutions of dihedral angle distribution shows an increase in the fraction of dihedrals in the trans state; from the intramolecular pair-correlation functions one can learn that chains become more extended during deformation in all three cases. Furthermore, in case of RCOM, from the evolution of both intermolecular and intramolecular pair-correlation functions it is observed that the spatial density fluctuations increase strongly during deformation.

All in all both the introduction of constrained bonds and the deformation protocol have a huge influence on results obtained from molecular simulation of glassy-polymer deformation. After studying three different combinations of constraint conditions and deformation protocol (FAA, FCOM, RCOM), the results obtained with the flexible bond model in combination with a deformation protocol where the positions of all monomers are scaled affinely with the box size (FAA) show the best agreement with experimental observations. However, the high value of the strain-hardening modulus remains a problem.

Chapter 5

Generalization of the EBMC algorithm to polymers of type $(AB)_n$: application to atactic PS

ABSTRACT

An end-bridging (EB) Monte Carlo (MC) algorithm has been developed, to create well-equilibrated atactic polystyrene (aPS) samples for molecular simulations. The algorithm is a modification of an algorithm that was originally developed for polyethylene (PE). Because of foreseen problems of applying the EB technique to atomistic PS, such as the infeasibility of implementation and a negligible acceptance of the EB move due to large non-bonded energy penalties, a coarse-grained description of aPS is used; monomers are represented by two coarse-grained atoms. Main points of concern for the implementation were the preservation of the correct chemistry and tacticity during reptation and EB moves. The algorithm produces correct polymer conformations on all length scales, beyond the size of the coarse-grained atoms. The code is also very efficient, even though the acceptance of 0.001-0.005% is approximately 10-100 times lower than in the original EB code for PE. Systems of aPS of the order of 5000 monomers can be equilibrated on all length scales within a week, in a single-processor run; the chain end-to-end-vector auto-correlations show complete decay to zero. The code is also adequate for simulations of other polymers that have the same regularity in their sequence of chemical groups and that are modeled at the same or at a coarser level of description.

5.1 Introduction

Connectivity-altering Monte Carlo (MC) algorithms like end-bridging Monte Carlo (EBMC) are very powerful tools for obtaining well-equilibrated polymer melts. EBMC was introduced in 1995 [54] for equilibration of polyethylene (PE) in the melt. A (united)-atom-level description of PE was used. Later it was also implemented for a few other polymers such as polypropylene (PP) [123] and polyisoprene [124, 125]. It would be interesting to apply the EB technique to many other polymers, such as PS and PC (typical examples of a brittle and a tough polymer respectively).

One possibility is developing a new code for any polymer that is somehow interesting. But this is not very smart: The implementation of the method for any polymer is a very tedious job, certainly if the polymer of interest is modeled at the atomistic or united-atomistic level. The change of connectivity in simulations already asks for a lot of administration for simple polymers, such as PE, that can be modeled with one type of bead for (half a) monomer, and even more so if the polymer is more complex. So for the development of an EB code for any new polymer a huge time investment is required. And the result is only of limited use since the final algorithm can be used for one specific polymer only. Even worse, one always runs the risk that the acceptance of the EB move is extremely low in case the polymer backbone is bulky and stiff, so low that hardly any moves will be accepted during the simulation. All-in-all the implementation of connectivity-altering moves for polymers described at the atomistic level becomes a risky embarkment.

However one should realize that the merit of EBMC is the possibility to equilibrate polymers on the largest length scales. Equilibration on small and intermediate length scales can also be accomplished by other techniques (MC with more local moves, or MD). Because of this one could follow a two-step approach to equilibrate the polymer sample. In the first step the sample is equilibrated on the long and intermediate length scales, i.e., at the length scales of the end-to-end distance and the length of a Kuhn segment respectively; during this step the polymer is described at a somewhat coarse-grained level and EBMC is used. To that end an existing algorithm for EBMC simulation of PE is generalized to coarse-grained polymers. In the second step atomistic detail is reintroduced and the sample is equilibrated at small length scales, i.e., a few bond lengths. The advantages of this approach over the one mentioned above is that implementation of EBMC at the coarse-grained level is much easier than at a more detailed level. Furthermore the resulting algorithm is applicable to the large class of polymers for which a coarse-grained description has a comparable functional form. A final advantage is that coarse-graining will increase the acceptance probability of connectivity-altering moves.

To execute the plan sketched in the previous paragraph, one has to decide on the degree of coarse-graining one prefers to use. Figure 5.1 gives an overview of the various levels of description for polystyrene. Apart from the most detailed levels of description, being the all-atom level and the united-atom level (where all hydrogen atoms are lumped into

neighboring carbon atoms) on the one hand, and the level of a freely-jointed chain (consisting of segments representing Kuhn elements) on the other hand, there is the level of intermediate detail $p:1$ (p coarse-grained beads represent 1 monomer). The all-atom level and the united-atom level are too detailed for our purposes. The freely-jointed model is too coarse to incorporate all important chemistry-specific details. The level of $p:1$ coarse-graining may be chosen detailed enough to distinguish different polymers and still coarse enough to make the development of connectivity-altering algorithms that can be used for many different polymers feasible. However, in this level of intermediate detail there are many possibilities. 1:1 coarse-graining has been performed a lot by Milano and coworkers, for example for vinyl polymers [53]. Later on it has been applied as well by Vettorel et al. [126] for PE and by Spyriouni et al. [127] for polystyrene (PS). In the group of Kremer 2:1 coarse-graining is performed for example by Tschöp et al. [128] for bisphenol-A-polycarbonate (BAPC) and by Harmandaris et al. [95] for PS. In some cases, especially for larger monomers, with more soft degrees of freedom than for example vinyl polymers, it seems desirable to represent monomers by more than one coarse-grained particle. To prevent artefacts in the melt structure, 1:4 coarse-grained representations have been used for both BAPC [129] and poly(ethylene terephthalate) [130].

We are interested in obtaining well-equilibrated polymers in the bulk; especially typical glassy amorphous polymers. To that end we decided to follow the two-step equilibration procedure sketched above. To execute the first step, the level of coarse graining has been chosen that forms the best compromise between feasible implementation of EB on the one hand and not losing structural detail on the other hand. Such a compromise has been found in the 2:1 level of coarse graining. Moreover at this level force fields of typical glassy amorphous polymers such as PS and PC are available.

For equilibrating at the 2:1 level of coarse-graining, an EB algorithm has been developed. An existing EBMC code for equilibration of PE in the melt has been used as the starting point. Rigorous modifications in all energy calculations and lists containing interacting particles had to be developed. Furthermore a proper administration of alterations in the connectivity had to be set up, involving measures to prevent undesired changes in chemistry or tacticity. These tasks proved very cumbersome, justifying a generic approach that should be applicable to a whole class of polymers. After implementation, the algorithm is demonstrated for the 2:1 coarse-grained PS model developed by Harmandaris et al. [95]. The algorithm is tested on internal consistency and on performance, in terms of the CPU time needed to obtain well-equilibrated polymer melts of coarse-grained PS. The coarse-grained polymer structures resulting from simulations using the 2:1 coarse-grained PS model are used as an input for a procedure to reinsert atomistic detail, see the next Chapter .

In the course of this project the work of Spyriouni et al. [127], dealing with connectivity-altering simulations of 1:1 coarse-grained PS, appeared. Spyriouni et al. were successful in preparing PS in the melt with correct global chain conformations; on the more local level, discrepancies were observed between their distributions of dyad conformations and

those suggested by NMR data of Robyr et al. [131–133]. This justifies renewed attempts, such as ours, to prepare well-equilibrated PS. In general, our algorithm, which is applicable to other polymers than PS as well, is very useful when more detail than provided by 1:1 models is required.

The remainder of this Chapter is structured as follows. In Section 5.2 the generalization of the EBMC algorithm to polymers of type $(AB)_n$ and the 2:1 coarse-grained model for PS from Harmandaris et al. [95] are thoroughly explained. Subsequently results of tests of the algorithm on dimers and oligomers are presented in Section 5.3. Finally the algorithm is applied for the equilibration of long-chain polymer melts, as reported in Section 5.4. Conclusions are drawn in Section 5.5.

5.2 Coarse-grained polymer models and generalization of EBMC

In all $p:1$ coarse-grained models mentioned in the introduction, the polymer underneath is represented by coarse-grained beads connected in a chain without side groups. The amount of different types of beads does not exceed p . For $p = 1$, the force field controlling the motions in any degree of freedom in the coarse-grained system is simple. One needs bonded potentials controlling bond lengths, bond angles and dihedrals of the polymer backbone, and non-bonded potentials to control interactions of beads in different chains or in the same chain but separated by more than (dependent on details of the model) three or four bonds (excluded volume effect have to be taken into account properly). Clearly, with increasing p necessarily more details are included in the force field; but in addition incorporation of tacticity can add to its complexity. In the 2:1 representation of PS, as developed by Harmandaris et al. [95], tacticity information is also incorporated. In our generalization of the EBMC algorithm for PE, we take this into account, since we are particularly interested in PS. In the remainder of this Section the model of Harmandaris et al. [95] is explained first. Subsequently its implementation in the EBMC algorithm is discussed.

5.2.1 The 2:1 coarse-grained model of PS

We make use of the force field developed by Harmandaris et al. [95]. The mapping they use is schematically depicted in Figure 5.1. A-beads represent CH_2 -groups on the polymer backbone, B-beads $\text{CH}(\text{C}_6\text{H}_5)$ -groups. Tacticity is incorporated by labeling the B-beads with a + or -. After defining the direction of propagation along the chain, the tacticity label of any B-bead can be unambiguously determined as the sign of $(\vec{u}_1 \times \vec{u}_2) \cdot \vec{u}_p$, see Figure 5.2.

The various bond lengths, bond angles and dihedral angles in the coarse-grained model

Molecular models: from fully atomistic to freely-jointed chains

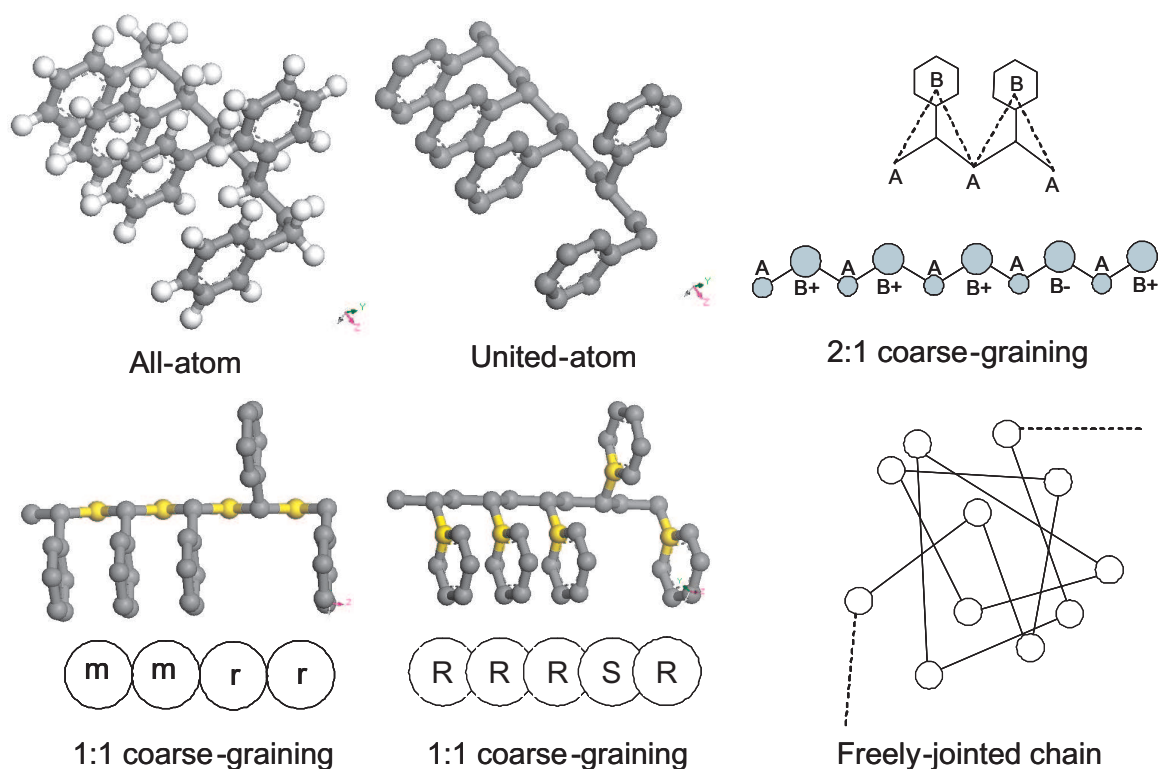


Figure 5.1: Overview of the various levels of description for polystyrene, from the most detailed (being the all-atom level), via the united-atom level (where all hydrogen atoms are lumped into neighboring carbon atoms) and the more coarse-grained levels 2:1 (2 CG beads represent 1 monomer) or 1:1 (1 CG bead represents 1 monomer), to the level of a freely-jointed chain (consisting of beads and joints representing Kuhn segments). In the 1:1 coarse-graining example in the lower part left the coarse-grained beads are centered at the CH_2 units, in the example in the lower part in the middle the coarse-grained beads are centered at the C-atoms at the first positions in the phenyl rings. The symbols in the beads contain information on tacticity (details can be found elsewhere [53]).

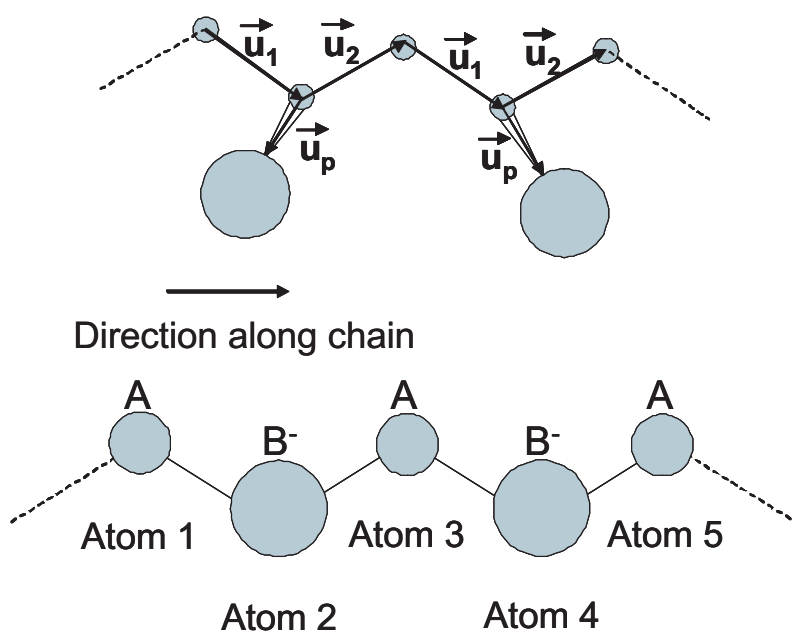


Figure 5.2: Elementary particles of the CG model. The upper part of the Figure shows a representation of PS that is very close to the atomistic one. The small beads represent backbone atoms lumped together with hydrogens, the large particles represent phenyl rings. The lower part concerns the CG description employed in this Chapter. Three elementary particles are used: A for the CH₂-backbone groups, and both B⁺ and B⁻ for CH(C₆H₅)-groups. The sign attached to the B contains information on tacticity.

are controlled by force-field terms that are potentials of mean force of the coarse-grained degrees of freedom. These potentials of mean force have been obtained in atomistic simulations of isolated PS dimers, by sampling conformational distribution functions $\rho^{CG}(\{b_i\}, \{\theta_i\}, \{\phi_i\}, T)$, where $\{b_i\}$, $\{\theta_i\}$, $\{\phi_i\}$ and T represent the bond lengths, bond angles, dihedral angles and temperature, respectively. After making the standard assumption that there exist no correlations between different degrees of freedom in the system, ρ^{CG} factorizes:

$$\rho^{CG}(\{b_i\}, \{\theta_i\}, \{\phi_i\}, T) = \prod_{i=1}^n \rho^{CG}(b_i, T) \prod_{i=1}^{n-1} \rho^{CG}(\theta_i, T) \prod_{i=1}^{n-2} \rho^{CG}(\phi_i, T) \quad (5.1)$$

The bonded potentials are obtained from inverse Boltzmann relations $U^{CG}(x, T) = -k_B T \ln \rho^{CG}(x, T)$, x being a spatial coordinate. The probability density functions $\rho^{CG}(x)$ for $x \in \{b_i\}$ and for $x \in \{\theta_i\}$ have been normalized by respectively r_i^2 and $\sin(\theta_i)$ to take into account the size of volume elements. From now on T will be left out since all simulations discussed here were done at one temperature (463 K) and the notation will be ρ_x^{CG} . The distributions before normalization will be referred to as P_x^{CG} from here onwards.

Details of the different bonded potentials are given in Table 5.1 and Figure 5.3. One type of bond length, three types of bond angles and four types of dihedral angles are distinguished. The potentials associated with bond length and ABA bond angles can be well approximated by harmonic functions, all the other bonded potentials are numerical and are shown in Figure 5.3. Tacticity is incorporated in the bond-angle and dihedral potentials. The use of improper torsional potentials [96] is therefore not necessary to maintain tacticity.

In addition to the bonded interactions mentioned, there are the non-bonded interactions between coarse-grained beads in different chains and interactions between coarse-grained beads within one chain of type 1-4 and beyond, i.e., separated by at least three coarse-grained bonds. Details on these non-bonded interactions are also given in Table 5.1. The relevant parameters for the pair interaction of A-beads are taken from the TraPPE-UA model [134] for atactic PS, those for the pair interaction of B-beads are derived from the potential of mean force between two toluene molecules as a function of the distance between them. Application of the Lorentz-Berthelot mixing rules [56] renders the parameter values of interaction of an A-bead with a B-bead: geometrical mixing ($\epsilon_{AB} = \sqrt{\epsilon_{AA}\epsilon_{BB}}$) for the energy parameter and linear mixing ($\sigma_{AB} = \frac{\sigma_{AA} + \sigma_{BB}}{2}$) for the length parameter.

Table 5.1: The coarse-grained PS force field from Harmandaris et al. [95]. The potentials for different types of coarse-grained bond lengths, bond angles and dihedral angles result from Boltzmann inversion of the corresponding distribution functions obtained from atomistic simulations; the potentials associated with the bond lengths and with θ_{ABA} -type bond angles can be approximated by harmonic functions. Bond angles are defined as $\theta = \pi - \arccos(\frac{\vec{u}_1 \cdot \vec{u}_2}{|\vec{u}_1||\vec{u}_2|})$, dihedral angles ϕ are defined such that $\phi \in [0, 2\pi)$ with $\phi = 0$ corresponding to the cis conformation and with clockwise direction of rotation. The Lennard-Jones-type potentials concern both the interactions between coarse-grained beads in different chains and the interaction between coarse-grained beads within one chain of type 1-4 and beyond, i.e., separated by at least three coarse-grained bonds.

Interaction type	Functional form	Parameters
Bond length b	$U_b = \frac{1}{2}k_b(b - l_0)^2$	$k_b = 700 \text{ kJ}\text{\AA}^{-2}\text{mol}^{-1}$, $l_0 = 3.4 \text{ \AA}$
Bond angles θ_{ABA} $\theta_{B^\pm AB^\pm}$ $\theta_{B^\pm AB^\mp}$	$U_{\theta_{ABA}} = \frac{1}{2}k_{\theta_{ABA}}(\theta_{ABA} - \theta_0)^2$ $U_{\theta_{B^\pm AB^\pm}}$ $U_{\theta_{B^\pm AB^\mp}}$	$k_{\theta_{ABA}} = 5.78 \times 10^3 \text{ kJ rad}^{-2}\text{mol}^{-1}$, $\theta_0 = 0.78 \text{ rad}$ numerical, see Figure 5.3 numerical, see Figure 5.3
Dihedral angles $\phi_{AB^- AB^-}$; $\phi_{B^+ AB^+ A}$ $\phi_{B^- AB^- A}$; $\phi_{AB^+ AB^+}$ $\phi_{AB^+ AB^-}$; $\phi_{B^+ AB^- A}$ $\phi_{AB^- AB^+}$; $\phi_{B^- AB^+ A}$	$U_{\phi_{AB^- AB^- / B^+ AB^+ A}}$ $U_{\phi_{B^- AB^- A / AB^+ AB^+}}$ $U_{\phi_{AB^+ AB^- / B^+ AB^- A}}$ $U_{\phi_{AB^- AB^+ / B^- AB^+ A}}$	numerical, see Figure 5.3 numerical, see Figure 5.3 numerical, see Figure 5.3 numerical, see Figure 5.3
Non-bonded r_{ij} , $i, j \in A, B$	$U_{\text{LJ},ij} = 4\epsilon_{ij} \left[\left(\frac{\sigma}{r-r_{ij}} \right)^{12} - \left(\frac{\sigma}{r-r_{ij}} \right)^6 + \frac{1}{4} \right]$	$\sigma = 4.25 \text{ \AA}$, $r_{\text{cutoff}} = r_{ij} + 2^{1/6}\sigma$ $\epsilon_{AA} = 0.383 \text{ kJ mol}^{-1}$, $r_{AA} = 2^{1/6}(\sigma_{AA} - \sigma)$, $\sigma_{AA} = 3.95 \text{ \AA}$ $\epsilon_{BB} = 3.85 \text{ kJ mol}^{-1}$, $r_{BB} = 2^{1/6}(\sigma_{BB} - \sigma)$, $\sigma_{BB} = 4.55 \text{ \AA}$ $\epsilon_{AB} = \sqrt{\epsilon_{AA}\epsilon_{BB}}$, $r_{AB} = 2^{1/6}(\sigma_{AB} - \sigma) = 0$, $\sigma_{AB} = \frac{\sigma_{AA} + \sigma_{BB}}{2}$

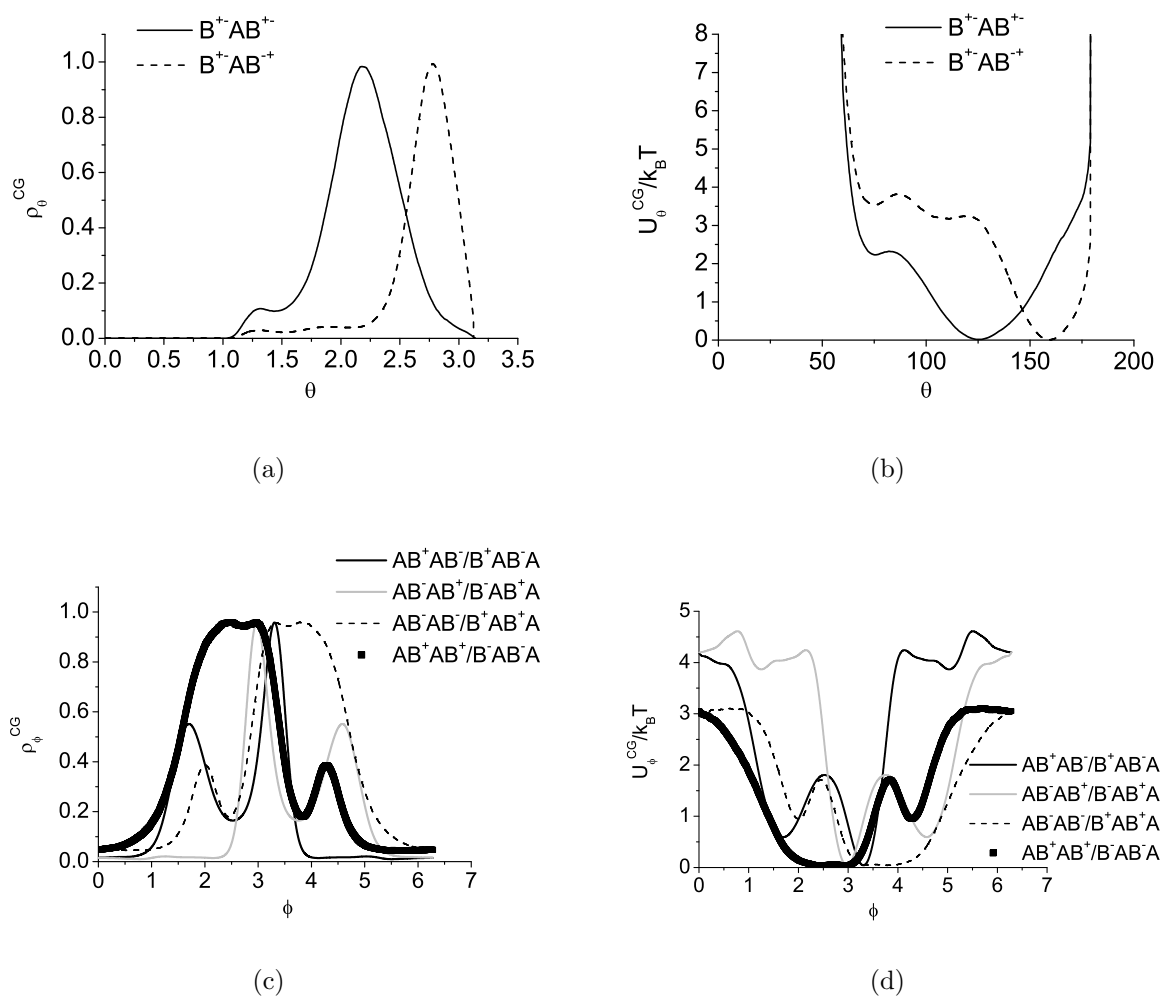


Figure 5.3: Distributions of coarse-grained bond angles (a) and dihedral angles (c), and the force-field components (b) and (d) obtained from these distributions using inverse Boltzmann relations.

5.2.2 Generalization of EBMC to simulate coarse-grained systems

The starting point was an EBMC algorithm designed for and particularly efficient in equilibrating systems of PE chains of realistic molecular weight ($M_w \gg 1$ kDa) in the melt, see refs [54, 55] and Section 2.3.2 of this thesis. All moves described there could be used again, although sometimes under constrictions, as explained below.

The force field described in Section 5.2.1 has been converted into tables which are read by the EBMC program. Onto the coarse-grained beads of the initial sample, type labels have been tagged (A, B⁺ or B⁻), in order to distinguish different kinds of beads and sequences of beads. In addition to changing the input, all routines dealing with energy calculations (or calculation of forces) have been modified. On top of this all kinds of lists have to be changed, see Section 2.3.2. The "overlap list" is now based on the largest Lennard-Jones parameter (σ_{BB}) in the force field; all atoms are allocated to cells of size $\sigma_{BB}(1 + \delta)$ with $0 < \delta \ll 1$. A similar modification was needed for the "linked-cell list"; the size of the linked cell is now dictated by the range $r_{cutoff} = 2^{1/6}\sigma_{BB}$ (see Table 5.1) over which Lennard-Jones interactions between particles of type B (B⁺ or B⁻) are calculated. For many local types of moves, such as flip, end rotation, intra-chain rebridging (see Chapter 3, in particular Figure 3.1) and volume fluctuations this suffices.

Moves involving connectivity changes, in this case reptation and end bridging, required more measures. One point of attention is the prevention of wrong bead sequences. Reptation moves of chains with an A-bead (B-bead) on both chain ends would result in a sequence of two A-beads (B-beads), which is undesirable and results in a crash of the program, since interactions involving these bead sequences are not defined. This could be prevented by forbidding reptation for chains with the same kind of beads on both chain ends. Alternatively one could try to reptate a whole monomer (an A- and a B-bead together). However, test runs showed that the chance of successful attempts to reptate B-beads is one to two orders of magnitude lower than the chance on successful attempts to reptate A-beads, due to the larger size of the B-beads, which give rise to larger non-bonded-energy penalties for reptation. The chance of moving a whole monomer will be even lower and therefore whole-monomer reptations have not been implemented. The result of forbidding reptation for chains with the same type of beads on both chain ends results in a strongly decreased translational mobility of the chain ends for those chains; reptation of monomers as a whole results in low chain-end mobility for all chains. The consequence of this low chain-end mobility is that the efficiency of the EB move deteriorates, because of "shuttling" [72], i.e., successive EB moves annihilating each other (moves involving the same chain end are performed forward and backward for many times). Reptation leads to considerable changes in the environment near chain ends, and with that in the candidates for performing an end-bridging move from a particular chain end. Because of the reasons mentioned, we chose for single-atom reptation moves; to prevent undesired chemistry changes, initial samples have been prepared with exclusively chains that have different types of beads at both ends.

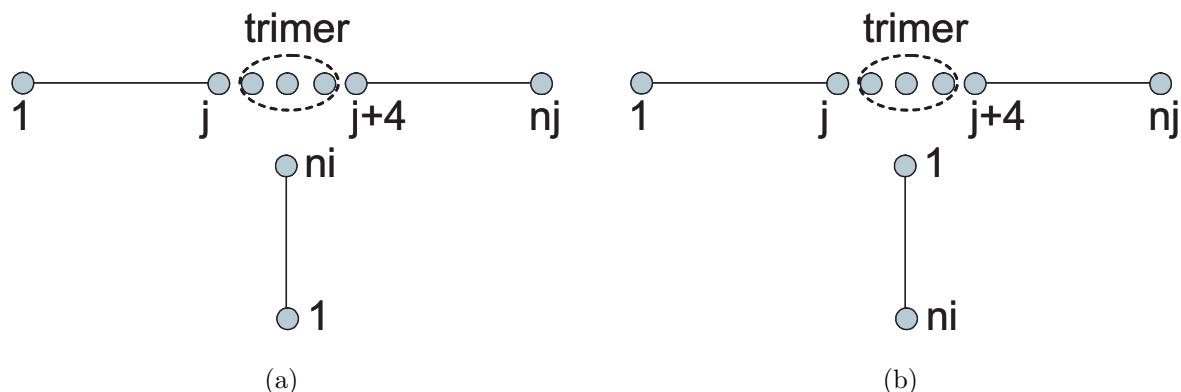


Figure 5.4: The end-bridging move often results in reversion of the chain direction for part of the chain. This is the case if the final bead n_i of the attacking chain attaches to bead j in the victim chain (see a)) or if the first bead of the attacking chain attaches to either bead j or bead $j+4$ of the victim chain (see b)).

During end-bridging wrong bead sequences have been prevented by adding the criterion that beads at both sides of the trimer bridge are of the same type. Furthermore, end-bridging moves that would result in chains with the same type of beads at both chain ends are prevented; this is necessary to prevent that subsequent reptation moves would result in undesired chemistry changes. A final issue is that in some cases the chain direction is reversed (at least for part of the chains involved in the particular end-bridging move), see Figure 5.4. The B-beads for which the chain direction is reversed change from B^+ into B^- and vice versa. This required additional administration involving temporary arrays with bead-type information of attempted configurations.

5.3 Testing the algorithm on small molecules

In order to test the algorithm for PS, various simulations have been done first for isolated dimers in vacuum. Comparison of Figures 5.3 and 5.5 shows that distributions of bond lengths, bond angles and dihedral angles in the dimer simulations are very similar to the distributions expected based on the force field.

To test how the algorithm performs as far as more global chain properties are concerned, simulations have been done of a melt consisting of short polymer chains ($M_w=1$ kDa). The distributions of bond lengths, bond angles and dihedral angles (all not shown here) reveal slight deviations from the distributions shown in Figure 5.3, that have to be attributed to intra-chain interactions beyond 1-4 and to inter-chain interactions. An additional test providing insight in the chain conformations on all length scales is via the intra-chain distance distribution, giving the average square spatial distance $\langle R^2(n) \rangle$ (or $\langle R^2(N) \rangle$)

between monomers in the same chain separated by n monomers (or by N coarse-grained beads) in the same chain. In Figure 5.6 this quantity, as obtained from the EBMC simulation mentioned, is given. $\langle R^2(n) \rangle$ is normalized by nb^2 , with b the average bond length in the coarse-grained representation of PS. This normalization is convenient since for large n there should exist a proportionality between $\langle R^2(n) \rangle$ and nb^2 (Gaussian chain conformations). Also shown is the same quantity from an MD simulation of the same system performed by Harmandaris [135]. The results are in close accordance.

After performing these initial checks, the performance of the algorithm regarding the equilibration of long-chain polymer melts has been studied. The results are presented in the next Section.

5.4 Equilibration of long-chain polymer melts

To study the performance of the EBMC algorithm for the equilibration of a melt ($T = 463$ K) of long PS chains, initial samples at the 2:1 level of coarse-graining are prepared according to the method discussed by Harmandaris et al. [92, 95]. In order to obtain a proper distribution of intra-chain distances, the approach described below is followed. Chains are created with a non-reversal random-walk algorithm [92]. For chains larger than 5 kDa all chains with a non-Gaussian conformation, i.e., not satisfying

$$R^2(N) = C_\infty^{CG} N b^2 \pm 0.15\% \quad \text{for } N > 100, \quad (5.2)$$

are discarded. The average bond length in the coarse-grained model is $b = 3.4$ Å. From b and the experimental value of the characteristic ratio C_∞ of polystyrene [136] it can be calculated that the characteristic ratio at the coarse-grained level C_∞^{CG} equals 3.5. (C_∞ equals 8.5 at 463 K and is based on atomistic PS models: $R^2(N) = C_\infty N l^2$ with $l = 1.54$ Å.)

Subsequently the chains are arranged randomly in a simulation box, which size is such that the density equals the experimental density [137] at the temperature studied. The resulting samples show huge local density fluctuations. In order to reduce the largest fluctuations, the samples are subjected to a zero-temperature MC simulation in which chains are only moved as rigid objects, thereby maintaining the correct distribution of intra-chain distances. In a next step MD simulations are performed, in which the non-bonded interactions are introduced slowly. As the initial distribution of intra-chain distances exhibits no overshooting at relatively small distances [92], it can be concluded that the preparation process did not result in locally overstretched chains.

After this thorough preparation process the sample is subjected to EBMC at an external temperature of 463 K and a pressure of 1 bar, i.e., the conditions under which the 2:1 coarse-grained force field for PS had been developed. Although the initial samples are

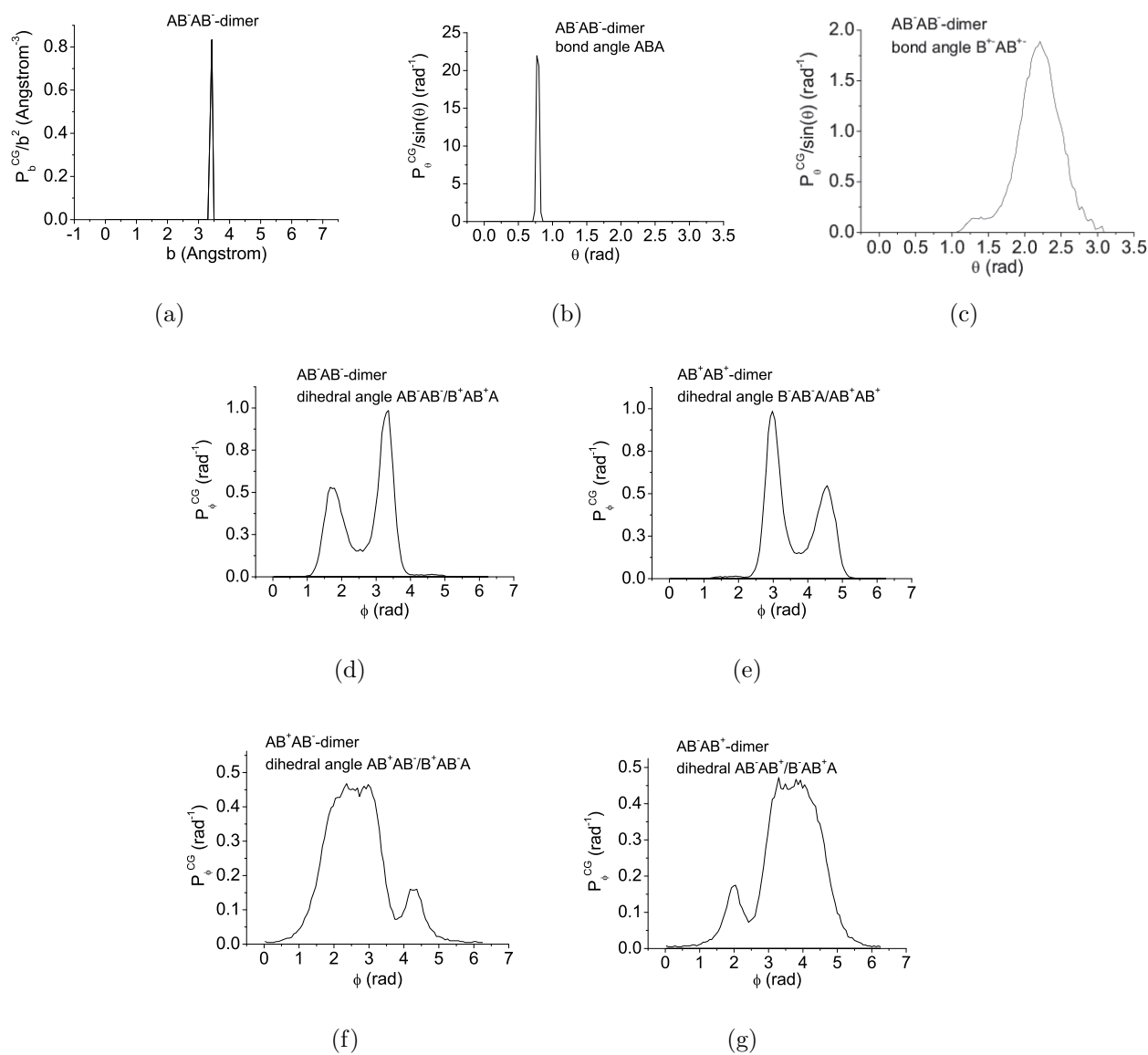


Figure 5.5: Results of various simulations of isolated dimers in vacuum. For an AB^-AB^- -dimer the distributions of bond lengths, bond angles and dihedral angles are shown, for three other dimers, an AB^+AB^+ -dimer, an AB^+AB^- -dimer and an AB^-AB^+ -dimer, only dihedral-angle distributions are shown. All distributions agree very well with the distributions expected on the basis of the force field, see Figure 5.3.

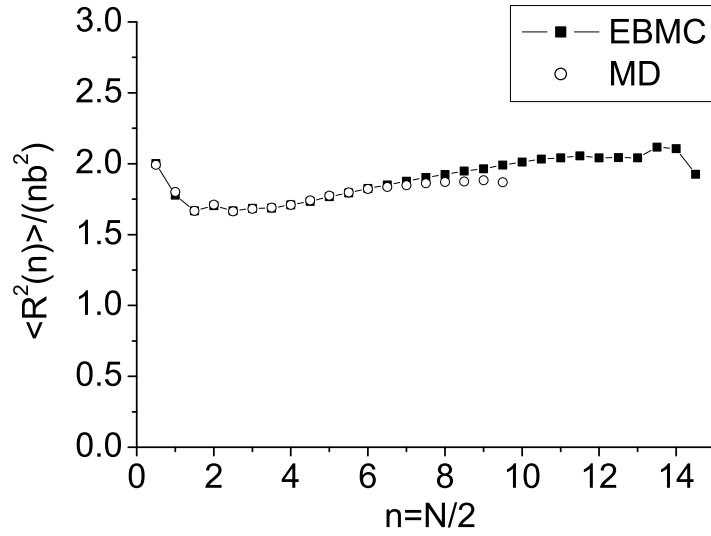


Figure 5.6: Distribution of intra-chain distances as obtained from simulations of short-chain polymer melts ($\langle M_w \rangle = 1$ kDa). Results from EBMC simulations agree well with those from MD simulations (red circles) performed by Harmandaris [135].

monodisperse (this is an arbitrary choice), in the EBMC run one has to allow for substantial polydispersity to make end-bridging moves possible. The spectrum of chemical potentials, see Chapter 2 and ref [54], is chosen such that the chain-length distribution is uniform in the interval from $\bar{X}(1 - \Delta)$ to $\bar{X}(1 + \Delta)$, where \bar{X} is the number-average degree of polymerization and Δ the half-width of the chain-length distribution reduced by the number-average chain length. The results below concern a sample of 50 chains for which $\bar{X}=96$ ($N=192$) and $\Delta =0.5$. To equilibrate the sample, end-bridging moves are combined with reptations, end rotations, flips and concerted rotations. The end-bridging moves constitute half of the attempt moves; the other half of the attempt moves is equally distributed over all the other types of moves. No volume fluctuations are allowed, because the non-bonded interactions are purely repulsive and unlimited expansion is only temporarily prevented by topological constraints (for unentangled systems expansion is not counteracted at all).

To judge the performance, the evolution of the internal energy has been studied, as well as the evolution of the M_w -distributions (from monodisperse at the start to uniform between $\bar{X}(1 - \Delta)$ and $\bar{X}(1 + \Delta)$); also the following autocorrelation function (ACF) of the end-to-end unit vector $\vec{u} = \frac{\vec{R}_{ee}}{|\vec{R}_{ee}|}$ has been calculated:

$$ACF_1(t) = \langle \vec{u}(0) \cdot \vec{u}(t) \rangle \quad (5.3)$$

In Figure 5.7 it is shown that the internal energy of the polymer sample, which is primarily related to local rearrangements, evolves to a final value within $(3 - 5) \times 10^3$ MCS. Full decorrelation of the end-to-end unitvector \vec{u} , which is an indication that the sample fully lost information on its initial state, requires 1×10^4 MCS, see Figure 5.8. For the evolution of the M_w -distribution from fully monodisperse towards uniform between $\bar{X}(1 - \Delta)$ and $\bar{X}(1 + \Delta)$ an equal amount of simulation time is required. The final M_w -distribution is given in Figure 5.9, together with the theoretical perfectly uniform distribution (grey line); the fact that the simulated distribution seems much higher can be attributed to very narrow bins used for its calculation. The acceptance of the end-bridging move was of the order of 0.001-0.005%, which is approximately 10-100 times lower than in the original EBMC code [55], developed for PE. The lower acceptance in case of PS is primarily caused by the larger excluded volume of the beads in PS than in of those in PE, whereas the bridgable distance is the same for both polymers. In spite of this low acceptance, equilibrating PS polymer melts with EBMC is very feasible: The simulations reported on here have been performed in one or two week's time using one Intel Itanium 2 processor (1,3 GHz, 3 Mbyte cache) on an SGI Altix 3700 system.

It would be interesting to compare the decorrelation of end-to-end unit vectors in the present EBMC simulations to the same decorrelation in an MD simulation of an equivalent system. Possibly for short chains (< 100 monomers) the difference is small. Still, because of the favorable scaling of the decorrelation time in EBMC simulations with the degree of polymerization [55], for systems of larger chains EBMC will definitely be the technique of choice for preparing well-equilibrated PS melts.

The correctness of the final result, i.e., the final structure, is checked via distributions of bond lengths, bond angles and dihedral angles, but also via the internal-distances distribution of the polymer chains and the single-chain static structure factor $S(\vec{q})$:

$$S(\vec{q}) = \frac{1}{N^2} \sum_{i=1}^N \sum_{j=1}^N \exp(i\vec{q} \cdot (\vec{r}_i - \vec{r}_j)) \quad (5.4)$$

where \vec{q} is the scattering vector and \vec{r}_i and \vec{r}_j are the position vectors of beads i and j . Distributions of bond lengths and angles again show slight deviations, from the distributions in Figure 5.3, caused by intra-chain non-bonded interactions and inter-chain interactions. The internal-distance distribution, shown in Figure 5.10(a), does indicate Gaussian chain conformations as it tends asymptotically to a constant value as N increases. However it does not approach $C_\infty^{CG} = 3.5$. Probably the chains are still too short. For example Spyriouni et al. [127] also observed that C_n approaches C_∞ only for $n \geq 300$. After rotational averaging of 5.4 one obtains:

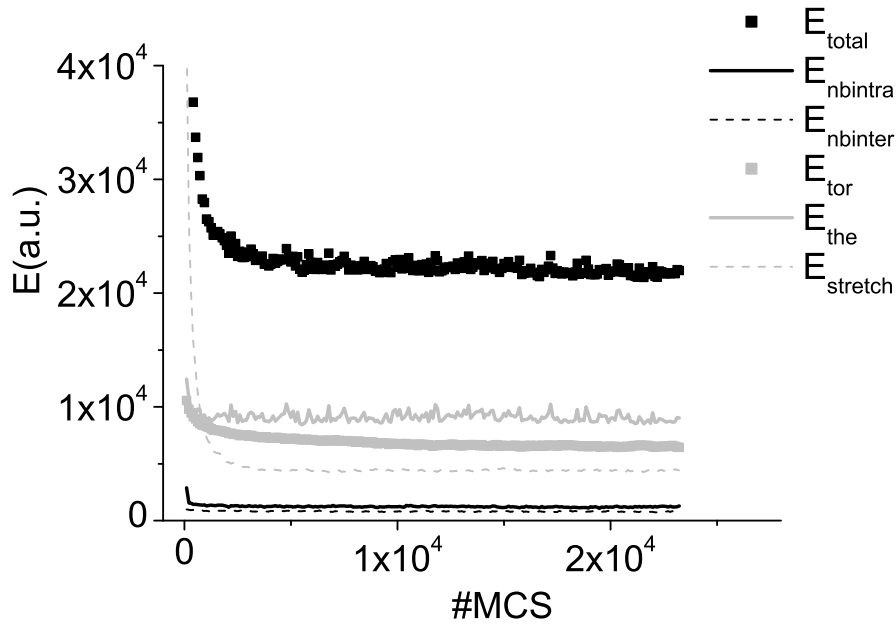


Figure 5.7: Internal-energy evolution, all components, i.e., the energies associated with respectively non-bonded interactions between monomers in the same chain ($E_{nbintra}$) or in different chains ($E_{nbinter}$), torsional angles (E_{tor}), bond angles (E_{the}) and bonds ($E_{stretch}$), are separated. Final values are reached within $(3 - 5) \times 10^3$ MCS.

$$S(q) = \frac{1}{N^2} \sum_{i=1}^N \sum_{j=1}^N \frac{\sin(q|\vec{r}_i - \vec{r}_j|)}{q|\vec{r}_i - \vec{r}_j|} \quad (5.5)$$

Kratky plots of 5.5 for chains of different length N (or, to be precise, chains with their degree of polymerization in different chain-length intervals) are given in Figure 5.10(b). The presence of a plateau in the curves indicates that the chain conformations are Gaussian.

All-in-all the end-bridging algorithm, modified for the equilibration of polymers at the 2:1 level of description, seems adequate for the equilibration of PS melts of polymer chains with a realistic M_w . Application of the algorithm to other polymers modeled at the 2:1 level of description, if necessary preceded by development of force fields that fit the EBMC algorithm, seems a road worthwhile to pursue. In this thesis work the focus will be on reinserting atomistic details of PS into the coarse-grained structures and studying various other structural properties at the atomistic level. The findings are presented in the next Chapter.

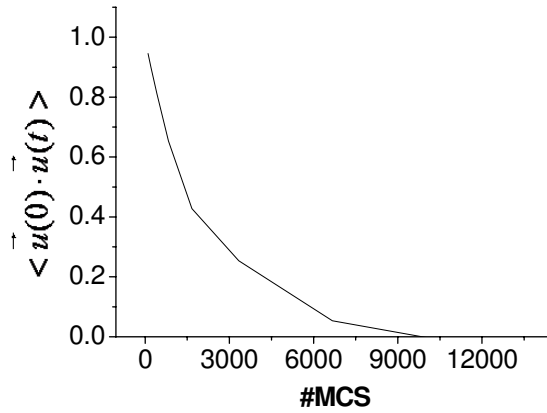


Figure 5.8: Autocorrelation function of the end-to-end unitvector $\vec{u} = \frac{\vec{R}_{ee}}{|\vec{R}_{ee}|}$.

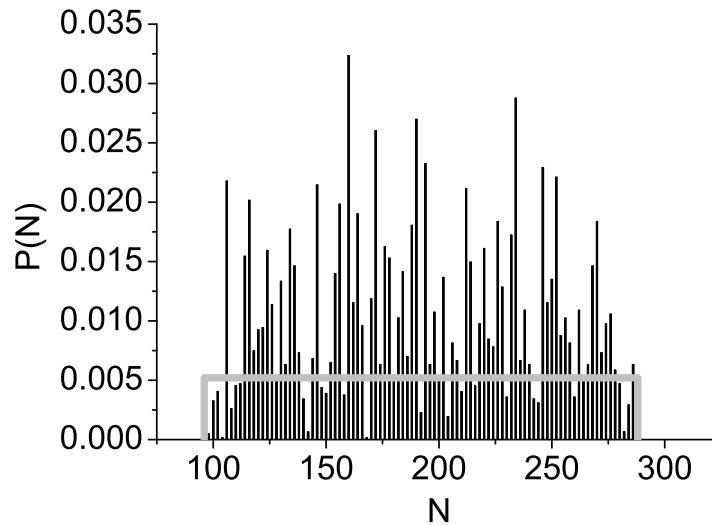


Figure 5.9: The distribution of chain lengths $P(N)$ (N being the number of beads in the chain) of the simulated PS melt is in accordance with the values chosen for the chemical potentials, which prescribe a uniform distribution between $\bar{X}(1 - \Delta)$ and $\bar{X}(1 + \Delta)$, with $\bar{X} = 96$ ($N = 192$) and $\Delta = 0.5$. The simulations started with a monodisperse sample ($N = 192$). The number of MCS required to obtain the final uniform distribution is of the same order as the number of steps to obtain a full decay of the ACF of the end-to-end unit vector.

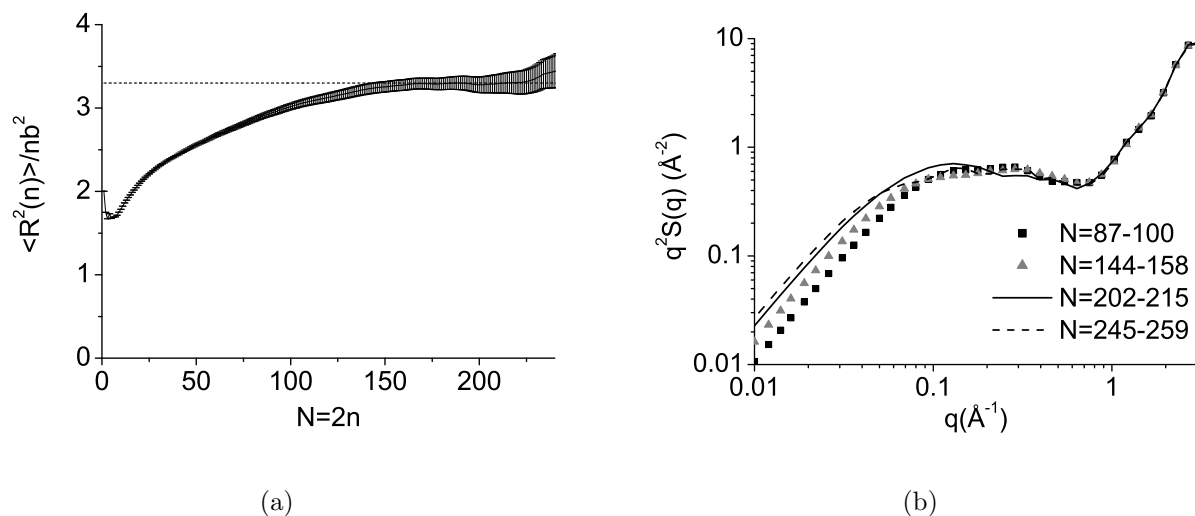


Figure 5.10: (a) Internal-distances distribution averaged over all chains. (b) Kratky plots for chains with their degree of polymerization in different intervals.

5.5 Conclusions

In order to create well-equilibrated atactic-polystyrene (aPS) samples, so-called end-bridging (EB) Monte Carlo (MC), a connectivity-altering MC technique, has been developed. Connectivity-altering MC techniques are very useful to equilibrate polymers on all length and time scales [55], as the route towards well-equilibrated structures is then not dictated by the slowest relaxation processes, that is by reptation, which would be the case for instance in straight-forward MD simulations.

EBMC already exists for polyethylene. The application of the technique to other polymers, such as PS, which is interesting in relation to the study of mechanical properties of polymers, is desirable. However, the development of an EBMC algorithm for atomistic PS is a non-trivial task, involving a lot of bookkeeping. Moreover, in case EB is applied to polymers with bulky monomers, such as aPS, there is the risk of negligible acceptance of the EB move. By developing an algorithm for PS described at a slightly coarse-grained level, these problems have been overcome. An additional advantage is that the algorithm can be applied to other polymers that are modeled at the same or at a coarser level of description.

The EB algorithm has been developed using a 2:1-coarse-grained description of aPS developed by Harmandaris, in which every PS monomer is represented by two coarse-grained atoms, A and B, for CH_2 and $\text{CH}(\text{C}_6\text{H}_5)$, respectively. Tacticity has also been taken into account via bending- and dihedral potentials. This description is simple enough to make

development of an end-bridging algorithm feasible. An EB algorithm for PE has been used as a starting point for the implementation of the method for PS.

Technically the implementation meant modification of all energy calculations and related issues such as linked-cell lists (for efficient calculation of non-bonded interactions) and hard-sphere-overlap lists. Furthermore measures had to be taken to prevent chemistry changes during reptation and end-bridging moves. An additional challenge has been to deal with tacticity; for that purpose a "view direction" along the chain had to be defined and updated during EB moves. Finally the interaction between different moves, primarily between reptation and EB had to be given special attention, both in relation to preventing changes in the chemistry and in relation to efficiency of the algorithm.

Once implemented, the code has been subjected to a number of tests. The results indicate correct implementation of the force field. All distributions of bond lengths, bond angles and dihedral angles are in accordance with the force field. The final polymer conformations show Gaussian statistics and the value for C_∞ (the characteristic ratio based on the atomistic PS model) is approximately 8.5 at 463 K, which is in agreement with values from literature.

The code is also very efficient, although the acceptance of the EB move is approximately 10-100 times lower than in the original EB code for PE. Systems of aPS of the order of 5000 monomers can be equilibrated on all length scales, in a single-processor run. The chain end-to-end vector auto-correlations show complete decay to zero. And a simulation that is started with a monodisperse mass distribution at the start, will evolve to an equilibrium system with a polydisperse mass distribution as dictated by the chemical-potentials settings.

Chapter 6

Structural properties of atactic-polystyrene samples of different thermal history, as obtained from a multi-scale preparation method

ABSTRACT

A method is presented to prepare well-equilibrated atactic polystyrene (aPS) samples to be used in molecular simulations. The method starts with equilibrating the polymer in the melt at length scales beyond the Kuhn length l_K , using end-bridging techniques; at this level a (2:1)-coarse-grained description of aPS is being employed. Subsequently atomistic detail is reintroduced and the sample is equilibrated at the smallest length scales as well. At length scales beyond l_K the polymer chain conformations obtained fulfil the random-coil hypothesis of Flory and $C_\infty = 8.7 \pm 0.1$ at 463 K. Eventually various glassy samples are created by subjecting the melt sample to different cooling rates. Pair correlations are in agreement with existing X-ray data and the amount of dihedral angles in the *trans* (t) state agrees with NMR data. On the level of dyads, the conformations of racemic dyads agree well with existing NMR results. At the same time, meso dyads conformations do not agree: 65% of meso dyads is in the *gt/tg* state (NMR: 80%), 25% is in *tt* state (NMR: < 10%). The structures obtained from the method described have been used to study aging type of phenomena; an attempt has been made to relate the observation

in simulations that an increase in cooling time effects an increase in yield stress to effects of the cooling rate on the polymer structure.

6.1 Introduction

One striking phenomenon originally introduced by Struik [14] in relation to glassy polymers is *physical aging*. It refers to the slow structural relaxation processes, not involving any chemical reactions, in polymer materials below their glass transition. The presence of aging is not restricted to polymers, but occurs in any structural glass.

Physical aging is of importance in relation to mechanical properties of materials. The work of Utz et al. [122] showed that for a binary mixture of Lennard-Jones particles the height of the yield peak and the presence or absence of strain-softening can be influenced by the heat treatment to which the system is exposed. The presence of physical aging and its influence on mechanical behavior of glassy polymers has been demonstrated by for example Struik et al. [14] and Hasan et al. [15]; slow cooling rates clearly support a high yield stress and the presence of strain-softening.

The age of a material increases with time and the aging is fastest at a temperature just below T_g . The age is determining for the height of the yield peak and the degree of strain softening [16]. The reverse of aging is rejuvenation, which can be accomplished by heating the polymer above T_g and subsequently quenching into the glassy state again. Alternatively one can subject the polymer to a mechanical pre-treatment, as has been demonstrated by Govaert et al. [17]. By mechanical preconditioning the brittle atactic polystyrene (aPS) is turned into a ductile polymer, albeit that this ductility is temporary. aPS appears to age very fast; already after a couple of minutes the height of the yield peak increases and strain softening returns and within two days the polymer turns brittle. In spite of the observations with respect to the changes in the mechanical behavior, rejuvenation should not be taken too literally; it has been demonstrated by Isner et al. [30], who use a rugged-energy-landscape model, that states produced by mechanical deformation are generally distinct from states traversed during thermal aging.

The observations mentioned make a polymer like aPS a very interesting material, which indeed has been studied a lot, also in simulations at the atomistic level. Lyulin et al. use molecular-dynamics simulations to study the stress-strain behavior of aPS, giving, in spite of deformation rates being orders of magnitude larger than in experiments, reasonable values for E-moduli, yield stresses and strain-hardening moduli [46]. Also aging effects, as seen in stress and energy vs strain plots, have been studied by Lyulin et al. [138] and explained in terms of ratios of time scales for cooling, deformation and segmental relaxation. An MD demonstration of the influence of cooling rate on stress-strain behavior, based on data from Lyulin [139], is given in Figure 6.1, where two samples of 8 chains of 80 monomers each are deformed uniaxially in tensile. Both samples have been prepared in the same way, starting from one chain in vacuum, which was allowed to relax under melt conditions. Subsequently the system was multiplied in all three Cartesian directions and the resulting system was equilibrated again. The resulting two melt systems of aPS are similar. One of the samples is cooled down through T_g at a rate of 0.01 K/ps, the other at a rate of 0.1

K/ps. Both samples have been subjected to deformation at a rate of $0.025 \text{ \AA}/\text{ps}$. Clearly there is a more pronounced yield peak for the sample cooled down slower.

Although aging refers to structural relaxation, it is very uncertain what structural properties actually change or evolve during aging. Molecular simulations could be useful to investigate this. Up to date molecular simulations have primarily been used to reproduce experimental data on polymer structures in the melt. Many computational attempts have been made to reproduce the correct conformations of dihedral angles, dyads, triads, etc. in the framework of rotational isomeric state (RIS) theories [140–142]. Although conformational distributions are not directly measured, there are NMR data suggesting that model calculations assuming fixed meso dyads with 80% tg/gt conformations and less than 10% tt , and racemo dyads with more than 50 % tt and less than 8% $t\bar{g}/\bar{g}t$, are close to experimental reality. In addition pair-correlation functions have been simulated, by for example Harmandaris et al. [95], which reasonably reproduce the X-ray data on aPS from Londono et al.[143]. Furthermore there are attempts to reproduce polymer structures on larger length scales. For example studies of the intra-chain distances between atoms as function of the number of backbone chemical bonds separating those atoms has been performed by Auhl et al. [92] for a model polymer, and by Harmandaris et al. [95] and by Spyriouni et al. [127] for aPS. At level of the largest length scales, entanglement networks have been studied by for example Everaers et al. [50] and Tzoumanekas et al. [51]. Utz et al. [122] studied the evolution of the pair correlations during the heat treatment of a binary Lennard-Jones system. The amount of studies on evolution of structural properties during aging is limited though.

In this Chapter we attempt on the one hand to reproduce experimental results on the structural properties of aPS in the glassy state. On the other hand we study how the structure evolves during cooling and what the effect of cooling rate is on the structure. Relevant questions are what properties evolve during aging and what are the relevant length scales.

Our approach is the following. First (2:1) coarse-grained aPS polymer samples are created and equilibrated, as described in the previous Chapter. Subsequently atomistic details are reintroduced, after which the structures are equilibrated at the smallest length scales, i.e., down to the chemical-bond length, using united-atom molecular-dynamics simulations. Afterwards, the equilibrated aPS melt samples are cooled below T_g at the two different cooling rates (0.01 K/ps and 0.1 K/ps) in MD. Finally the glassy aPS samples are used for MD production runs, from which structural properties have been calculated. Dihedral distributions and dyad conformations have been calculated, as well as distance factors as measured by e.g. Robyr and Suter [131]. In addition the distribution of angles between phenyl rings have been determined as a function of the spatial distance between them. Also pair-correlation functions have been calculated and compared to the data of Londono et al.[143]. And finally, intra-chain distances have been computed, to look into the longer length scales.

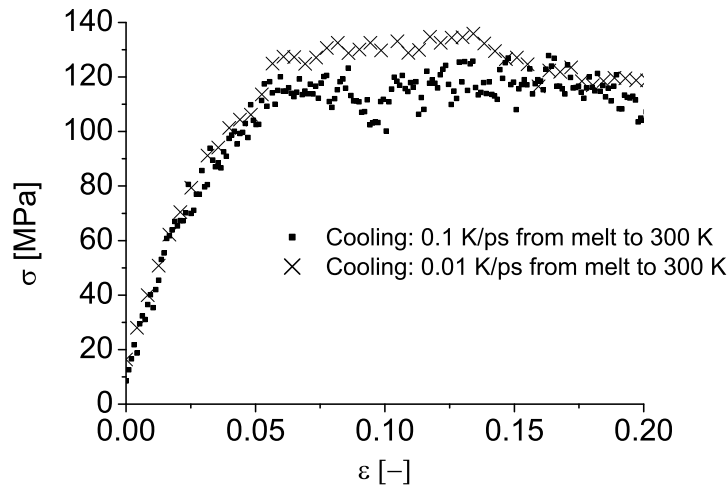


Figure 6.1: Stress-strain curves obtained during uniaxial deformation of two different glassy aPS samples prepared by using different cooling rates. The height of the yield peak and the degree of strain-softening are dependent on the cooling rate; the lower cooling rate gives rise to a higher yield peak and a higher degree of strain softening.

In Section 6.2 the details of the reinsertion of atomistic detail are described, as well as the further details of the sample-building process and the production runs. In Section 6.3 the aPS structures, in the melt and in the glass, are compared vs various results from the literature, and details regarding the calculation of various distributions and quantities are provided. In Section 6.4 the samples resulting after the different cooling rates are compared in their structural details. Finally conclusions are presented in Section 6.5.

6.2 Reinsertion of atomistic detail

An aPS sample consisting of (2:1)-coarse-grained polymer chains has been prepared following the method described in the previous Chapter, starting from initial chain configurations down to rigorous equilibration using the end-bridging method. The sample prepared consists of 50 chains within a uniform mass distribution with an average chain length of $\bar{X} = 100$ monomers and a width of $2\Delta\bar{X}$, where $\Delta = 0.5$. The pressure is 1 bar and the temperature is 463 K, which is well above the glass-transition temperature. (Experimentally observed values for T_g are around 373 K. In simulations this value is higher due to higher cooling rates. Lyulin et al. [144] show a logarithmic dependence of T_g on cooling rate, and for PS they find, for typical cooling rates in simulations (0.1-0.01 K/ps) values for T_g in the range 390-400 K.)

In order to be able to calculate the properties mentioned in the introduction, more structural detail is needed than available in the (2:1)-coarse-grained description. At least the positions of the C-atoms are indispensable. Therefore all C-atoms are reintroduced following a three-step procedure. The resulting structures have been used in united-atom MD production runs afterwards.

In the first step C-atoms are reintroduced. In the (2:1)-coarse-grained description of aPS, the CG-atoms of type A represent a CH₂ unit and the CG-atoms of type B represent a CHC₆H₅ unit. In order to reconstruct the seven C-atoms represented by every B atom, use is made of the positions of the coarse-grained beads and previously inserted atoms, as well as of the average distances between the different types of atoms $d_{ij,av}$ within the same monomer or monomers nearby (i and j represent any type of C-atom or CG-atom). These distances have been obtained from atomistic simulations by Harmandaris. C-atoms are now introduced in trial positions, from which the distances d_{ij} to three atoms nearby are calculated. Subsequently the length differences $d_{ij} - d_{ij,av}$ are minimized using a quasi-Newton algorithm [145].

In a next step the united-atom polymer sample is equilibrated for 50 ps in MD, still at 463 K and 1 bar, using a soft-core potential for the repulsive Van der Waals interactions to prevent large local conformational distortions due to spatial overlap of atoms:

$$U_{LJ,soft}(r) = \begin{cases} 24\epsilon(1 - r/\sigma) + 228\epsilon(1 - r/\sigma)^2 & r \leq \sigma \\ 4\epsilon((\sigma/r)^{12} - (\sigma/r)^6) & r > \sigma \end{cases} \quad (6.1)$$

The complete force field with all details is given elsewhere [146]. The pressure is controlled using the Berendsen barostat [56] ($\beta_p=0.2$, where β_p is the ratio of the isothermal compressibility and the time constant of the barostat) and the temperature is controlled via the collisional-dynamics thermostat [147] ($\lambda=3$ ps, $m_0=1$ Da).

After equilibration with the soft-core potential, the full Lennard-Jones potential is introduced, and a 50 ps simulation is performed. From the obtained trajectories structural properties are calculated and compared to data from literature; the results are given in Section 6.3. Finally the sample is used for two different cooling simulations, one sample at a rate of 0.01 K/ps and the other at 0.1 K/ps, which are typical state-of-art cooling rates employed in atomistic molecular simulations [144]. The two resulting aPS glass samples are compared with regard to their structural properties, calculated from 50 ps simulation runs at the final temperatures; this is discussed in Section 6.4.

6.3 Structural properties of aPS resulting from the multi-scale preparation method

The main purpose of the coarse-graining and the connectivity-altering Monte Carlo method described in the previous Chapter, was to improve the equilibration at longer length scales, beyond the level of the Kuhn length. To verify to what extent this was successful, the intra-chain distances, i.e., the average distance between monomers on the same chain separated by N backbone chemical bonds, have to be verified. For this purpose the characteristic ratio C_N has been studied as a function of the number of backbone atoms:

$$C_N = \left\langle \frac{R^2(N)}{Nl^2} \right\rangle \quad (6.2)$$

where $R^2(N)$ is the squared distance between atoms separated by N backbone chemical bonds and l the length of the chemical bond in the aPS backbone.

In Figure 6.2 (a) C_N of aPS has been given, as obtained from the simulations, at three different temperatures, one above T_g ($=373$ K [136]) and two below T_g . For all temperatures R/Nl^2 tends to a constant value for large N , in agreement with Flory's random-coil hypothesis [32]. In Figure 6.2 (b-d) the values of C_∞ have been determined from linear fits to the curves of C_N vs $1/N$. (Flory [32] shows for freely rotating chains that $\left\langle \frac{R^2(N)}{Nl^2} \right\rangle = C_\infty(1 - \frac{\alpha}{N})$, with α independent of N . Because the aPS polymer chains studied here could be mapped onto freely rotating chains, linear fits of C_N vs $1/N$ data are used here as well.) At $T = 463$ K we obtain $C_\infty = 8.7 \pm 0.1$, which compares well to the value 8.5 predicted from literature at that temperature (for aPS $C_\infty = 9.85$ at 300 K and $d(\ln C_\infty)/d(\ln T) = -0.9 \times 10^{-3}$ [136]).

At lower temperature the value of $C_\infty = 9.85$ is not approached. Whereas C_∞ should increase during cooling, this is not observed in our simulations; it even decreases a few %. For $T = 300$ K (after cooling from 463 K at a rate of 0.1 K/ps) a value of 8.3 ± 0.1 has been found and for $T = 323$ K (after cooling from 463 K at a rate of 0.01 K/ps) 8.5 ± 0.1 . These observations can be understood by realizing that the polymer chains have no chance to undergo conformational changes at length scales beyond the Kuhn length during cooling by either cooling rate employed here; probably the changes in intra-chain distances at those length scales can be largely attributed to the increase in density during cooling (the size of the sample reduces by 1.5% for both cooling rates).

To make a comparison at length scales of a few monomer segments or smaller, the pair-correlation function g_{rem} has been studied. This correlation function, which excludes correlations between atoms separated by less than three chemical bonds or atoms belonging to the same phenyl ring, has been extracted by Londono et al. [143] from X-ray measurements on various polymers, among which aPS. In the left part of Figure 6.3 g_{rem} has been given

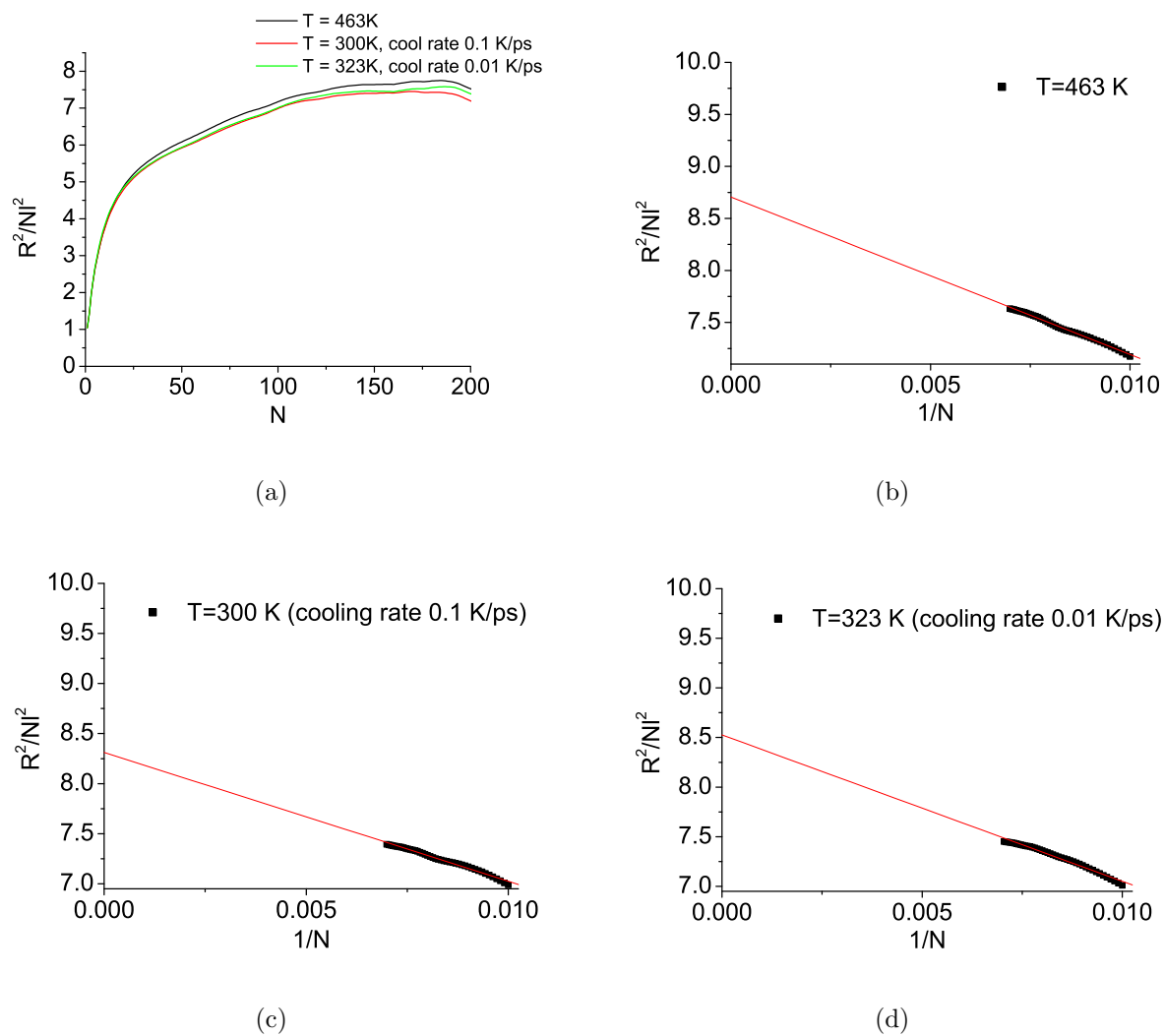


Figure 6.2: Internal distance distributions (a) in the melt at $T = 463\text{ K}$, and in the glass at $T = 300\text{ K}$ and $T = 323\text{ K}$. All curves tend asymptotically to a constant value, in accordance with Flory's random-coil hypothesis. The values of C_∞ have been determined for all three temperatures from linear fits to the internal distance distributions, see (b)-(d).

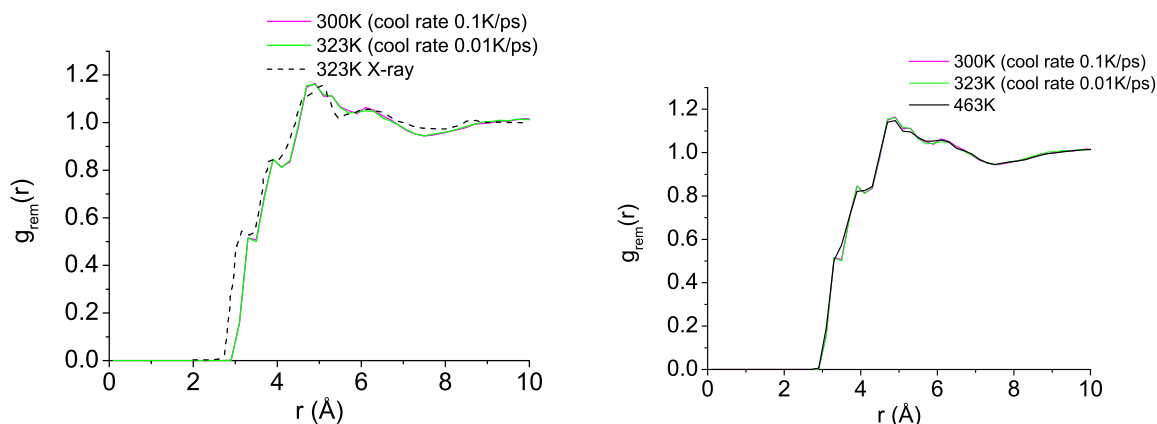


Figure 6.3: Pair-correlation functions g_{rem} in the melt at $T = 463$ K and in the glass at $T = 300$ K and at $T = 323$ K. In these functions the trivial contributions from atoms separated by less than three chemical bonds or between atoms in the same phenyl ring have been left out.

for both simulations in the glassy state ($T = 300$ K and $T = 323$ K), together with the data of Londono et al. The agreement of either of the simulations with the experimental data is excellent.

In addition to pair correlations, distributions of dihedral angles have been determined from the simulations, see Figure 6.5; dihedral angles are defined as explained in Figure 6.4. According to the NMR measurements of Dunbar et al. [148], at room temperature, the amount of dihedral angles in the t state is $(68 \pm 10)\%$. The results from our simulations are in agreement with this result of Dunbar et al.; the agreement is best for the simulated aPS structure that has been created with the slowest cooling rate (0.01 K/ps).

Apart from having a correct dihedral-angles distribution, a simulated polymer structure must also be able to capture the correct distribution of dyad conformations, determined by two consecutive dihedral angles in the polymer chain's backbone. In Figure 6.6 the percentages of dyads in the various possible conformations are given for all simulated aPS structures. A good way of testing whether these dyad-conformational distributions are close to those in experimental reality, is by calculating so-called geometrical rate factors, which can be measured by solid-state NMR. These geometrical rate factors $g(\omega_A, \omega_B)$, which are very sensitive to the distribution of dyads over their various possible conformations, determine the rate of magnetization exchange between two spin packets A and B that have their chemical-shift anisotropy (CSA) tensor differently oriented in the static magnetic field \vec{B}_0 , and therefore resonate at different frequencies, ω_A and ω_B [131]. In various experimental studies to determine geometrical rate factors for aPS [131–133], aPS with ^{13}C labels at position 1 in the phenyl group has been used, see Figure 6.7. The orientation of the phenyl ring with respect to the external magnetic field \vec{B}_0 determines its resonance

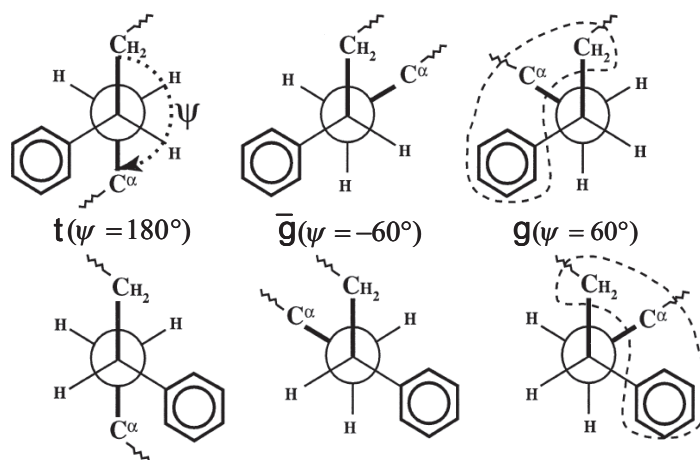
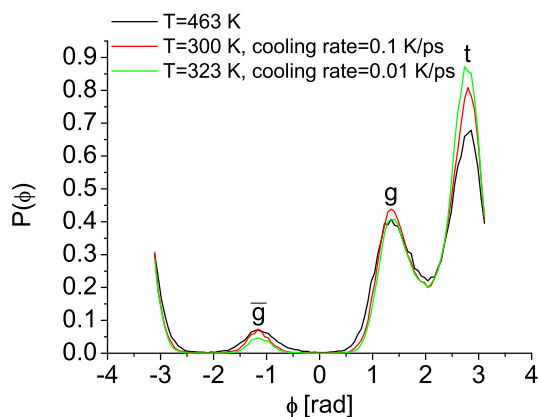


Figure 6.4: All backbone dihedrals (determined by positions of 4 consecutive atoms in the backbone) are viewed in the same direction, that is, always starting from a CH_2 -unit: $\text{CH}_2\text{-CH}(\text{C}_6\text{H}_5)\text{-CH}_2\text{-CH}(\text{C}_6\text{H}_5)$. The direction of positive orientation is such that sterically equivalent conformations are assigned the same dihedral angle. Reprinted from Dunbar et al. [148]



	T=463K	T=300K (0.1K/ps)	T=323K (0.01K/ps)
t	56.2	60.2	63.9
\bar{g}	5.4	3.7	2.5
g	38.4	36.1	33.6

Figure 6.5: Distribution $P(\phi)$ of dihedral angles in the melt at 463 K and in the glassy state at 323 K and 300 K. The percentages of t , g and \bar{g} , resulting from integrating $P(\phi)$ over $(-\pi, -\frac{\pi}{3}]$, $(-\frac{\pi}{3}, \frac{\pi}{3}]$ and $(\frac{\pi}{3}, \pi]$, respectively, are given in the Table .

frequency ω . $g(\omega_A, \omega_B)$ determines the rate at which spin exchange takes place between an ensemble of phenyl groups with a particular orientation with respect to the external magnetic field that corresponds to a Larmor frequency ω_A , and an ensemble of phenyl groups with an orientation with respect to \vec{B}_0 that corresponds to a Larmor frequency ω_B .

For an ensemble of N interacting spins the geometrical rate factor g_{AB} is given by:

$$g(\omega_A, \omega_B) = \frac{N}{n_A n_B} \left(\frac{\mu_0 \hbar \gamma^2}{4\pi} \right) \sum_i^{n_A} \sum_j^{n_B} \left(\frac{1 - 3 \cos^2 \theta_{ij}}{r_{ij}^3} \right)^2 \quad (6.3)$$

where n_A and n_B are the numbers of spins with frequencies in small intervals around ω_A and ω_B , respectively. The vacuum magnetic permeability is μ_0 , the gyromagnetic ratio is γ , r_{ij} is the distance between spins i and j , θ_{ij} is the angle between the internuclear vector and the static magnetic field \vec{B}_0 . The geometrical rate factor provides information on local orientational order between the phenyl rings. In absence of such order a 2D plot of $g(\omega_A, \omega_B)$ will be totally flat; deviations from flatness indicate preferred angles between spatially proximate phenyl groups.

A quantity that is similar to the geometrical rate factor but that is measured under magic-angle spinning (MAS) conditions [149] (where the angular dependence drops out) is the distance factor. Although the results in this Chapter concern geometrical rate factors, for further discussion the distinction will not be relevant.

The rate constants $R(\omega_A, \omega_B)$ ($\sim g(\omega_A, \omega_B)$) for polarization-transfer between phenyl rings, as obtained from the simulations at the various temperatures, have been shown in Figures 6.8(a-c); those reported by Robyr et al. [131] are shown in Figure 6.8(d). Clearly there exists local order between the phenyl rings; and the order is exaggerated in the simulations, as can be seen from the stronger deviations from a flat profile for the simulations than for the experiments. To extract more information from these rate factors, one should look into separate contributions from different types of dyads, and contributions from orientational correlations between phenyl groups in different chains. Some experimental results on the separate contributions of meso and racemic dyads already exist [132].

Much less involved than calculating and comparing distance factors, is using the results of Robyr, Gan and Suter [132]. They showed that distance factors, calculated using RIS models with for meso dyads more than 80% tg/gt and less than 10% tt and for racemic dyads more than 50% tt and less than 8% $t\bar{g}/\bar{g}t$, approach experimental distance factors very reasonably. From our simulations we obtain conformations of racemic dyads that agree with these results. For the meso dyads the percentage of dyads in tg/gt found in the simulations, 63%, is too low; the amount of meso dyads in tt , 28%, is much too high.

The reason for the discrepancies between the simulation results for meso-dyad conformations and the results of Robyr et al. is not obvious. However, some insight in the causes of the discrepancies may be obtained from comparing the aPS structures prepared by the

		T = 463 K	T = 300 K (0.1 K/ps)	T = 323 K (0.01 K/ps)
Meso	tt	19.8	24.8	27.7
	\overline{gg}	0.0	0.0	0.0
	gg	5.5	4.3	4.1
	$\overline{gt/tg}$	7.5	5.8	4.2
	gt/tg	64.9	63.5	63.2
	$\overline{gg/gg}$	2.3	1.6	0.8
Racemic	tt	43.8	48.9	55.2
	\overline{gg}	0.0	0.0	0.0
	gg	24.6	22.3	18.3
	$\overline{gt/tg}$	6.1	3.0	1.9
	gt/tg	19.4	21.4	21.6
	$\overline{gg/gg}$	6.1	4.4	3.0

Figure 6.6: Conformations of dyads at 463K in the melt and in the glassy state at 300 K and at 323 K.

methods described in this thesis to an approach similar to ours, that was followed by Spyriouni et al. [127]. In our work aPS sample preparation is initiated with equilibration at the (2:1) level of coarse graining, followed by reinsertion of atomistic detail and equilibrating locally afterwards. Spyriouni et al. start by equilibrating using a 1:1-coarse-grained model of aPS. Subsequently a backmapping scheme, i.e., a scheme for reinsertion of atomistic detail has been used that is necessarily much more complicated than ours, as their coarse-grained model is further away from the atomistic one than ours.

Spyriouni et al. report on the conformational properties of their PS samples at a temperature of 500 K an overall amount of dihedrals in the t state of around 60%, which is comparable to our 56% at 463 K. And, considering the temperature difference, the conformational data found by Spyriouni et al. at 500 K are probably also in agreement with the experimental result of Dunbar et al. [148] at room temperature ($(68 \pm 10)\%$ of the dihedrals in the t state). For the conformations of dyads Spyriouni et al. observe the following. The amount of meso dyads in the gt/tg conformation is 60% and of all racemic dyads 45% is in the tt conformation. These results are again comparable to our results, see Figure 6.6.

The agreement between our results on conformational properties of PS and those of Spyriouni et al. is remarkable. The fact that both Spyriouni and the author of this thesis use the same force field for the final atomistic simulations does not trivially explain the agreement between their data.

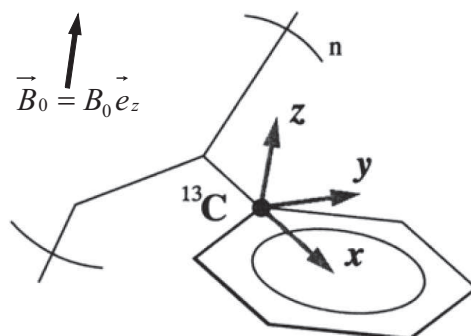


Figure 6.7: A phenyl ring in an external magnetic field \vec{B}_0 . The carbon atoms at positions 1 in the phenyl ring are ^{13}C and are thus sensitive to NMR. The orientation of \vec{B}_0 with respect to the phenyl ring determines the resonance frequency of the ^{13}C atom. Reprinted from Robyr et al. [131]

6.4 Comparison of structural properties obtained from the different cooling rates

After checking all the properties vs experimental knowledge, we would like to compare the different properties of the sample created by slow cooling from the melt (at 0.01 K/ps to a final temperature of 323 K) and the sample created by fast cooling (0.1 K/ps to a final temperature of 300 K). As already observed in the introduction, the cooling rate is reflected in the mechanical behavior. The stress-strain curves obtained using two different cooling rates are different, primarily in the height of the yield peak, the sample resulting from the lower cooling rate giving the highest yield stress, see Figure 6.1. From the previous discussion of the intra-chain distances distribution, it became already clear that chain conformations change little at the long length scales, and intra-chain distances essentially scale with size of the sample.

At the level of pair-correlation functions, one observes stronger peaks at lower temperatures, see Figure 6.3. Especially peaks at the length scales below 4-5 Å become sharper, which is a signature of increased local order upon cooling. The influence of cooling rates, however, on the pair-correlation functions is hardly noticeable. This information is however very general and does not give much insight. It would be more interesting to look at specific, carefully chosen correlations, such as correlations between atoms in spatially close phenyl rings, either in the same chain or in different chains.

As an example we studied the distribution of angles β between phenyl planes as a function of their distance. The distribution $P(\beta)/\sin\beta$ is given in Figure 6.9. Small angles are preferred, both at high temperature (463 K) and in the glassy state. For temperatures below the glass transition this ordering effect is more pronounced. Again the influence

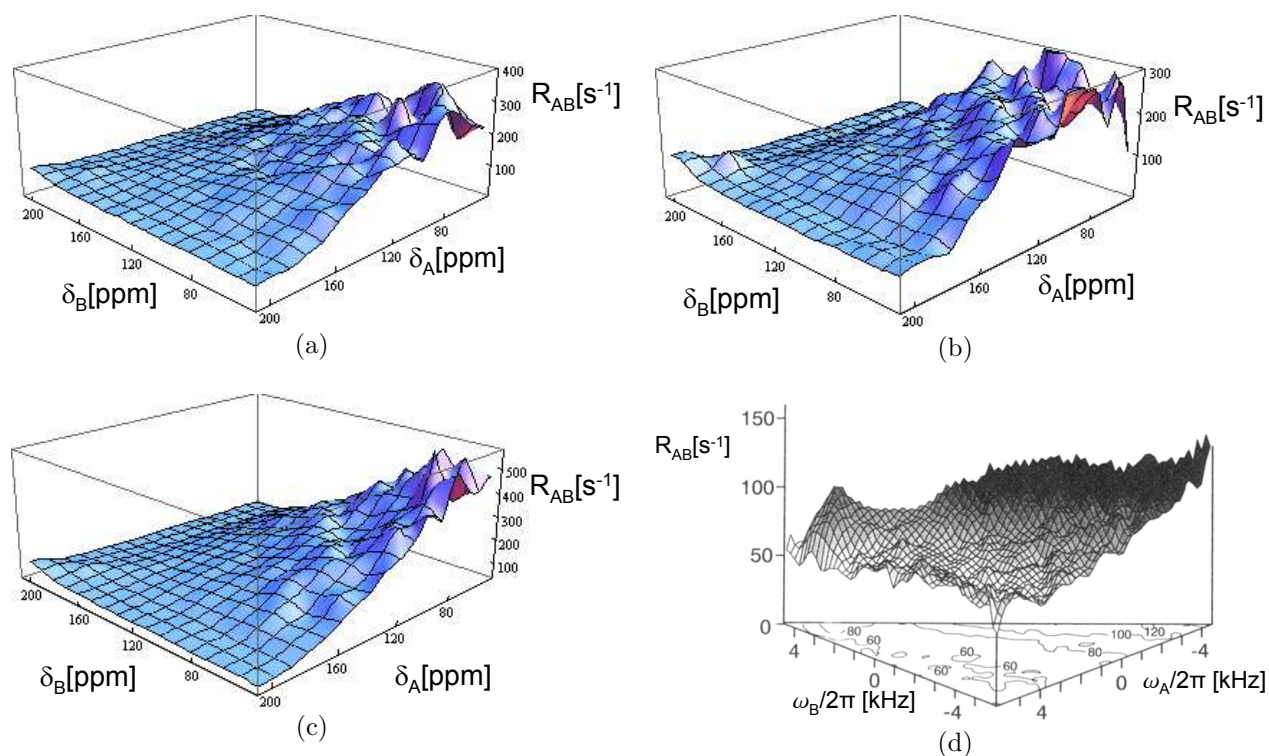


Figure 6.8: Rate constants for polarization transfer obtained from the simulations (a-c) and from experiments by Robyr [131]. The distance factors at 300 K (b) compare reasonably to the distance factors measured by Robyr et al. (d), but not perfectly. Further improvement of the dyad statistics, see discussion on dyad conformations, is needed to obtain better agreement between distance factors as obtained from experiment and simulation. In (a) through (c) the parts-per-million scale has been used, in (d) the kHz scale. (For details on both scales see for example [131] or [150].)

of cooling rate is very small, compare Figure 6.9 (b) and (c). Probably for length scales smaller than 5 Å, the only effect is that the thermal fluctuations of angles β around their average values become less as the temperature is decreased. For length scales above 5 Å no changes are observed; both above and below the glass transition, no preferred angles are present. This could mean that in real aPS at distances beyond 5 Å no orientational correlation between phenyl rings exists. However alternatively it could mean that although there exist such correlations in real aPS, this is not seen in the simulations because of the huge cooling rates.

The dihedral-angle distributions, see Figure 6.5, show an increase, upon cooling, in the number of dihedral angles in the t state, at the cost of both dihedral angles in the g state and in the \bar{g} state. This decrease is twice stronger for the slower cooled sample than for the faster cooled one. These effects are also seen in dyad conformations, see Figure 6.6. For the racemic dyads, upon cooling, an increase of 11% in the number of dyads in the tt conformation is seen and a decrease in essentially all other conformations. With regard to the meso dyads, the amount of tt dyads increases by 8%. Again the cooling rates are important.

Although interesting, the observations with respect to cooling rate differences still do not answer the question what structural properties are important to aging, and how differences in the yield peak, see Figure 6.1, have to be understood. As a next step, one should subject the samples resulting from both cooling rates to deformation and monitor the evolution of structural properties (primarily of dihedral distributions and distributions of dyad conformations); a major question is whether these structural properties of both samples become equal after strain-softening, beyond which the stress-strain curves seem to coincide.

6.5 Conclusions

A new method to generate aPS polymer samples has been explained. In a first stage the aPS is modeled using a (2:1)-coarse-grained description, i.e., PS monomers are described by two coarse-grained atoms. At this level of description the polymer has been equilibrated using end-bridging Monte Carlo techniques. After this equilibration at coarse-grained level, atomistic detail (only hydrogen atoms are left out) has been reintroduced. Subsequently equilibration above T_g has been carried out. Finally to obtain room-temperature aPS, the sample is cooled through the glass transition at 373K. Two different cooling rates have been used to study their effect on structural evolution.

On the longest length scales, beyond the Kuhn length, the sample preparation resulted in polymer conformations in agreement with Flory's random-coil hypothesis, as could be concluded from the fact that C_N goes asymptotically to a constant value as N becomes large. Moreover, the value $C_\infty = (8.7 \pm 0.1)$ found for the sample above T_g is similar to the

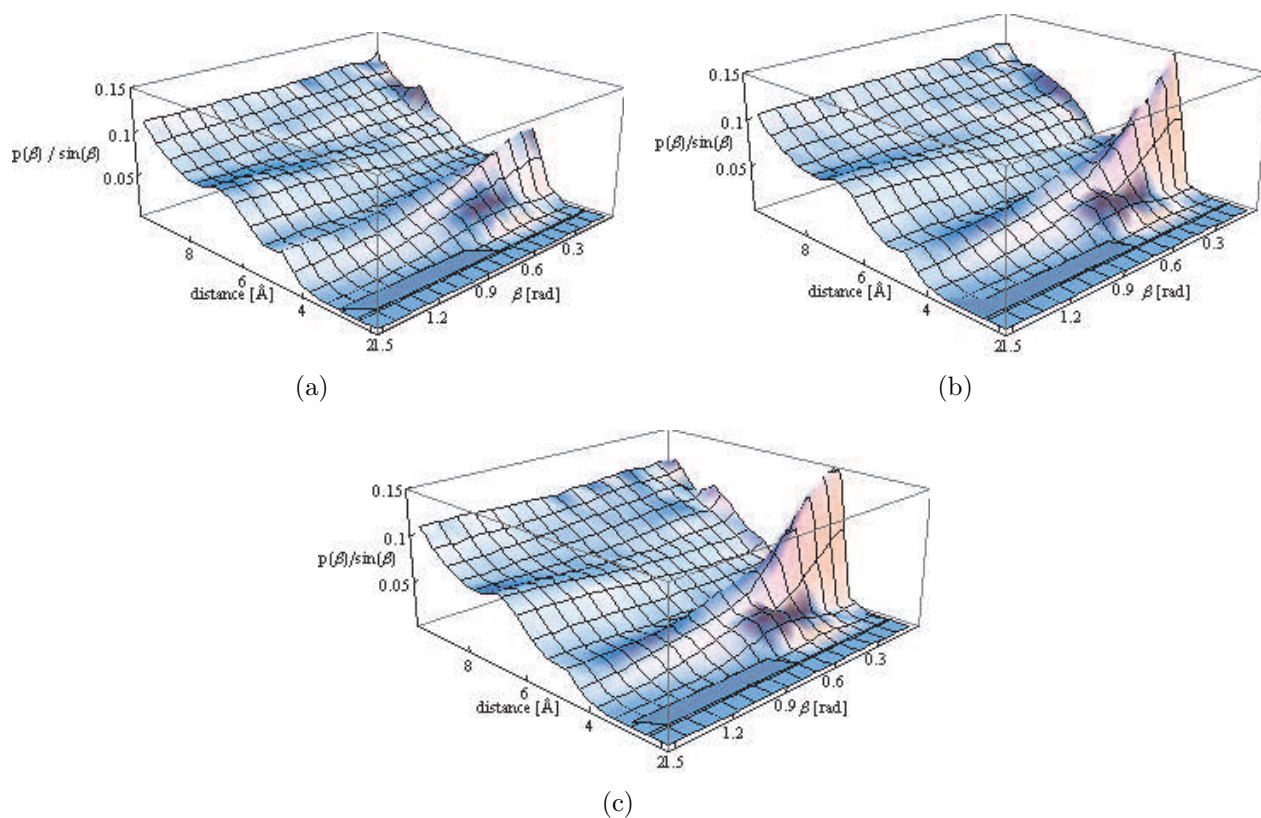


Figure 6.9: Distribution $P(\beta)/\sin\beta$ of angles between phenyl groups as a function of their distance, for the aPS sample above T_g at 463 K (a), and for the aPS samples below T_g resulting from the cooling with 0.01 K/ps (b) and from the cooling with 0.1 K/ps (c). For distances shorter than 5 Å small angles between phenyl planes are preferred; this effect is especially pronounced below T_g . The cooling rate seems hardly of influence on this type of ordering.

literature value [136]. At temperatures below T_g the conformations at the longest length scales are essentially the same; for the samples below T_g the values obtained for C_∞ are (8.5 ± 0.1) and (8.3 ± 0.1) . The slight decrease in C_∞ can be attributed to the decrease of the sample volume upon cooling.

The pair correlations found are in excellent agreement with X-ray data [143]. On top of that, dihedral-angle conformations as predicted by NMR [148] are reproduced in the simulations reported here. At the level of dyad conformations, important differences are observable between the simulated aPS structures, and existing NMR results [131]. The conformations of racemic dyads found in the simulations are in agreement with the experimental data. For the meso dyads large differences can be observed; whereas NMR data suggest more than 80% in the tg/gt and less than 10% in the tt conformations, the simulated structures show only 65% of the meso dyads in tg/gt and as much as 25% in tt . The cause of these differences is not clear.

Another simulational approach to prepare aPS, by Spyriouni et al. [127], comparable to the one presented here, starts with equilibration of aPS at a 1:1-coarse-grained level, also using connectivity-altering Monte Carlo. After equilibrating the coarse-grained polymer, a complicated backmapping scheme is used to reinsert atomistic details. Finally the aPS sample is equilibrated at $T = 500$ K. In spite of the conceptual similarity, there are obvious differences with our approach. In our approach we employ a more detailed description of the aPS monomer unit, and as a consequence our backmapping is simpler. In spite of these clear technical differences, both approaches perform equally well with regard to reproducing experimental observations on structural properties of aPS. Both the method of Spyriouni and the method presented here are successful in reproducing polymer conformations at length scales beyond the Kuhn length. Also distributions of dihedral angles are in agreement with experiments [148]. Experimental data on dyad conformations are not correctly reproduced. Both approaches show racemic dyad conformations that follow experimental observations. The problem arises, again for both approaches, for the meso dyads, where NMR results predict 80 % tg/gt conformations and less than 10% tt conformations. The reason for the similarities in the results from both approaches is not a priori obvious; it can not be trivially ascribed to the fact that in both approaches the same force field is applied at the atomistic level.

Finally the structures resulting from the preparation method presented here have been used to look into effects related to aging. An attempt has been made to relate differences in stress-strain behavior observed between two samples prepared by using different cooling rates, to differences in the structures of both samples. At the level of the pair-correlation function, sharper peaks indicating stronger local ordering have been observed for temperatures below T_g than for temperatures above T_g . However, no influence of the cooling rate was seen. Also the distribution of angles between phenyl rings as a function of the distance between the rings did not reveal any influence of the cooling rate. The only clear differences were observed in the distributions of dihedral angles and consequently in the distributions of the meso and racemic dyads over their various possible conformations.

Such observations are insufficient to answer the question on what structural properties are important to aging, and how differences in the yield peak, see Figure 6.1, have to be related in detail to e.g. particular Lennard-Jones interactions. In a possible follow-up study one should focus on the evolution (during deformation) of structural properties, especially dihedral angle distributions and distributions of dyad conformations, in samples obtained from different cooling rates; a key question is whether beyond strain-softening, where stress-strain curves coincide, differences in structural properties have been erased.

Chapter 7

Molecular-dynamics simulation of PS under deformation: The role of equilibration

ABSTRACT

The role of sample preparation in the stress-strain relations for glassy polystyrene as obtained from atomistic molecular-dynamics simulations has been studied. A sample preparation method (extended-chain condensation, ECC) that is based solely on molecular-dynamics simulations has been compared to a method (coarse-grained end-bridging, CGEB) involving connectivity-altering (end-bridging) Monte Carlo and coarse graining. Whereas CGEB results in polymer conformations obeying Gaussian statistics, ECC results in polymer structures that are too compact. The stress-strain relations are different in the strain-hardening regime. For samples prepared according to the CGEB method a stronger strain hardening is observed and the modulus is more realistic (For the CGEB sample $G_R = 9 \pm 1$ is found vs $G_R = 4 \pm 2$ for the ECC samples.). These differences have to be attributed to a steeper increase in the contributions to the total stress from bond- and dihedral angles for CGEB than for ECC samples. In the CGEB sample the same strain value necessarily results in larger chain extensions at the large length scales (beyond the length of a Kuhn segment) than in the ECC sample; this difference is compensated by more local conformational changes via dihedral angles and via stronger deviations of both bond angles and dihedral angles from their equilibrium values.

7.1 Introduction

The mechanical properties of polymers are known to depend on the processing history [14]. For example the yield stress is dependent on the age of a polymer material; aging leads to an increase of the yield stress with time. By heating a polymer above its melting point and subsequently quenching into the glassy state, the age can be reduced (rejuvenation) and therewith the yield stress. Mechanical predeformation can result in even stronger rejuvenation; the yield stress can be reduced such that the material exhibits no strain softening anymore [17]. Ultimately, processing can turn a brittle polymer into a ductile one.

Also in simulations these observations have been made. Lyulin et al. [46] were able to reproduce typical stress-strain curves for the amorphous polymers polystyrene (PS) and bisphenol-A polycarbonate (PC). They succeeded in approximately reproducing quantities like E-moduli, yield point and strain-hardening moduli; deviations of the values obtained in the simulations from experimental values were of the order of 20%. Note however that, due to limitations of the molecular-dynamics method used, deformation rates had to be applied that are orders of magnitude larger than typical experimental deformation rates. Later Lyulin et al. [138] also reported on their extensive study of the energy development during aging and rejuvenation for the same two polymers; the differences in behavior between those two polymers could be interpreted by considering ratios between time scales for cooling, deformation and segmental relaxations.

As explained in previous Chapters, in all simulations involving polymers, especially simulations of polymers in melts, initial-sample preparation is a serious challenge. Primitive sample-generation methods such as excluded-volume chain growth (EV) and phantom-chain growth (PCG), see Chapter 2, followed by attempts to equilibrate by basic simulation techniques (Monte Carlo (MC), molecular dynamics (MD) and Brownian Dynamics (BD), to name a few) will not result in samples that are equilibrated on all length and time scales. Still these approaches are being used [46, 138, 151] to obtain initial samples that are subsequently used for simulations in which statistical and dynamical quantities have to be studied. The effect of poor equilibration on simulated mechanical behavior has not extensively been studied yet. Brown and Clarke [108] prepared on purpose a number of model polymer samples with large differences in both persistence length and percentage of dihedral angles in the trans conformation, and found large differences in the post-yield stress-strain behavior. Whether differences between existing equilibration methods result in differences in polymer structures that have a strong effect on mechanical behavior is an open question.

To learn more on the role of the sample-preparation method in the mechanical behavior observed in simulations, one could subject samples that are prepared by widely different methods to the same mechanical tests. Here we follow such an approach for PS. One PS sample is prepared by starting from one all-trans chain in vacuum that is allowed to

collapse, under melt conditions, to a coil in an orthorhombic box. The orthorhombic box is subsequently multiplied in all three directions in Euclidian space. Finally the sample is subjected to equilibration at elevated temperature. The second sample has been prepared by making use of coarse-graining and end-bridging MC techniques to equilibrate at intermediate to large length scales, see Chapter 5, and united-atom PS MD to equilibrate at length scales of a few monomer segments, see Chapter 6. After preparation, the initial samples are characterized first, using pair-correlation functions and internal-distance distributions [92, 95], to clearly show the structural differences resulting from the different preparation methods. Subsequently both samples undergo the same cooling and deformation. The mechanical stress response to applied strain is carefully analyzed for both samples; in addition the contribution of the various interaction types in the system to the total stress has been investigated. Also the amount of energy stored in the various degrees of freedom of the sample, i.e., energy partitioning, has been studied. Finally structural evolution during deformation has been looked at.

The remainder of this Chapter is organized as follows. In Section 7.2 the details of both the sample-preparation methods and the deformation protocol are explained. An extended comparison of the mechanical behavior of samples prepared by two very different preparation methods, based on stress partitioning, energy partitioning and evolution of various structural properties, is described in Section 7.3. Conclusions are drawn in Section 7.4.

7.2 Details of the simulations

As explained, two different sample-preparation methods are compared. One method, from now on referred to as the extended-chain-condensation (ECC) method, is quite primitive. The other, more sophisticated, method, based on coarse graining and end bridging (EB), will be referred to as the CGEB method. The CGEB method has been extensively described in Chapters 5 and 6. First a polymer sample is prepared in the melt phase as described in Section 5.4, at a 2:1 level of coarse-grained description. Subsequently the sample is further equilibrated at the intermediate and long time scales, i.e., beyond the length scale of a few monomer segments, with the EB technique. After the system has completely forgotten its initial state, as could be concluded from the decay to zero of the autocorrelation function of the end-to-end unit vectors, see Chapter 5, atomistic detail is reintroduced in the system. The atomistically detailed system is subjected to MD simulation to obtain a sample that is also locally, i.e., at the scale of a few monomer segments, equilibrated. In this way a sample is prepared consisting of 50 chains of on average 100 monomers.

The ECC method starts from an extended chain in vacuum, a situation that is mimicked by putting the chain in an orthorhombic box with periodic boundary conditions, with a box size larger than the size of the chain. This system is subjected to melt-pressure and -temperature conditions, resulting in a collapse of the chain and an evolution of the density towards its melt value [137]. After the collapse the sample is doubled in all three directions

of Euclidian space; in this way a sample of 8 chains of 80 monomers is generated. This final system is equilibrated for another 10 ns at 540 K, again using periodic boundary conditions. More details can be found in refs [152] and [146]. Using this method 5 samples are prepared in order to have comparable statistics as in case of the much larger system created by the CGEB method.

After preparation via either of the methods we have samples in the melt; in both cases the same united-atom description of the PS polymer is employed. Details of this force field can be found elsewhere [146]. Since the purpose is to study and compare the ECC and the CGEB sample in the glassy state the samples have to be cooled down. To that end all samples are cooled into the glassy state in NpT MD simulations, employing the velocity Verlet integration scheme with a time step of 4 fs. The pressure is controlled using the Berendsen barostat [56] ($\beta_p=0.2$, where β_p is the ratio of the isothermal compressibility and the time constant of the barostat) and the temperature via the collisional-dynamics thermostat [147] ($\lambda=10$ ps, $m_0=0.1$ Da). The cooling rate employed is 0.1 K ps⁻¹, which is a typical cooling rate used in molecular simulations [46, 138]; the final temperature is 300 K. From the plot of the specific volume vs temperature we deduce, similarly as done in ref [46], that our systems vitrify at approximately 400 K. The glassy samples resulting from cooling are deformed uniaxially at a deformation velocity of 0.05 Å ps⁻¹.

7.3 Differences between CGEB and ECC samples

In order to obtain insight in the importance of careful equilibration on all length and timescales, both the samples prepared according to the CGEB method and the samples prepared according to the ECC method are subjected to uniaxial deformation. To understand the comparison, we start by presenting some structural properties of both equilibrium samples and make a short reference to established literature on those properties. Subsequently, both samples are deformed and the mechanical behavior is compared. Finally the evolution of the polymer structures is studied in both cases.

7.3.1 Structural properties prior to deformation

The structural properties can be compared using pair-correlations functions. Most pair-correlation functions of polymer systems are dominated by the trivial correlations between atoms that are separated by one or two chemical bonds. These correlations are very similar for many polymers [143]. Londono et al. subtracted these trivial correlations from the total structure functions obtained by their X-ray measurements on PS and other polymers. The remaining parts of the structure functions are Fourier transformed into pair-correlation functions $G_{rem}(r)$. As shown by Londono et al. these functions G_{rem} contain very specific

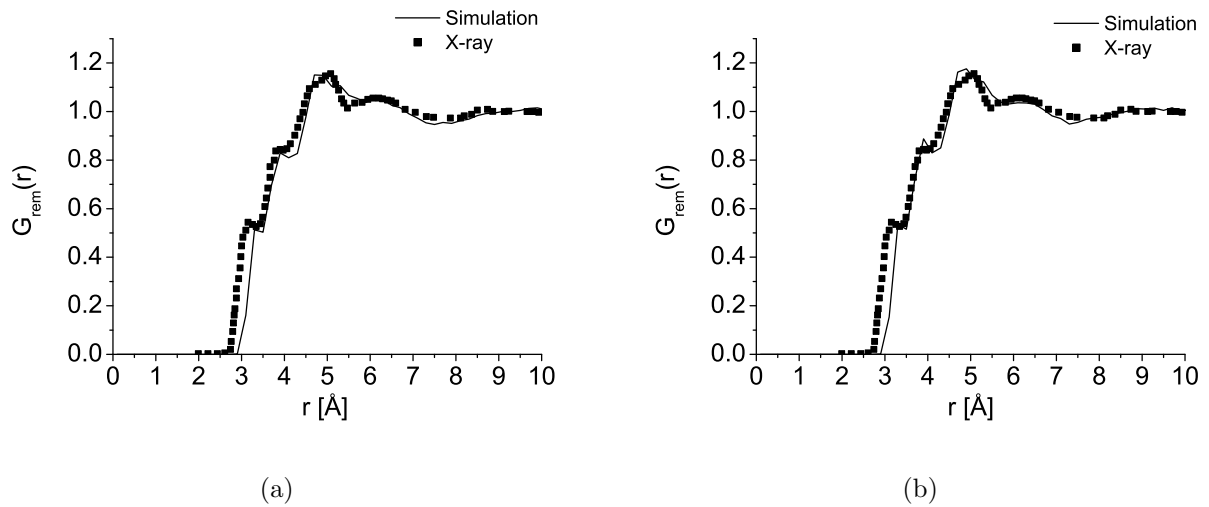


Figure 7.1: Pair-correlation functions G_{rem} for both the polymer sample from CGEB (a) and from ECC (b). Trivial correlations between atoms separated by less than three chemical bonds or atoms in the same phenyl ring are excluded. Clearly, the experimentally reported correlations are accurately reproduced.

structural information, from conformational and intermolecular degrees of freedom, on the basis of which chemically different polymers can be distinguished.

Following their approach, we calculated G_{rem} for our PS samples, see Figure 7.1. Both preparation methods resulted in samples that possess the same structural features as measured by Londono et al. [143]. Small discrepancies between G_{rem} as calculated in either of the simulations on the one hand, and as obtained from the experiments on the other hand, can probably be attributed to details of the force field rather than to the sample preparation method applied.

The pair-correlation functions discussed here are indicative for how well realistic polymer structures are resembled on short length scales. However, especially at larger length scales clear differences should be expected, since the approach to equilibration followed in this thesis aims at improving equilibration at the longest length and time scales; for local equilibration similar approaches are followed for both samples. To investigate the structures at larger length scales one could calculate gyration radii or end-to-end distances. A better alternative chosen here, providing information on all length and time scales, is the internal-distance distribution.

The distribution of internal distances in a chain is very informative on how well a sample has been equilibrated. The precise quantity calculated here is C_N , defined as:

$$C_N = \left\langle \frac{R^2(N)}{Nl^2} \right\rangle \quad (7.1)$$

where R is the spatial distance between two atoms in the backbone of the same polymer, N is the number of backbone bonds separating those atoms and l is the length of a chemical backbone bond. The averaging is done over all pairs in all chains and also over time. Figure 7.2 shows these distributions for both polymers. For large N the curve should tend asymptotically to C_∞ . Clearly, for the well-equilibrated polymer sample this requirement is met. From a linear fit of the data $R^2(N)$ vs $1/N$ for $N > 100$, it is found that, for large N , C_N approaches 8.5, which is lower than typical values of C_∞ reported in literature; Mark et al. [136] report 9.85 for PS at room temperature. The cause for this is that the sample has been equilibrated at a temperature corresponding to the melt phase, producing the correct value for C_∞ at that temperature, and subsequently cooled down many orders of magnitude faster than experimentally achievable. Apparently at this cooling rate the system is not capable of adjusting its value of C_∞ towards the value at room temperature. For the non-equilibrated sample the situation is much worse: first $R^2(N)$ shows an increase, however for larger N $R^2(N)$ decreases again to a plateau at 4.3 ± 0.5 . According to Auhl and Everaers [92] this is indicative for locally overstretched polymer chains. The low plateau value from ECC can be understood from the fact that the sample preparation started from extended chains in vacuum and not in the melt. In the melt, the attractive interactions between monomers in the same chain are shielded beyond a distance of a few monomer segments, whereas in vacuum this is not the case. In other words, the effective intra-chain attractive interactions are larger during the ECC sample preparation than in a PS melt. The result is a much more compact structure obtained from the ECC procedure than should be expected for a PS melt.

7.3.2 Stress-strain behavior

Both samples are deformed uniaxially in tension. The true stress is monitored and plotted versus strain in Figure 7.3. In both cases the stress-strain curve has the typical form as known experimentally [8]; one can observe the characteristic regimes of initial quasi-elastic response, yield at a few percent strain, then further deformation at constant stress, and finally an increase in stress for large extensions, called strain hardening. Strain softening, i.e., a drop (up to a few tens of MPa) in the stress after the onset of yielding, can be observed also if upon sample preparation a slower cooling rate (0.01 K ps^{-1}) is used, see e.g. Lyulin et al. [46].

To make a quantitative comparison among the two polymer samples, Young's moduli E , yield points (ϵ_y, σ_y) and strain-hardening moduli G_R have been determined. The E -moduli are determined as the slopes of the stress-strain curves during the first percent deformation, the yield point as the intersection of the stress curve with the straight line $f(\epsilon) = E(\epsilon - 0.02)$

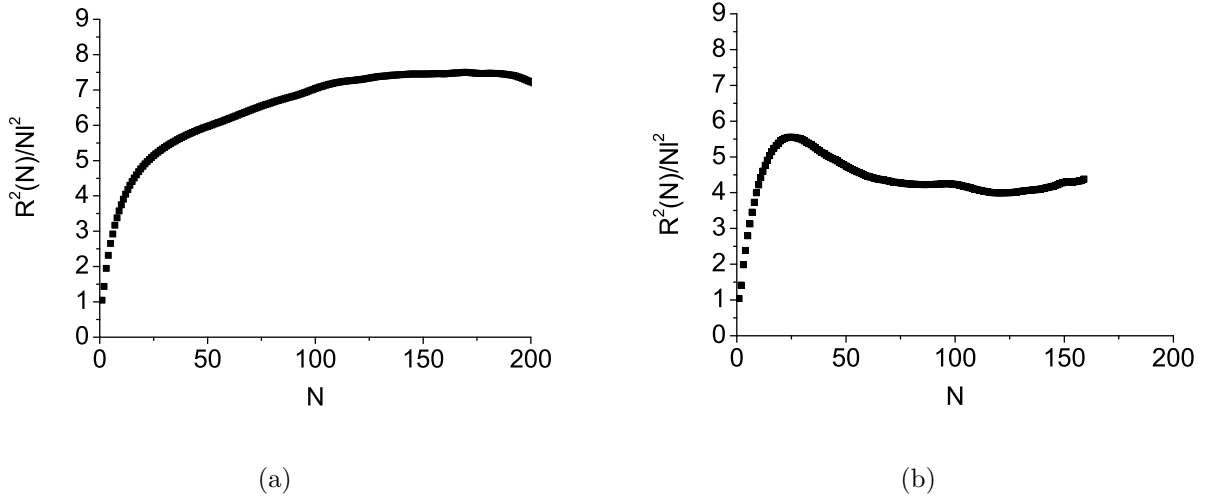


Figure 7.2: Distribution of internal distances in the polymer prepared by the CGEB method (a) and in the ECC method (b).

[7] and the G_R -moduli as the slope of the linear fit to the stress curve for $\epsilon > 0.6$ [7]. The values of these quantities are collected in Table 7.1. The value of the E -modulus from the CGEB sample is low compared to typical experimental values (3.2-3.4 GPa [153]), whereas the value from the ECC sample is closer; the cause of this is not clear. The yield stresses from both samples are overestimated by approximately 30% [8], and are comparable to those reported by Lyulin et al. [46]. The strain-hardening moduli are underestimated again (Van Melick et al. [8] report 13 MPa for PS); G_R from the CGEB sample is closer to the experimental value than the G_R from the ECC sample. This last observation is correlated with the fact that the chains in the ECC sample are less extended than in the EB sample.

Table 7.1: Mechanical properties of both the PS glass samples prepared by the CGEB method and those prepared via the ECC method. Young moduli, yield stress, yield strain and strain-hardening moduli of PS take realistic values.

sample	E (GPa)	σ_y (MPa)	ϵ_y (-)	G_R (MPa)
CGEB	2.3 ± 0.3	115 ± 5	0.045 ± 0.005	9 ± 1
ECC	3.3 ± 0.2	105 ± 5	0.05 ± 0.005	4 ± 2

7.3.3 Stress partitioning and energy partitioning

In order to learn which degrees of freedom are important in which stages of deformation, the separate contributions of the various types of interactions to stress (its normal component

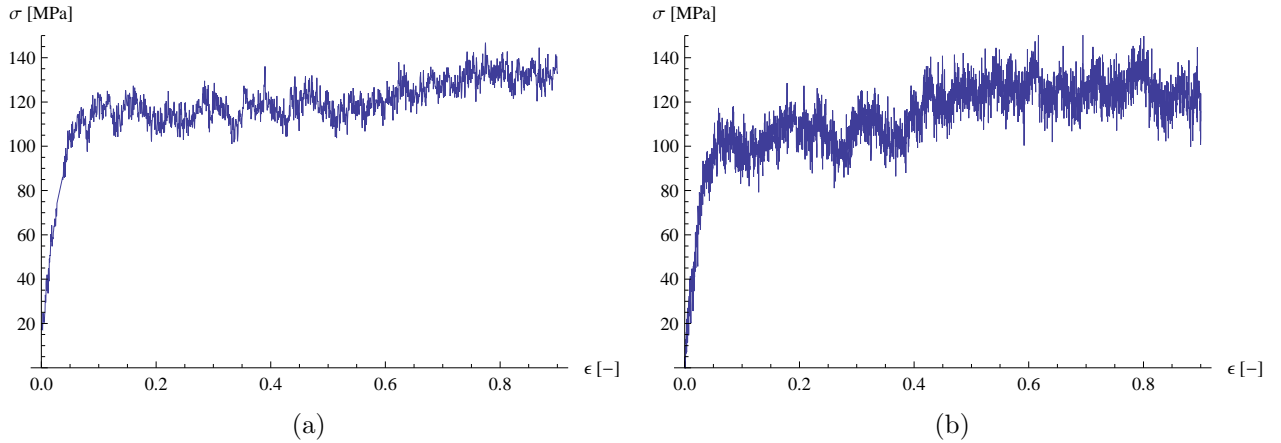


Figure 7.3: Stress vs strain for both the polymer prepared by the CGEB method (a) and the polymer prepared following the ECC method (b). The typical form of experimentally known stress-strain curves are reproduced in both cases, although the CGEB case exhibits a more pronounced strain hardening. Quantitative data on the comparison of both cases are given in Table 7.1.

in the direction of active deformation) and energy, i.e., the partitioning of stress and energy, have been calculated.

Figures 7.4 (a) and (b) show the contributions from all types of interactions to the stress for the CGEB and ECC samples, respectively. In first approximation the attractive contribution from the bonds is balanced by repulsive intra-chain Van der Waals interactions, i.e., Van der Waals interactions between monomers within the same polymer chain, before and during deformation, see Figures 7.5 (a) and (b) for the CGEB and the ECC sample respectively. Most remarkable is that the absolute value of both the stress contribution due to the bond lengths and the contribution from the intra-chain Van der Waals interactions is decreasing during deformation. Apparently the deformation induces structural rearrangements reducing internal stresses in the material. The sum of these two contributions, plotted in Figures 7.5 (c) for the CGEB sample and (d) for the ECC samples, is attractive and goes over a maximum at a strain at $\epsilon \approx 0.05$, suggesting some potential-energy barrier at the onset of yield, and is constant for larger strain. The physical picture could be that non-bonded stresses require only very small atom displacements and react therefore immediately to deformation, whereas local conformational transitions via dihedral angles are needed for stresses from chemical bonds to relax. Such conformational changes are promoted in active deformation, but occur beyond the yield point, see for example the work of Capaldi et al.[45] or Lyulin et al.[46]. Therefore the stresses from the chemical bonds start to relax later, and consequently the sum of these two stress contributions goes over a maximum.

The kinetic stress contribution is more or less constant, since the settings of the thermostat

were such that our deformations are isothermal and the volume is constant (apart from a few percent increase at the onset of yield, not shown). In experimental situations there will be, unless special measures have been taken for heat exchange, some heating of the sample. Further study will be necessary to determine the extent to which this influences stress-strain relations.

The remaining contributions, coming from bond angles, dihedral angles and inter-chain Van der Waals interactions, are given in Figures 7.5 (e) and (f), corresponding respectively to the CGEB and the ECC case. At the first glance the evolutions of all three components are the similar for CGEB and ECC. But there are differences in the details. For example in the stress contributions σ_{13} from bond angles and σ_{14} from dihedrals: prior to deformation for the ECC case the contribution from bond angles is repulsive ($\sigma_{13} = -6$ MPa) and the contribution from dihedrals vanishes ($\sigma_{14} = 0$ MPa), whereas for the CGEB case both contributions are attractive ($\sigma_{13} = 5$ MPa and $\sigma_{14} = 2$ MPa). Furthermore, for larger strain values ($\epsilon > 0.5$) the contributions σ_{13} and σ_{14} rise faster for CGEB than for ECC. This can be understood by realizing that the chains in the ECC samples are in more compact conformations than the chains in the CGEB sample. Consequently, in the CGEB sample bond angles and dihedrals will be more seriously affected by the deformation. The average slope of the curve of $(\sigma_{13} + \sigma_{14})$ vs ϵ (not shown), in the interval beyond $\epsilon = 0.6$, have been determined for both samples; in case of CGEB a value $\partial(\sigma_{13} + \sigma_{14})/\partial\epsilon = (60 \pm 1)$ MPa is obtained and in case of ECC a value $\partial(\sigma_{13} + \sigma_{14})/\partial\epsilon = (44 \pm 1)$ MPa. This has to be at least partly responsible for the fact that in case of the CGEB sample the presence of strain hardening is more convincing than in the case of ECC, see Figure 7.3. On the contrary, if one compares the slopes of the contributions σ_{Vinter} (from inter-chain Van der Waals interactions) for both samples, then a larger negative value is found for the CGEB case ($\partial(\sigma_{Vinter})/\partial\epsilon = (-18 \pm 1)$ MPa) than for the ECC case ($\partial(\sigma_{Vinter})/\partial\epsilon = (-9 \pm 1)$ MPa). The cumulative effect of the different slopes $\partial\sigma_{13}/\partial\epsilon$, $\partial\sigma_{14}/\partial\epsilon$ and $\partial\sigma_{Vinter}/\partial\epsilon$ for the CGEB and the ECC cases, is the difference in strain-hardening modulus.

A possible explanation lies in the fact that the CGEB sample starts from more extended-chain conformations, and during deformation this difference remains, since at larger length scales (longer than the Kuhn length) the simulated polymer chains are not able to relax and their conformations are determined by the overall deformation of the sample. The differences at larger length scales are compensated by the fact that more local conformational changes via dihedrals occur in the CGEB case than in the ECC case, see next subsection. In addition to that, bond- and dihedral angles show larger departures from their equilibrium values in the CGEB case than in the ECC case. The result is more severe structural reordering in case of CGEB, which leads to stronger reduction in the stresses that are due to inter-chain Van der Waals interactions.

In Figure 7.6 the partitioning of energy is shown for both samples. How does this partitioning of energy fit into the total picture? In the CGEB case we observe an instantaneous increase in the energies from bond lengths, bond angles and dihedrals. This instantaneous increase is not observed in case of ECC, because the chains are already initially less ex-

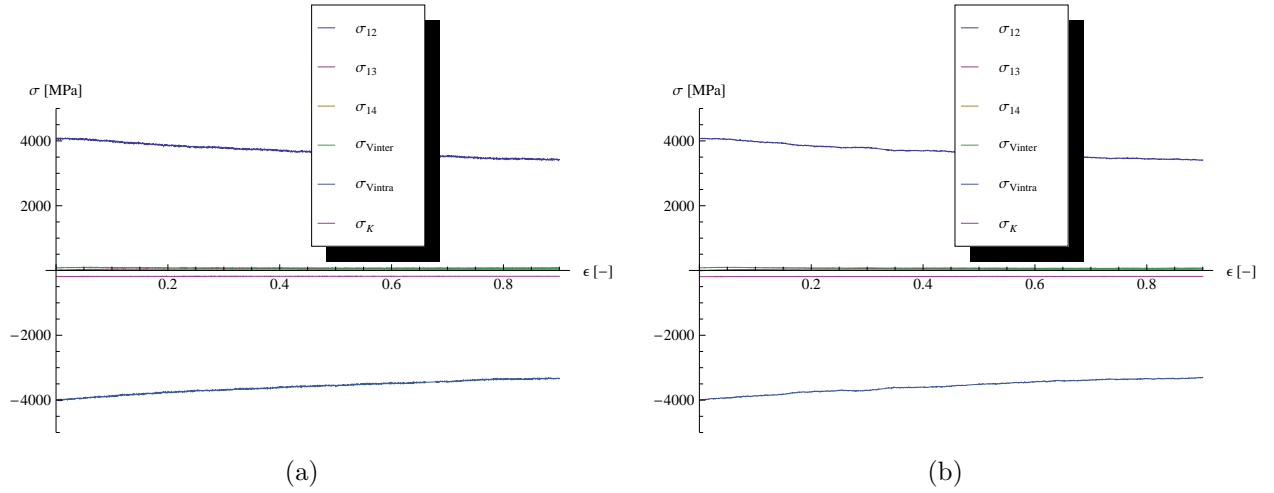


Figure 7.4: Stress partitioning as a function of strain for both the polymer prepared by the CGEB method (a) and the polymer prepared following the ECC method (b). There are six contributions to the total stress: contributions from bond lengths (σ_{12}), bond angles (σ_{13}), dihedral angles (σ_{14}), intra-chain ($\sigma_{V_{intra}}$) and inter-chain ($\sigma_{V_{inter}}$) Van der Waals interactions and a kinetic contribution (σ_K). The dominant contributions, σ_{12} and $\sigma_{V_{intra}}$, are more than an order of magnitude larger than all other contributions. More detailed information on the separate contributions is given in Figure 7.5.

tended for ECC. In case of ECC even a decrease in dihedral energy with strain is observed. This difference in dihedral-energy evolution can not be ascribed to more transitions from gauche states to the trans states for the ECC sample than for the CGEB sample; further discussion on this point can be found in the next subsection. A further interesting issue is the difference between inter-chain Van der Waals interactions. For the CGEB case the inter-chain Van der Waals energy rises first, then goes over a maximum at $\epsilon = 0.25$ and subsequently decreases again. Such a barrier is absent for ECC. These observations support the picture that once bonds (and angles) feel the deformation, which only happens in the CGEB case, where the chain conformations are not too compact, some local orderings are disturbed, giving rise to the barrier, see Figure 7.6(c), in the inter-chain Van der Waals energy.

7.3.4 Evolution of structures

In order to obtain insight in the influence of deformation on chain conformations, from the level of a few monomer segments to the level of the size of a polymer chain, distributions of dihedral angles in the polymer backbones, pair correlations and internal distances have been studied as a function of strain. In Figure 7.8 the distributions of dihedral angles for both cases are given. The convention that has been used to calculate dihedral angles, is

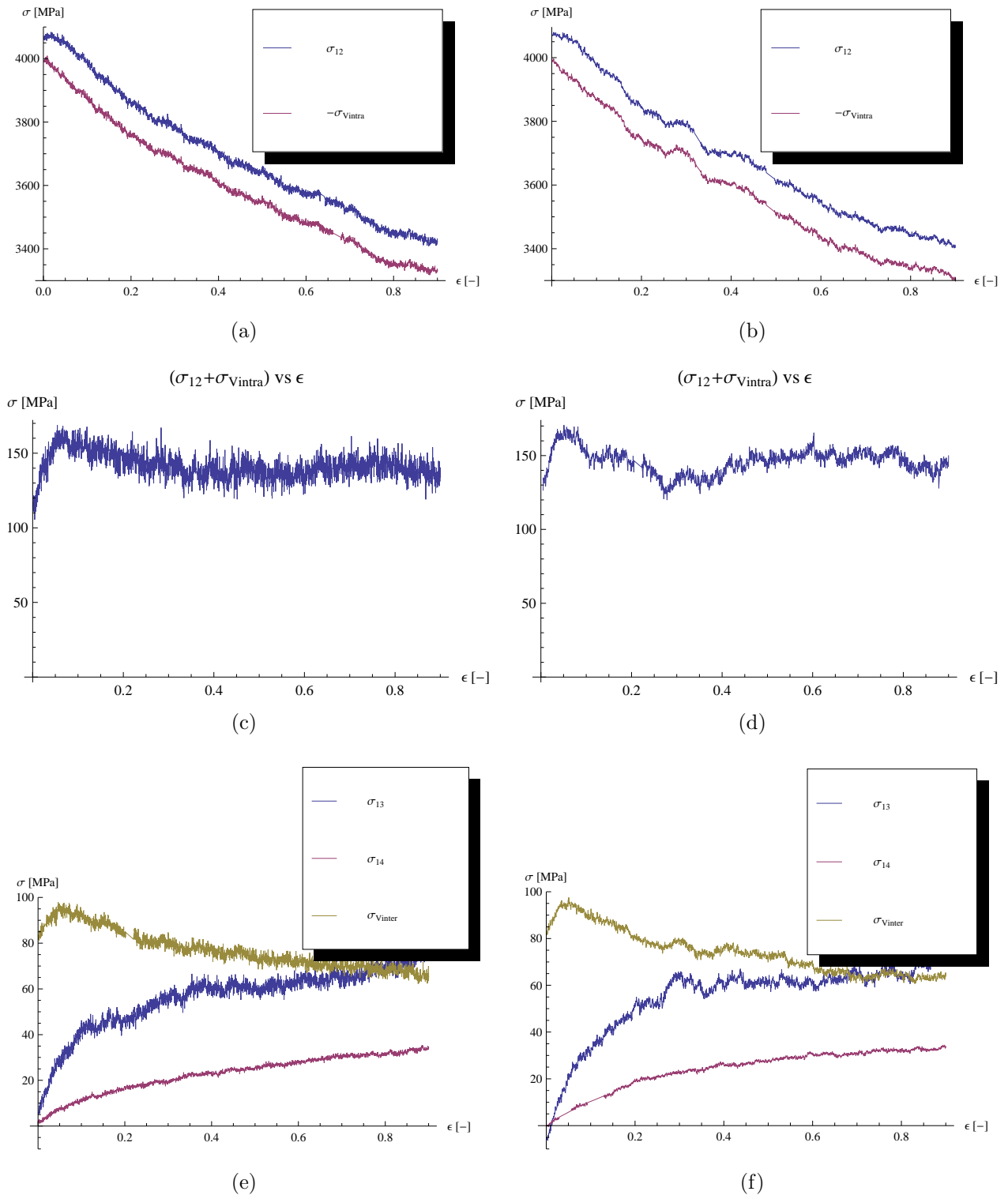


Figure 7.5: Stress partitioning as a function of strain for both the polymer prepared by the CGEB method (subfigures (a), (c), (e)) and the polymer prepared following the ECC method (subfigures (b), (d), (f)). The largest stress contributions, coming from bond lengths (σ_{12}) and intra-chain angles (σ_{vintra}), are given for the CGEB sample in (a) and (c) and for the ECC samples in (b) and (d). σ_{vintra} and σ_{12} largely cancel each other. All other contributions, concerning bond angles, bond lengths and dihedral angles, are given in (e) for the CGEB sample and in (f) for the ECC sample.

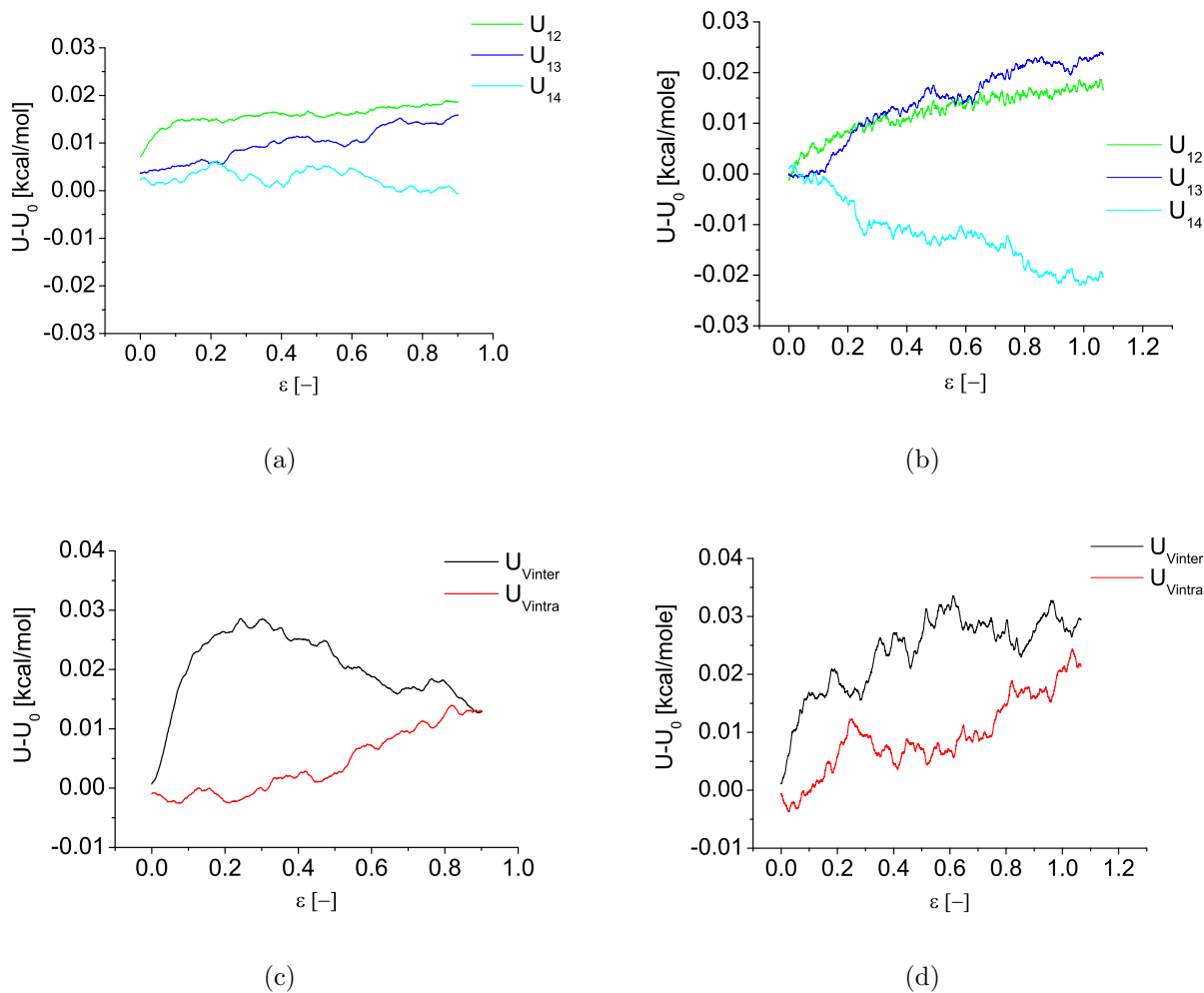


Figure 7.6: Energy partitioning for both polymer samples. The evolution of the energies related to bond lengths U_{12} , bond angles U_{13} and dihedral angles U_{14} is given in (a) for the CGEB and in (b) for the ECC samples. The intra-chain and inter-chain Van der Waals energies, respectively U_{Vintra} and U_{Vinter} , and the total energy U_{pot} are plotted vs strain in (c) and (d), for the CGEB and the ECC samples respectively.

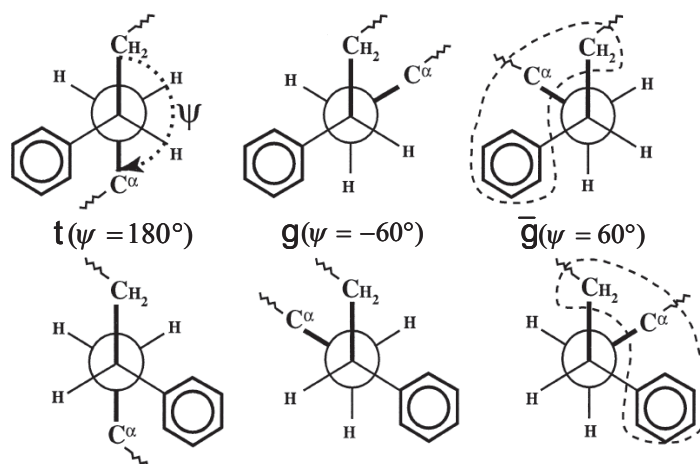


Figure 7.7: Backbone dihedrals are calculated as explained in ref [148]. All backbone dihedrals (determined by positions of 4 consecutive atoms in the backbone) are viewed in the same direction, that is, always starting from a CH₂-unit: CH₂-CH(C₆H₅)-CH₂-CH(C₆H₅). The direction of positive orientation is such that sterically equivalent conformations are assigned the same dihedral angle. (Conformations that are mirror-images of each other have the same dihedral angle.) Note that the convention used here is slightly different from the convention used in the previous Chapter. Reprinted from Dunbar et al. [148]

explained in Figure 7.7. Clearly both in the case of the CGEB and in the case of the ECC samples, the amount of dihedrals in the trans conformation increases during deformation, although more so for CGEB (from 60.4% to 64.7%) than for ECC (from 69.3% to 70.4%). In case of CGEB this increase is completely at the cost of the number of dihedrals in the \bar{g} state; the number of angles in the g state remains unchanged. For the ECC case also an increase is observed in the g state (from 1.1% to 1.9%).

Given the fact that the trans state is lower in energy than either of the other states, the stronger increase in the trans population for the CGEB sample may seem in contrast with the observation in the previous Section that the ECC sample shows the larger decrease in dihedral energy. However, this can probably be explained by a broadening of the peaks in the distribution in the CGEB case; on average dihedrals are forced, by deformation, away from values corresponding to local energy minima. This effect is probably less for the ECC case, since the intra-chain degrees of freedom are less affected at the level of a few bonds, again because the chains were less extended from the beginning.

Also the pair-correlation functions G_{rem} have been studied. The changes with strain are negligible; therefore the curves have been omitted here. Finally the internal distance distributions have been studied, see Figures 7.9 (a) for CGEB and (b) for ECC. Both in the case of the CGEB and of the ECC sample all intra-chain distances for atoms separated by more than 20 backbone bonds are increased by the deformation. Most distances are

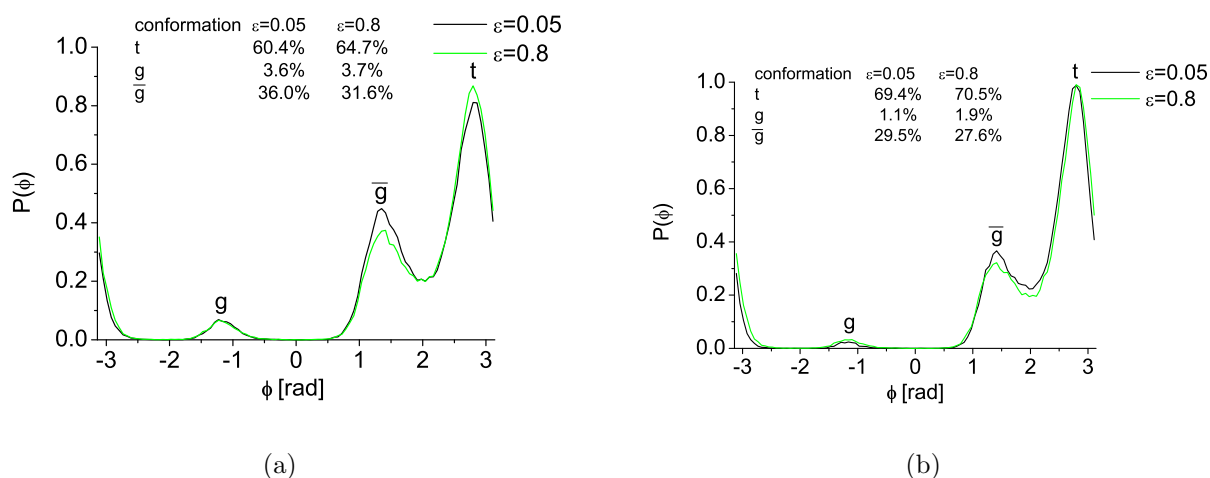


Figure 7.8: Dihedral distributions for both the CGEB (a) and the ECC (b) sample, before yield and in the strain hardening regime. In both cases the amount of dihedrals in the trans state increases upon deformation.

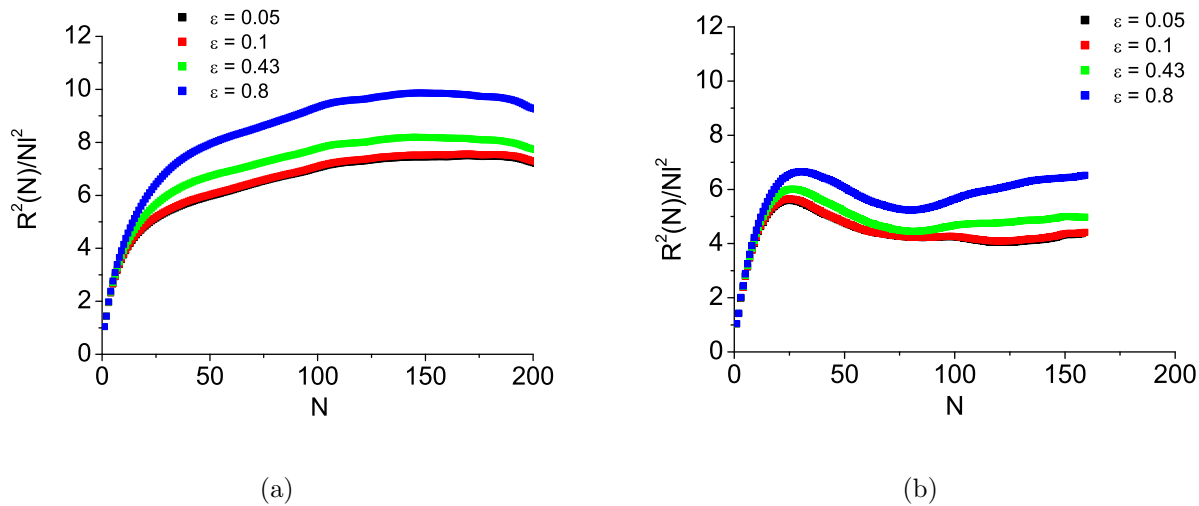


Figure 7.9: Distributions of intra-chain distances as a function of the strain for both the CGEB (a) and the ECC (b) sample, before yield and in the strain-hardening regime. The physical pictures of the two cases are comparable: for atoms separated by less than 20 backbone bonds, the intra-chain distances are not influenced by deformation, whereas for atoms separated by more than 20 backbone bonds, intra-chain distances are multiplied by the same factor, suggesting affine deformation.

increased by a comparable factor, which suggests that at length scales corresponding to intra-chain separations beyond 20 backbone bonds the samples deform affinely.

7.4 Conclusions

In this Chapter the importance of proper equilibration on all length scales for simulating the mechanical properties of PS in the glassy state has been investigated. Two sample-preparation methods have been compared. One method, termed the Extended-Chain-Collapse (ECC) method, starts from an extended chain in vacuum, which is allowed to relax at melt temperature and at ambient pressure in an NpT MD simulation. Subsequently the system is duplicated in all three Euclidian directions, after which additional equilibration in MD is performed. The other method is called the CGEB method. It uses end-bridging Monte Carlo in combination with a coarse-grained description of PS, to equilibrate the PS sample at length scales beyond the length scale of a few monomer segments. In a next step atomic details are reintroduced and the sample is equilibrated, using MD, at the length scales below that of a few monomer segments as well.

The structures obtained from both methods have been compared on all length scales. The intra-chain distances between atoms separated by more than 20 backbone chemical bonds are very different for the two samples. Whereas for the CGEB sample the characteristic ratio C_N as a function of chain length approaches a value of 8.5 (vs $C_\infty=9.85$ [153]) for large values of N , for the ECC sample the situation is much worse ($C_N \rightarrow (4.3 \pm 0.5)$).

The stress-strain behavior observed when both samples are subjected to uniaxial extension is similar. The most clear difference is that for the CGEB sample a stronger strain hardening is observed than for the ECC sample, in accordance with too compact chains in the ECC sample.

With regard to this strain-hardening difference between the two samples, the following is observed. The contributions from bond- and dihedral angles to the stress show a stronger increase for larger strains ($\epsilon > 0.5$) for the CGEB sample than for the ECC sample. On the contrary, a steeper decrease is observed of the inter-chain Van der Waals contribution to the stress. The net effect is a larger slope of the total stress for large strain values, i.e. a larger strain hardening. These observations can be understood by realizing that at larger length scales chain conformations are not able to relax during deformation and are essentially dictated by the size and shape of the simulation box. Since, already before deformation, chains in the CGEB sample are in more extended conformations than chains in the ECC sample, the chains in the CGEB sample are in more extended conformations at any strain value. These large-scale differences are compensated at length scales of a few monomer segments in two ways. The first is by more local conformational changes via dihedral angles: For the CGEB sample an increase in the amount of dihedrals in the trans-state is 4%, for the ECC sample the amount in the trans-state increases by only 1%. The second way is

by larger deviations of bond- and dihedral angles from their equilibrium values. The result of these differences in local conformational changes is more severe structural reordering in the case of CGEB, which leads to stronger reduction in stresses due to inter-chain Van der Waals interactions.

Energy partitioning as a function of the strain confirms the picture that during active deformation the polymer conformations are affected at smaller length scales for the CGEB sample than for the ECC sample. Energies related to intra-chain degrees of freedom exhibit for the CGEB sample an almost instantaneous increase, which is not observed for the ECC sample; for the energy related to dihedral angles, even a decrease is observed in the ECC case. Moreover a barrier in the intra-chain Van der Waals energies for the CGEB sample, which is absent for the ECC sample, may suggest that some local ordering involving monomers of different chains is disturbed.

In summary, we observe that two different sample-preparation methods, our new CGEB and the existing ECC, result in large structural differences beyond the length scale of a Kuhn segment. These structural differences give rise to differences in the degree of strain hardening, which can be explained as follows. Chains prepared by the CGEB method are in more extended conformations than chains prepared according to the ECC method; the chains resulting from the latter method are too compact, because screening of excluded-volume interactions was not properly taken into account. Because of this, during deformation, bond- and dihedral angles are more seriously affected for the CGEB sample than for the ECC sample; contributions from bond- and dihedral angles to the stress show a stronger increase for larger strains ($\epsilon > 0.5$) for the CGEB sample. At the same time more structural reordering takes place in the CGEB sample than in the ECC sample, which translates in a steeper decrease, after $\epsilon = 0.5$, of the inter-chain Van der Waals contribution to the stress. The net effect accounts for the difference in strain-hardening moduli observed for both samples.

Chapter 8

Conclusions and outlook

Mechanical behavior of amorphous polymers involves processes occurring at widely varying length- and especially time scales. Understanding mechanical behavior of these materials therefore calls for a multi-scale research approach. The supergoal in such an approach is to link different scales, in order to couple details at the atomistic level to macroscopic behavior.

This thesis concerns an attempt to cover as wide a range in length and time scales as possible, where the atomistic level is taken as the starting point, by means of molecular simulations. Three main issues can be identified in molecular-simulation approaches for glassy-polymer deformation. The first is the preparation and equilibration of polymer samples in the melt, the second is the vitrification by cooling down and the third is deformation under applied stress or strain. All these issues are related to limited accessible time windows in molecular simulations. For equilibration and also for calculation of equilibrium properties, of condensed polymer systems, connectivity-altering Monte Carlo (MC) techniques are very promising. However, its application involves very complicated and extensive bookkeeping issues and it cannot be applied directly to any polymer at will. With regard to the vitrification and deformation, which are dynamical processes, the application of molecular dynamics (MD) techniques seems a logical choice; the problem, however, is that, by the available time window in these simulations, one is limited to rates that are orders of magnitude larger than typical experimental rates. By using MC for deformation one may be able to extend the accessible time window available for deformation by one order of magnitude.

Two different polymers have been studied: PE and PS. In experimental reality, PE is semicrystalline and at room temperature it is not glassy (vitrification only occurs at 150-170 K, [136]). Still PE was attractive for simulation for its chemical simplicity and the availability of algorithms. Crystallinity has been prevented in simulations by quenching from the melt. In order to be able to simulate real amorphous glassy (at room temperature) polymers such as PS, a very involved multi-scale procedure to create well-equilibrated

polymer samples had to be developed first; studies of the behavior of PS have been done afterwards.

8.1 Main results

MC simulations of glassy amorphous PE under deformation, in which strain increments are alternated by short MC runs for local relaxation, see Chapter 3, result in stress-strain curves that show the typical regimes characteristic for amorphous-polymer deformation, with realistic values for E-moduli, yield stresses and -strains, but with strain-hardening moduli that are one order of magnitude too large. Stress-strain relations show correct dependencies on strain rate and temperature. And also a correct evolution of density with strain is obtained. The following physical picture is obtained. Initially, up to a strain slightly beyond the yield point, non-bonded interactions dominate stress- and energy response to the prescribed strain. During further deformation, non-bonded interactions do not contribute to further stress or energy increase anymore, whereas bonded interactions become more important; beyond a strain value of approximately 0.5 bonded interactions associated with bond lengths and bond angles are responsible for strain hardening. Finally during deformation a very severe chain stretching is observed, also at length scales of a few chemical bonds.

In many simulations it is advantageous to constrain bond lengths or bond angles, since these hard degrees of freedom evolve on very short time scales and simulation of their time evolution requires a lot of CPU time. The possibility to use constrained bond lengths in simulations of deformation forms the subject of Chapter 4. Since the use of constraints requires modification of the deformation protocol, both the influence of constraints and the influence of deformation protocol have been studied. More specifically we have looked into three cases: in one case flexible bonds are used and deformation has been done by scaling monomer positions with the size of the sample, in a second case flexible bonds have been used and deformation is performed by scaling positions of centers-of-mass of chains with the sample size, and in the third case rigid bonds are used and center-of-mass positions of chains are scaled with sample size under deformation. Only the first case gives reasonable qualitative agreement with experimental knowledge on stress-strain curves; however the strain-hardening modulus remains one order of magnitude too high.

To be able to generate well-equilibrated samples of typical amorphous polymers in the melt, see Chapter 5, an end-bridging MC algorithm for the equilibration of linear PE has been generalized to linear polymers of type $(AB)_n$, where A and B are coarse-grained particles, representing groups of atoms, forming the monomer. The algorithm has been applied to PS, where $A \equiv \text{CH}_2$ and $B \equiv \text{CH}(\text{C}_6\text{H}_5)$. The desire to be able to apply the end-bridging technique to a whole class of linear polymers is not the only reason for developing a general end-bridging algorithm for coarse-grained $(AB)_n$ polymers instead of atomistically detailed polymers. Enormous bookkeeping burdens could be restricted and a risk of negligible

acceptance of the end-bridging move (which would make the algorithm as inefficient as MD algorithms in sampling configuration space of long-chains polymer melts) could be prevented by doing so. With this algorithm correct chain conformations are obtained above T_g . Although the acceptance of the end-bridging move is 10-100 times lower in case PS is simulated than in case PE is simulated, it is still possible to equilibrate a system of thousands of PS monomers divided over chains of hundreds of monomers in a single-processor run in a week's time.

Atomistically detailed PS polymer samples have been obtained by backmapping details into the well-equilibrated coarse-grained PS polymers and subsequent equilibration in MD, see Chapter 6. This procedure does not influence polymer conformations on the long length scales; polymer conformations are in agreement with Flory's random-coil hypothesis. Also at the levels of pair-correlation functions and dihedral distributions the polymer conformations are in agreement with existing experimental knowledge. Only at the level of dyad conformational distributions discrepancies between the simulations and experimental results are seen for the meso dyads. The cause of this is not clear; remarkable however is that a method (by Spyriouni et al.) for obtaining well-equilibrated PS that is conceptually the same as ours, but with different details, shows the same shortcomings.

The atomistic PS samples obtained are used for studying effects related to aging. In more detail, an attempt is made to relate differences in stress-strain behavior between two samples prepared with different cooling rates to differences in structure. Clear differences, between the two samples, are found in dihedral angles and in dyad conformations.

Finally, the importance of the new end-bridging MC equilibration of PS polymer chains at all length scales for the simulation of mechanical properties has been looked into, see Chapter 7. A comparison of the sample preparation involving the end-bridging method with a more standard sample-preparation method shows that, whereas the end-bridging method is reliable for producing correct Gaussian chain conformations, the standard method results in too compact and non-Gaussian chain conformations, because non-bonded interactions were not sufficiently shielded during preparation. This important conformational difference translates into differences in the post-yield stress response; the strain hardening for the end-bridged sample is in agreement with experiment, for the other sample (with too compact chains) a too low strain-hardening modulus has been obtained. This strain-hardening difference can be explained by realizing that for more extended chains the effect of deformation is a stronger local change in conformation. In particular more local conformational changes via dihedrals and stronger departures from equilibrium angles are observed (and a stronger rise in angular stress contributions) for the sample with the more extended chains. These local conformational changes give rise to structural rearrangements that lead to a steeper decrease of inter-chain Van der Waals contribution to stress. The net effect directly translates in a higher strain-hardening modulus than for the sample prepared by the standard method.

A comparison of the MC deformation simulations on amorphous PE and the MD simu-

lations on PS leads to two important observations. First of all, in the MD simulations a strain hardening is obtained that is in agreement with experimental results, whereas from the MC simulations a strain-hardening modulus has been obtained that is one order of magnitude too high. At the same time, conformational changes, during deformation, at short length scales seen in the MC simulations are much stronger than those seen in the MD simulations. Apparently, the applied mix of MC moves is not sufficiently able to relax the sample in between strain increments, not even at small length scales.

8.2 Outlook

Possible research directions for future projects are the following. First of all, due to its proven superiority over most other methods, the sample-preparation method introduced here for PS should be used to prepare a variety of PS polymer samples; for example to investigate the influence of the mass distribution and of a much larger average chain length on mechanical properties. In this context it is also relevant to look into the evolution of entanglement networks, during both cooling and deformation, in the polymers. In addition, the sample-preparation method presented here should be applied to various other polymers of the same $(AB)_n$ structure. This would enable one to exclude equilibration issues from studies in which mechanical behavior of chemically different polymers is compared.

As a next step in the multi-scale modeling approach an important research line would be to really go beyond the time scales accessible for cooling and deformation in atomistic-level simulation studies. This requires molecular-dynamics studies employing, in contrast to the present study, coarse-grained models also to the dynamics of cooling and deformation. Such models should originate from atomistic ones (no toy models!). To interpret the dynamics in such models, which is distinct from the dynamics at atomistic level, will be a major challenge.

Furthermore we want to stress that the work in present thesis is limited to the study of evolution of structural properties and specific contributions to stress and energy in polymer materials during deformation experiments. An even more complete picture could be obtained by studying various dynamical properties, such as translational or rotational mobility of (groups of) atoms. This will allow verification by spectroscopic analysis.

Finally, a few very specific questions raised during this thesis work should be answered. It is important to sort out how to improve the reproduction of experimental distributions of meso-dyad conformations in PS, since distributions of dyads seem to play a role in aging-like processes. In this context it may be useful to thoroughly compare the details of the method of Spyriouni et al. and the method presented in this thesis. A further relevant extension concerns the work on aging of PS. We have seen already that some structural properties do depend on the cooling rate used to vitrify the sample. A key question here is

whether, during deformation, these structural differences will have been erased after strain softening.

Bibliography

- [1] M.D. Ediger, C.A. Angell, and S.R. Nagel. *J. Phys. Chem.*, 100:13200, 1996.
- [2] C.A. Angell. *Science*, 267:1924, 1995.
- [3] M. Rubinstein and R.H. Colby. *Polymer physics*. Oxford University Press, Oxford, 2003.
- [4] M.T. Shaw and W.J. McKnight. *Introduction to polymer viscoelasticity*. Wiley-Interscience, Hoboken, New Jersey, 2005.
- [5] G.R. Strobl. *The physics of polymers*. Springer-Verlag, Berlin Heidelberg New York, 1997.
- [6] L.R.G. Treloar. *Introduction to polymer science*. Wykeham Publications Ltd, London Winchester, 1970.
- [7] I.M. Ward and J. Sweeney. *An introduction to the mechanical properties of solid polymers*. J. Wiley and Sons, Chicester, England, 2004.
- [8] H.G.H. van Melick. *Deformation and failure of polymer glasses, Ph.D. thesis*. Eindhoven University of Technology, Eindhoven, The Netherlands, 2002.
- [9] C. Chui and M.C. Boyce. *Macromolecules*, 32:3795, 1999.
- [10] E.M. Arruda and M.C. Boyce. *Int. J. Plast.*, 9:697, 1993.
- [11] E.J. Kramer and L.L. Berger. *Advances in polymer science*, 91/92:1, 1990.
- [12] H.H. Kausch. *Polymer fracture*. Springer, Berlin, 1978.
- [13] G. Kraus. *Reinforcement of elastomers*. Wiley Interscience, London, 1965.
- [14] L.C.E. Struik. *Physical aging in amorphous polymers and other materials*. Elsevier, Amsterdam, 1978.
- [15] O.A. Hasan and M.C. Boyce. *Polymer*, 34:5085, 1993.

- [16] H.G.H. van Melick, L.E. Govaert, B. Raas, W.J. Nauta, and H.E.H. Meijer. *Polymer*, 44:1171, 2003.
- [17] L.E. Govaert, H.G.H. van Melick, and H.E.H. Meijer. *Polymer*, 42:1271, 2001.
- [18] G.B. McKenna. *J. Phys.*, 15:S737, 2003.
- [19] D. Cangialosi, M. Wübbenhorst, H. Schut, A. van Veen, and S.J. Picken. *J. Chem. Phys.*, 122:064702, 2005.
- [20] R. Haward and G. Thackray. *Proc. R. Soc. London A*, 302:453, 1968.
- [21] M.C. Boyce, D.M. Parks, and A.S. Argon. *Mech. Mater.*, 7:15, 1988.
- [22] M.C. Wang and E.J. Guth. *J. Chem. Phys.*, 20:1144, 1952.
- [23] P.D. Wu and E. van der Giessen. *J. Mech. Phys. Solids*, 41:427, 1993.
- [24] T.A. Tervoort, R.J.M. Smit, W.A.M. Brekelmans, and L.E. Govaert. *Mech. Time-Dep. Mater.*, 1:269, 1998.
- [25] A.I. Leonov. *Rheol. Acta*, 15:85, 1976.
- [26] F.P.T. Baaijens. *Rheol. Acta*, 30:284, 1991.
- [27] L.E. Govaert, P.H.M. Timmermans, and W.A.M. Brekelmans. *J. Eng. Mater. Techn.*, 122:177, 2000.
- [28] R.J.M. Smit. *Toughness of heterogenic polymeric systems: a modelling approach*, Ph.D. thesis. Eindhoven University of Technology, Eindhoven, The Netherlands, 1998.
- [29] F.H. Stillinger. *Science*, 267:1935, 1995.
- [30] B.A. Isner and D.J. Lacks. *Phys. Rev. Lett.*, 96(025506), 2006.
- [31] E.J. Kramer. *J. Polym. Sci. B*, 43:3369, 2005.
- [32] P.J. Flory. *Statistical mechanics of chain molecules*. Hanser Publishers, New York, 1989.
- [33] K. Binder. *Phil. Mag. B*, 77:591, 1998.
- [34] W. Götze. *J. Phys.: Condens. Matter*, 11:A1, 1999.
- [35] J. Han, R.H. Gee, and R.H. Boyd. *Macromolecules*, 27:7781, 1994.
- [36] S. Yip, M.F. Sylvester, and A.S. Argon. *Comp. Theor. Polym. Sci.*, 10:235, 2000.
- [37] S.U. Boyd and R.H. Boyd. *Macromolecules*, 34:7219, 2001.

-
- [38] R.J. Roe. *J. Non-Cryst. Solids*, 235-237:308, 1998.
- [39] D. Brown and J.H.R. Clarke. *Macromolecules*, 24:2075, 1991.
- [40] J. Zhou, T.M. Nicholson, G.R. Davies, and I.M. Ward. *Comp. Theor. Polym. Sci.*, 10:43, 2000.
- [41] I. Ogura and T. Yamamoto. *Polymer*, 36:1375, 1995.
- [42] I.M. Neelov, A.A. Darinskii, and J. Clarke. *Vysokomol. Soedin. (Polymer Science USSR)*, 38:1373, 1996.
- [43] F.M. Capaldi, M.C. Boyce, and G.C. Rutledge. *Polymer*, 45:1391, 2004.
- [44] L.S. Loo, R.E. Cohen, and K.K. Gleason. *Science*, 288:116, 2000.
- [45] F.M. Capaldi, M.C. Boyce, and G.C. Rutledge. *Phys. Rev. Lett.*, 89:175505, 2002.
- [46] A.V. Lyulin, B. Vorselaars, M.A. Mazo, N.K. Balabaev, and M.A.J. Michels. *Europhys. Lett.*, 71:618, 2005.
- [47] A.F. Terzis, D.N. Theodorou, and A. Stroeks. *Macromolecules*, 33:1385, 2000.
- [48] A.F. Terzis, D.N. Theodorou, and A. Stroeks. *Macromolecules*, 33:1397, 2000.
- [49] A.F. Terzis, D.N. Theodorou, and A. Stroeks. *Macromolecules*, 35:508, 2002.
- [50] R. Everaers, S.K. Sukumaran, G.S. Grest, C. Svaneborg, A. Sivasubramanian, and K. Kremer. *Science*, 303:823, 2004.
- [51] C. Tzoumanekas and D.N. Theodorou. *Macromolecules*, 39:4592, 2006.
- [52] F. Müller-Plathe. *ChemPhysChem*, 3:754, 2002.
- [53] G. Milano and F. Müller-Plathe. *J. Phys. Chem. B*, 109:18609, 2005.
- [54] P.V.K. Pant and D.N. Theodorou. *Macromolecules*, 28:7724, 1995.
- [55] V.G. Mavrantzas, T.D. Boone, E. Zervopoulou, and D.N. Theodorou. *Macromolecules*, 32:5072, 1999.
- [56] M.P. Allen and D.J. Tildesley. *Computer simulation of liquids*. Clarendon Press, Oxford, 1987.
- [57] D. Frenkel and B. Smit. *Understanding molecular simulations: from algorithms to applications*. Academic Press, London, 2002.
- [58] D. Chandler. *Introduction to modern statistical mechanics*. Oxford University Press, New York, 1987.

- [59] N. Metropolis, A.W. Rosenbluth, M.N. Rosenbluth, A.H. Teller, and E. Teller. *J. Chem. Phys.*, 21:1087, 1953.
- [60] B.J. Alder and T.E. Wainwright. *J. Chem. Phys.*, 27:1208, 1957.
- [61] B.J. Alder and T.E. Wainwright. *J. Chem. Phys.*, 31:459, 1959.
- [62] A. Rahman. *Phys. Rev.*, 136A:405, 1964.
- [63] L. Verlet. *Phys. Rev.*, 159:98, 1967.
- [64] R.W. Hockney and J.W. Eastwood. *Computer simulations using particles*. McGraw-Hill, New York, 1981.
- [65] C.R.A. Catlow, S.C. Parker, and M.P. Allen. *Computer simulations of liquid crystals and polymers*. Springer, 1989.
- [66] D.P. Landau, S.P. Lewis, and H.-B. Schüttler. *Computer simulation studies in condensed-matter physics XIII*. Springer, 2001.
- [67] P. Pasini, S. Zumer, and C. Zannoni. *Computer simulations of liquid crystals and polymers*. Springer, 2005.
- [68] S. Plimpton. *J. Comput. Phys.*, 117:1, 1995.
- [69] L. Nyland. *J. Parallel and Distributed Computing*, 47:125, 1997.
- [70] Y. Deng, R.F. Peierls, and C. Rivera. *J. Comput. Phys.*, 161:250, 2000.
- [71] P. Nielaba, M. Mareschal, and G. Ciccotti. *Bridging time scales: molecular simulations for the next decade*. Springer-Verlag, Berlin, Germany, 2002.
- [72] N.Ch. Karayiannis, A.E. Giannousaki, V.G. Mavrantzas, and D.N. Theodorou. *J. Chem. Phys.*, 117:5465, 2002.
- [73] H.J.C. Berendsen, J.P.M. Postma, W.F. Van Gunsteren, A. DiNola, and J.R. Haak. *J. Chem. Phys.*, 81:3684, 1984.
- [74] P.H. Mott, A.S. Argon, and U.W. Suter. *Phys. Conden. Struct. Defect. Mech. Properties, Philos. Mag.*, 67:931, 1993.
- [75] M. Utz, Q. Peng, and M. Nandagopal. *J. Pol. Sci. B*, 42:2057, 2004.
- [76] S.A. Ospina, J. Restrepo, and B.L. Lopez. *Mater. Res. Innov.*, 7:27, 2003.
- [77] S.A. Ospina, M. Hess, and B.L. Lopez. *E-Polymers*, (024), 2004.
- [78] T. Hölzl, C. Mesner, S. Kreitmeier, and D. Goritz. *Comput. Theor. Polym. Sci.*, 9:99, 1999.

-
- [79] I. Carmesin and K. Kremer. *Macromolecules*, 21:2819, 1988.
- [80] H.P. Deutsch and K. Binder. *J. Chem. Phys.*, 94:2294, 1991.
- [81] V. Tries, W. Paul, and J. Baschnagel. *J. Chem. Phys.*, 106:738, 1997.
- [82] K. Binder, J. Baschnagel, C. Bennemann, and W. Paul. *J. Phys.: Condens. Matter*, 11:A47, 1999.
- [83] J. Li, T. Mulder, B. Vorselaars, A.V. Lyulin, and M.A.J. Michels. *Macromolecules*, 39:7774, 2006.
- [84] J.I. McKechnie, D. Brown, and J.H.R. Clarke. *Macromolecules*, 25:1562, 1992.
- [85] M. Hutnik, F.T. Gentile, P.J. Ludovice, U.W. Suter, and A.S. Argon. *Macromolecules*, 24:5962, 1991.
- [86] R. Khare, M.E. Paulaitis, and S.R. Lustig. *Macromolecules*, 26:7203, 1993.
- [87] D. Rigby and R.J. Roe. *J. Chem. Phys.*, 87:7285, 1987.
- [88] M. Kotelyanskii, N.J. Wagner, and M.E. Paulaitis. *Macromolecules*, 29:8497, 1996.
- [89] M. Müller, J. Nievergelt, S. Santos, and U.W. Suter. *J. Chem. Phys.*, 114:9764, 2001.
- [90] S. Santos, U.W. Suter, M. Müller, and J. Nievergelt. *J. Chem. Phys.*, 114:9772, 2001.
- [91] W.L. Mattice and U.W. Suter. *Conformational theory of large molecules, the rotational isomeric state model in macromolecular systems*. Wiley, New York, 1994.
- [92] R. Auhl, R. Everaers, G.S. Grest, K. Kremer, and S.J. Plimpton. *J. Chem. Phys.*, 119:12718, 2003.
- [93] D.N. Theodorou and U.W. Suter. *Macromolecules*, 18:1467, 1985.
- [94] L.R. Dodd, T.D. Boone, and D.N. Theodorou. *Molecular Physics*, 78:961, 1993.
- [95] V.A. Harmandaris, N.P. Adhikari, N.F.A. Van de Vegt, and K. Kremer. *Macromolecules*, 39:6708, 2006.
- [96] A.R. Leach. *Molecular modelling. Principles and applications*. Pearson Education Limited, Harlow, 1996.
- [97] A.V. Lyulin, N.K. Balabaev, M.A. Mazo, and M.A.J. Michels. *Macromolecules*, 37:8785, 2004.
- [98] M. Vacatello, G. Avitabile, P. Corradini, and A. Tuzi. *J. Chem. Phys.*, 73:548, 1980.
- [99] J.I. Siepmann and D. Frenkel. *Mol. Phys.*, 75:59, 1992.

- [100] L.R. Dodd and D.N. Theodorou. *Adv. Polym. Sci.*, 116:249, 1994.
- [101] M. Wittkop, J.U. Sommer, S. Kreitmeier, and D. Goritz. *Phys. Rev. E*, 49:5472, 1994.
- [102] W. Brostow and R.D. Corneliusen. *Failure of plastics*. Hanser, New York, 1986.
- [103] J.P. Ryckaert and A. Bellemans. *Chem. Phys. Lett.*, 30:123, 1975.
- [104] D.N. Theodorou, T.D. Boone, L.R. Dodd, and K.F. Mansfield. *Makromol. Chem. Theory Simul.*, 2:191, 1993.
- [105] W. Smith. *CCP5 Info. Quart.*, page 14, 1993.
- [106] J. Bandrup and E.H. Immergut. *Polymer handbook*. J. Wiley and Sons, New York, 1966.
- [107] M.A. Kennedy, A.J. Peacock, and L. Mandelkern. *Macromolecules*, 27:5297, 1994.
- [108] J.I. McKechnie, R.N. Haward, D. Brown, and J.H.R. Clarke. *Macromolecules*, 26:198, 1993.
- [109] R.E. Robertson. *J. Chem. Phys.*, 44:3950, 1966.
- [110] A.S. Argon. *Philos. Mag.*, 28:839, 1973.
- [111] P.B. Bowden. *The physics of glassy polymers*. Appl. Sci., London, UK, 1973.
- [112] A.S. Argon. *Glass science and technology*. Academic, New York, USA, 1980.
- [113] B. Escaig and C. G'Sell. *Plastic deformation of amorphous and semicrystalline materials*. Les Editors de Physique, Les Ulis, France, 1982.
- [114] J.-C. Bauwens. *Plastic deformation of amorphous and semicrystalline materials*. Les Editors de Physique, Les Ulis, France, 1982.
- [115] I. Ward. *Polym. Eng. Sci.*, 24:724, 1984.
- [116] A.S. Krausz and H. Eyring. *Deformation kinetics*. Wiley, New York, USA, 1985.
- [117] E.F. Oleinik, O.B. Salamantina, S.N. Rudnev, and S.V. Shenogin. *Polym. Sci. USSR*, 35:1532, 1993.
- [118] H.G.H. van Melick, L.E. Govaert, and H.E.H. Meijer. *Polymer*, 44:3579, 2003.
- [119] H.G.H. van Melick, L.E. Govaert, and H.E.H. Meijer. *Polymer*, 44:2493, 2003.
- [120] G. Marechal and J.P. Ryckaert. *Chem. Phys. Lett.*, 101:548, 1983.
- [121] R. Edberg, G.P. Morriss, and D.J. Evans. *J. Chem. Phys.*, 86:4555, 1987.

-
- [122] M. Utz, P.G. Debenedetti, and F.H. Stillinger. *Phys. Rev. Lett.*, 84:1471, 2000.
- [123] C.T. Samara. *Simulation of polypropylene of various tacticities with the Monte Carlo method, Ph.D. thesis*. University of Patras, Patras, Greece, 2000.
- [124] M. Doxastakis, V.G. Mavrantzas, and D.N. Theodorou. *J. Chem. Phys.*, 115:11339, 2001.
- [125] M. Doxastakis, V.G. Mavrantzas, and D.N. Theodorou. *J. Chem. Phys.*, 115:11352, 2001.
- [126] T. Vettorel and H. Meyer. *J. Chem. Theory Comput.*, 2:616, 2006.
- [127] T. Spyriouni, C. Tzoumanekas, D.N. Theodorou, F. Müller-Plathe, and G. Milano. *Macromolecules*, 40:3876, 2007.
- [128] W. Tschop, K. Kremer, J. Batoulis, T. Bürger, and O. Hahn. *Acta Polymer*, 49:61, 1998.
- [129] C.F. Abrams and K. Kremer. *Macromolecules*, 36:260, 2003.
- [130] K. Kamio, K. Moorthi, and D.N. Theodorou. *Macromolecules*, 40:710, 2007.
- [131] P. Robyr, M. Tomaselli, C. Grob-Pisano, B.H. Meier, R.R. Ernst, and U.W. Suter. *Macromolecules*, 28:5320, 1995.
- [132] P. Robyr, Z. Gan, and U.W. Suter. *Macromolecules*, 31:8918, 1998.
- [133] P. Robyr, M. Müller, and U.W. Suter. *Macromolecules*, 32:8681, 1999.
- [134] C.D. Wick, M.G. Martin, and J.I. Siepmann. *J. Phys. Chem. B*, 104:8008, 2000.
- [135] V.G. Harmandaris. Private communication, 2007.
- [136] J. Mark, K. Ngai, W. Graessley, L. Mandelkern, E. Samulski, J. König, and G. Wignall. *Physical properties of polymers*. Cambridge University Press, Cambridge, U.K., 2003.
- [137] P. Zoller and D.J. Walsh. *Standard pressure-volume-temperature data for polymers*. Technomic Publishing co., Lancaster Basel, 1995.
- [138] A.V. Lyulin and M.A.J. Michels. *Phys. Rev. Lett.*, 99:085504, 2007.
- [139] A.V. Lyulin. Private communication, 2007.
- [140] D.Y. Yoon, P.R. Sundararajan, and P.J. Flory. *Macromolecules*, 8:776, 1975.
- [141] R.F. Rapold and U.W. Suter. *Macromol. Theory Simul.*, 3:1, 1994.

- [142] M. Rehahn, W.L. Mattice, and U.W. Suter. *Advances in polymer science*, 131/132, 1997.
- [143] J.D. Londono, A. Habenschuss, J.G. Curro, and J.J. Rajasekaran. *J. Polym. Sci., B*, 34:3055, 1996.
- [144] A.V. Lyulin, N.K. Balabaev, and M.A.J. Michels. *Macromolecules*, 36:8574, 2003.
- [145] W.H. Press, B.P. Flannery, S.A. Teukolsky, and W.T. Vetterling. *Numerical recipes*. Cambridge University Press, Cambridge, 1985.
- [146] B. Vorselaars, A.V. Lyulin, and M.A.J. Michels. *Macromolecules*, 40:6001, 2007.
- [147] A.S. Lemak and N.K. Balabaev. *J. Comput. Chem.*, 17:1685, 1996.
- [148] M.G. Dunbar, B.M. Novak, and K. Schmidt-Rohr. *Solid State Nuclear Magnetic Resonance*, 12:119, 1998.
- [149] Z. Gan and R.R. Ernst. *Chem. Phys. Lett.*, 253:13, 1996.
- [150] D. Neuhaus and M.P. Williamson. *The nuclear Overhauser effect in structural and conformational analysis*. VCH Publishers, New York, 1989.
- [151] A.V. Lyulin, J. Li, T. Mulder, B. Vorselaars, and M.A.J. Michels. *Macromol. Symp.*, 237:108, 2006.
- [152] A.V. Lyulin and M.A.J. Michels. *Macromolecules*, 35:1463, 2002.
- [153] J.E. Mark. *Polymer data handbook*. Oxford University Press, Oxford, U.K., 1999.

Summary

Equilibration and deformation of glass-forming polymers: molecular simulation via connectivity-altering Monte Carlo and scale-jumping methods

A deep understanding of the structure and dynamics of glasses poses a great challenge in soft condensed matter physics. On approaching the glass transition the molecular relaxation times in simple glass-formers are observed to grow to such an extent that these systems do not reach thermal equilibrium on experimentally accessible time scales. For polymers with complex microstructure the problem of the glass transition is even more difficult. While universal features of glassy dynamics should exist, superimposed chemistry-specific aspects do lead to apparently widely different behavior, such as brittle (e.g. polystyrene) vs. very ductile (e.g. polycarbonate) macroscopic failure. A better understanding of the mechanical properties of amorphous polymers is essential both for predicting the material properties after polymer processing and for the development of new materials.

The objective of this thesis project is to bridge the gap between current continuum multi-level finite-element polymer modeling and coarse-grained mesoscopic network modeling of amorphous polymers on the one hand, and molecular chemistry insights on the other hand. Suitable tools for exploring the structure and properties of bulk amorphous polymers at the molecular level are molecular dynamics (MD) and Monte Carlo (MC). One serious drawback however of many detailed MD or MC simulations of chemically-specific polymers is the problem of preparing well-equilibrated initial samples when approaching the glass transition. The result is an inefficient sampling of phase space and unreliable estimations of both statistical and dynamical properties.

For a few simple linear polymers this problem had been solved by the development of connectivity-altering MC (CAMC) algorithms. We use such an algorithm to obtain a well-equilibrated polyethylene (PE) sample in the melt. Subsequently the sample is cooled into the glassy state and deformed uniaxially, see Chapter 3. Typical experimental stress-strain curves, with E-moduli, yield-stresses, Poisson ratios of the correct order of magnitude, are found. Also dependencies on temperature, strain rate and cooling rate show the right trends. In addition the simulations provide a window into the material.

More insight into molecular-level processes during polymer deformation has been obtained both from separating contributions of different interactions to stress and energy at varying strain and by studying the evolution of the structure on all sub-continuum length scales.

Special attention was given to the selection of a suitable implementation of deformation in the simulations; various deformation methods have been compared, see Chapter 4. In this respect also the possibility to constrain the hard degrees of freedom, in order to save CPU time, has been looked into. It is found that the combination of constrained bonds with simple deformation protocols, in which positions of monomers or chains are scaled with the sample size, are not adequate for the simulation of polymer deformation; typical features of amorphous polymer mechanical behavior are then not reproduced.

Since PE is only one polymer and one of the main purposes of the project was to study and compare various chemically different polymers, we generalized the CAMC algorithm for PE to one for a broad class of linear polymers, see Chapter 5. This could be done by describing the polymers at a slightly coarse-grained (CG) level, such that the functional form of the force field becomes similar for all these polymers. By this approach the polymers are equilibrated at the CG level. Especially the distribution of intra-chain distances is important: from this we can judge whether the polymer chains adopt conformations that can be described as Gaussian chains of Kuhn segments (Flory's theorem). After equilibration at the CG level atomistic details are reintroduced, see Chapter 6, and the polymers are equilibrated on the length scales of the atomistic details as well. In the present work this whole procedure is followed for atactic PS as an example. Extensive comparisons with literature demonstrate that our approach results in microstructures that show much similarity to those in experimentally known PS.

Finally, the effect of sample preparation on the stress-strain relations for glassy polystyrene as obtained from atomistic molecular-dynamics simulations has been studied, see Chapter 7. A conventional sample-preparation method ("extended-chain condensation", ECC) that is based solely on molecular-dynamics simulations has been compared to the method ("coarse-grained end-bridging", CGEB) involving connectivity-altering (end-bridging) Monte Carlo and coarse graining. The stress-strain relations are different in the strain-hardening regime. For samples prepared according to the CGEB method a stronger strain hardening is observed and the modulus is more realistic. These differences have to be attributed to the fact that screening of excluded-volume interactions is not properly taken into account in ECC, which results in too compact chain conformations.

List of Publications

Architecture and Conformation of Uncharged and Charged Hyperbranched Polymers: Computer Simulation and Mean-Field Theory

Tim Mulder, Alexey V. Lyulin, Paul van der Schoot, and M.A.J. Michels
Macromolecules **38**, 996 (2005)

Monte Carlo Simulation of Uniaxial Tension of an Amorphous Polyethylene-like Polymer Glass

Jing Li, Tim Mulder, Bart Vorselaars, Alexey V. Lyulin, and M.A.J. Michels
Macromolecules **39**, 7774 (2006)

Atomistic Simulation of Bulk Mechanics and Local Dynamics of Amorphous Polymers

Alexey V. Lyulin, Jing Li, Tim Mulder, Bart Vorselaars, and M.A.J. Michels
Macromol. Symp. **237**, 108 (2006)

Monte Carlo Simulation of Uniaxial Deformation of Polyethylene-like Polymer Glass: Role of Constraints and Deformation Protocol

Tim Mulder, Jing Li, Alexey V. Lyulin, and M.A.J. Michels
Macromol. Theory Simul. **16**, 348 (2007)

Tim Mulder, V.A. Harmandaris, Alexey V. Lyulin, N.F.A. van der Vegt, and M.A.J. Michels, in preparation, to be submitted to Macromolecules

Tim Mulder, Alexey V. Lyulin, Bart Vorselaars, and M.A.J. Michels, in preparation, to be submitted to Macromol. Theory Simul.

Dankwoord

Eenieder die direct of indirect heeft bijgedragen aan de voltooiing van dit proefschrift wil ik hartelijk danken. Een aantal personen wil ik hier expliciet noemen.

Allereerst wil ik graag mijn promotor Thijs Michels en mijn copromotor Alexey Lyulin bedanken. In het begin moesten we elkaar nog goed leren kennen en verliep de samenwerking zo nu en dan wat stroef. Later is er naar mijn mening efficiënt samengewerkt. Thijs wil ik bedanken voor zijn sturing in de breedste zin des woords. Alexey is altijd een uitstekende vraagbaak geweest, met name met betrekking tot moleculaire simulaties.

De overige leden van de vakgroep Polymeerfysica wil ik danken voor gezelligheid, wijze lessen en praktische tips. In het bijzonder wil ik noemen mijn kamergenoot Bart Vorselaars van wie ik onder andere veel nuttige programmeertips heb gehad.

Vervolgens wil ik diverse collega's in het veld, die mij met hun specialistische kennis vooruit hebben geholpen, bedanken voor de prettige samenwerking. Doros Theodorou voorzag mij van een End-Bridging Monte Carlo code voor polyetheen, wat mij een goed uitgangspunt opleverde. Voor tal van drukberekeningen waren tips van Wim Briels en Wilfred van Gunsteren nuttig. Voor wat betreft coarse-graining en multischaal modelleren heb ik veel gehad aan de samenwerking met Nico van de Vegt en Vagelis Harmandaris. Als laatste wil ik in dit verband nog noemen Nikolaj Balabaev en Mikhail Mazo voor hun helpdeskfunctie bij het doen van atomistische simulaties van polystyreen.

Twee studenten wil ik hier ook noemen. Jing Li heeft een grote bijdrage geleverd aan het simuleren van polyetheen; dit werk is later ook gepubliceerd. Ruud Boesten heeft gewerkt aan visualisatie en analyse van entanglement networks; helaas ben ik niet meer in staat geweest zijn werk verder uit te bouwen en eventueel op te nemen in dit proefschrift, hopelijk krijgt zijn werk nog een vervolg. Behalve voor hun bijdrage aan het werk wil ik beide heren bedanken voor de prettige omgang!

Dan het ondersteunend personeel. Helmi en Clazien, onze secretaresses, zijn altijd heel behulpzaam (Ik herinner me i.h.b. een hotelkamer met babybed, centraal gelegen en met goede geluidsisolatie.) en gezellig geweest. Verder wil ik danken de heren Arieh Tal, Tarik Gammoun en Willem-Pieter Sukkel van de ict-ondersteuning voor hun inzet.

In het eindstadium heeft de promotiecommissie (Nico van de Vegt, Wim Briels, Han Slot,

Doros Theodorou, Peter Bobbert en Gerrit Kroesen) goed werk gedaan door het kritisch onder de loep nemen van het proefschrift en het aandragen van suggesties ter verbetering ervan.

Tot slot heeft ook een aantal personen uit de privésfeer een grote rol gespeeld bij de totstandkoming van dit proefschrift. Mijn vrouw Marianne heeft zich met name in de aanloop naar het versturen van "het boekje" naar de leescommissie het vuur uit de sloffen gelopen; naast haar eigen professionele activiteiten heeft zij én de zorg voor onze dochter Anne-Sophie én de huishouding gemanaged. Ook mijn ouders hebben hier hun steentje bijgedragen door Anne-Sophie regelmatig een dagje op te halen. Anne-Sophie op haar beurt heeft voor de broodnodige afleiding gezorgd en mijn relativiseringsvermogen vergroot. Ontzettend bedankt!

Curriculum Vitae

6 August 1977

Born in Eindhoven

1990-1996

VWO at Strabrecht College, Geldrop

1996-2003

M.Sc. in Applied Physics at Eindhoven University of Technology

-Traineeship at the Physics of Surfaces and Interfaces group of the Physics department of Eindhoven University of Technology. Subject: *Iron oxide reference measurements for low-energy ion scattering*, under supervision of Ir. M. de Ridder and dr. R.G. van Welzenis.

-Traineeship at FyMaZ, Aachen. Subject: *Finite-element modeling of lubrication of piston ring and cylinder liner in internal combustion engines*, under supervision of dr. A.P.J. Voncken and dr. H.J.H. Clercx.

-Master thesis project at the Polymer Physics group of the Physics department of Eindhoven University of Technology. Subject: *Architecture and conformation of hyperbranched polymers via Brownian dynamics simulation and mean-field theory*, under supervision of dr. A.V. Lyulin and prof. dr. M.A.J. Michels.

Extracurricular activities include active participation in various student associations and organizations, such as a fraternity, a general students association, a physics students association and, on behalf of that physics students association, in the organization of a university-wide career event.

2003-2008

Ph.D. at the Polymer Physics group of the Physics department of Eindhoven University of Technology, within a research project of the Dutch Polymer Institute (DPI). Subject: *Equilibration and deformation of glass-forming polymers: molecular simulation via connectivity-altering Monte Carlo and scale-jumping methods*, under supervision of dr. A.V. Lyulin and prof. dr. M.A.J. Michels. In addition, the master thesis project was given a short follow-up.

2008-

Researcher at Océ-Technologies, Venlo.